J Mater Sci (2020) 55:6195–6241

Review

Review of supported metal nanoparticles: synthesis methodologies, advantages and application as catalysts

Matumuene Joe Ndolomingo[1], Ndzondelelo Bingwa[1], and Reinout Meijboom[1,*]

[1] Department of Chemical Sciences, University of Johannesburg, PO Box 256, Auckland Park, Johannesburg 2006, South Africa

Received: 11 June 2019
Accepted: 31 January 2020
Published online: 12 February 2020

ABSTRACT

Supported metal nanoparticles, M-NPs, are of great scientific and economic interest as they encompass application in chemical manufacturing, oil refining and environmental catalysis. Oxidation and hydrogenation reactions are among the major reactions catalyzed by supported M-NPs. Although supported M-NPs are preferable due to their easy recovery and reuse, there are still some practical issues regarding their catalytic activity and deactivation. This review highlights the general features of supported M-NPs as catalysts with particular attention to copper, gold, platinum, palladium, ruthenium, silver, cobalt and nickel and their catalytic evaluation in various reactions. The catalytic performance of noble M-NPs has been explored extensively in various selective oxidation and hydrogenation reactions. In general, noble metals are expensive and sensitive to poisons. Despite their significant merits and potential (easily available, comparatively inexpensive and less sensitive to poisons), catalysis by base M-NPs is relatively less explored. Therefore, activity of base M-NPs can be improved, and still, there is potential for such catalysts.

Introduction

Catalysis is a crucial technology permitting the functionalization and utilization of a myriad of raw materials that can be used for the formation of products of great value. Catalysis at an interface is called heterogeneous catalysis, where the reactants and catalyst are in different phases. In most cases, the catalysts used in heterogeneous catalysis are solids or powders and the reactants are gases or liquids. For a solid catalyst, the catalytically active components, such as metals or metal oxides (usually in a low concentration), are immobilized in a dispersed state on a support or carrier.

Over the past years, metal nanoparticles (M-NPs)—generally so-called when their size is between 1 and 100 nm—have been widely used in synthetic organic chemistry [1–10]. Recently, catalysis by supported transition M-NPs has been attractive and received strong attention for many selective oxidation

Address correspondence to E-mail: rmeijboom@uj.ac.za

https://doi.org/10.1007/s10853-020-04415-x

[5, 10–15] and hydrogenation [16–21] reactions under mild conditions.

This review presents an up-to-date overview of supported M-NPs emphasizing Cu, Au, Pt, Pd, Ru, Ag, Co and Ni nanoparticles, NPs (active phase), their synthesis methodologies, their characteristics and their advantages and application as catalysts for various oxidation and hydrogenation reactions. A brief view of the ligand adsorption-based technique for M-NP surface area determination and kinetic models of the liquid-/gas-phase reaction over M-NPs is also provided. This review will contribute to develop novel and efficient reusable catalytic nanomaterials for various catalytic transformations. Nanomaterials are of high scientific importance and are subject of research in the materials science community due to the unique properties that they exhibit. Materials scientists emphasize understanding of the structures and properties of materials (natural, synthetic or composite), and also the way their processing influences their structures and properties, and thus their performance. Therefore, this review would likely help on designing efficient catalytic systems.

Properties of nanoparticles

Nanoparticles (NPs) are of high scientific interest as they show unusual properties compared to their bulk counterparts [13, 22]. At the nanoscale, the properties of the materials generally change. The effect that causes changes in the properties of the materials is referred to as the size-induced metal–insulator transition (quantum size effect) [23]. As the size of a material decreases in the nanorange, the percentage of atoms at its surface becomes substantial. Therefore, the subsequent surface-to-volume ratio increases substantially, which influences the surface-related properties of the material. In general, the interesting properties and the advantageous characteristics of NPs are:

- High surface-to-volume ratios, which provide a large number of active sites per unit area compared to their bulk counterparts [24].
- Higher zeta potential, averting the aggregation of nanoclusters in solution [25].
- Possible separation and recyclability, reducing the probability of contamination of the catalyst with the product and making them cost-effective [26].

Transition metal nanoparticles in catalysis

Transition M-NPs are clusters comprising from tens to thousands transition metal atoms (Fig. 1). Their sizes vary between one nanometer to hundreds of nanometers in diameter. However, in catalysis, the most active is only of few nanometers [6]. The size of the M-NP catalysts is therefore crucial aspect of the catalytic steps. Modern transition M-NPs (1–10 nm in diameter) differ from classical colloids (typically > 10 nm in diameter) in several aspects, including size and stability in solution [27].

Due to their unusual properties based on their intrinsic large surface-to-volume ratios, modern transition M-NPs with narrow size distribution have gained strong interest in scientific research as well as industrial applications [27, 29]. Transition M-NPs are awarded with various features of an efficient catalyst [30, 31]. Colloidal M-NPs as catalysts are used in homogeneous systems or otherwise can be heterogenized using a support such as alumina, silica, titania, carbon materials or zeolite. The support can be either a powder or a pre-shaped cheap solid with a high surface area that usually shows no catalytic activity on its own.

Homogeneous catalysis is very efficient and selective, but suffers from its limited thermal stability and the difficulty of extraction of the catalyst from the reaction media. Unlike homogeneous catalysis, heterogeneous catalysis benefits from possible use of high temperatures and easy recovery of catalyst materials, but suffered of low selectivity and clear understanding of the mechanistic aspects, vital for parameters improvement [6]. However, transition M-NPs in catalysis is fundamental as they mimic metal surface activation and catalysis at the nanoscopic scale and thus bring efficiency and selectivity to heterogeneous catalysis.

Copper nanoparticles as catalysts

Like many nanomaterials, Cu at nanometer-sized dimensions shows notable activity in various applications from material to medicine. Due to its easy availability, low cost and environmentally friendly character, Cu has received more consideration in organic synthesis. Many catalytic systems have been established in recent years, providing excellent selectivity in various copper-catalyzed organic reactions, such as Suzuki reaction [32], Heck reaction [33],

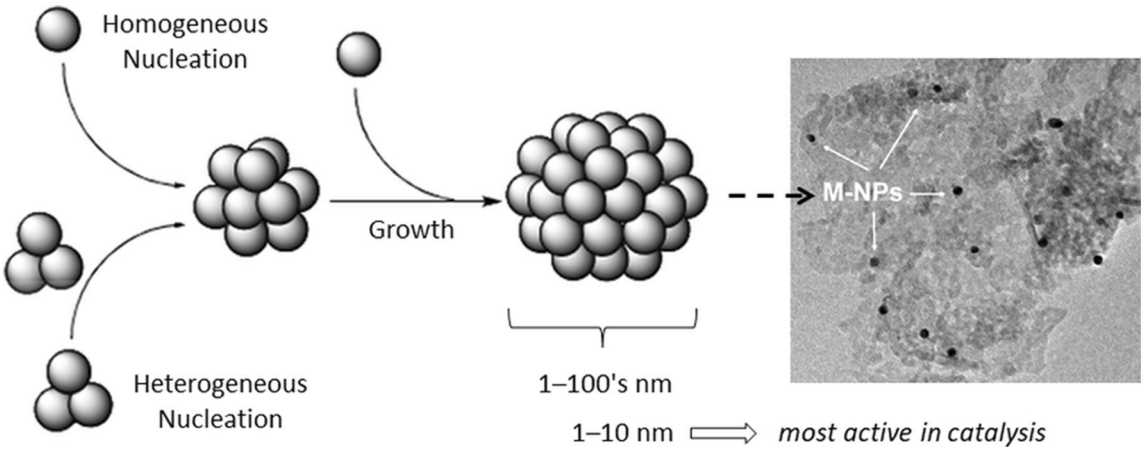

Figure 1 Nucleation and growth process of nanoparticles (spheres represent metal atoms). Adapted with permission from [28].

Click reaction [34] and oxygen arylation reaction [35] as well as many other useful reactions [5, 10, 36, 37]. We reported on the performance of copper-based catalysts in the oxidation of methylene blue [38]. An appreciable activity of 99% was obtained within 45 min of the reaction under mild conditions. Despite several merits and potential of Cu nanoparticles (Cu-NPs) as an efficient catalyst, catalysis by Cu-NPs is relatively less explored in comparison with other metals, such as Pd, Mg, Zn and Ni.

Gold nanoparticles as catalysts

The initial discovery of the catalytic efficiency of gold [39, 40] was surrounded by some confusion. It was observed by Bond and co-workers [41, 42] that very small particles of Au were active on the hydrogenation reaction. However, many reports stated that the catalytic activity observed may just be due to impurities [43]. In the last three decades, there have been a number of discoveries which demonstrate that catalysis by Au nanoparticles (Au-NPs) offers a myriad of possibilities to activate and reacting molecules [39, 40, 44–49]. Those discoveries, given the long believed chemical inertia of Au, have entirely changed researcher's perception of that metal. Au-NPs were therefore used in many catalytic systems including low-temperature CO oxidation [48], acetylene hydrochlorination [50], selective hydrogenation of nitro compounds [46] and selective oxidation of alcohols [49] along with many other important reactions [51, 52]. The performance of Au-based nanocatalysts on the liquid-phase oxidation of benzyl alcohol to benzaldehyde was investigated [53]. A good activity as well as selectivity toward benzaldehyde was obtained from the Au-based catalysts compared to the other catalysts. Nowadays, Au-NPs are not just good catalysts, but they are the best [45].

Platinum nanoparticles as catalysts

The use of platinum in catalysis presumably represents the most important application of platinum. Platinum nanoparticles (Pt-NPs) are widely used in the catalysis of many reactions, including the hydrogen evolution reaction used in fuel cells [54]. It is well known that the activity of M-NPs increases with the decrease in the particle sizes. However, a study by Tan and co-workers [55] revealed that for the hydrogen evolution reaction the catalytic activity of the Pt-NPs is unfavorably affected by size in the 1–3 nm range. That was explained by the fact that edge sites on small Pt-NPs bind too strongly to hydrogen atoms and become catalytically inactive [55]. Supported Pt-NPs are known to have good catalytic activity in many reactions, including oxidation of organic compounds [56, 57], alcohol oxidation [58], hydrogenation of biomass-derived compounds [59], NO reduction reaction [59], ethylene glycol reforming [60] and a variety of processes such as the ones used in oil refinery [61]. Recently, we have evaluated the activity of the Pt-NPs in gas-phase oxidation of ethanol [62]. It was reported that the activity of the catalysts was boosted by the immobilization of Pt-NPs on the surface of the mesoporous materials, and the immobilization of Pt-NPs favors complete oxidation to carbon oxide (CO_x).

Palladium nanoparticles as catalysts

Palladium was used earlier in catalysis for organic transformations. The use of palladium as catalyst in organic chemistry was mostly stimulated by the discovery of palladium-catalyzed oxidation of ethylene to acetaldehyde by air [63]. The Nobel Prize in Chemistry 2010 was awarded to R.F. Heck, E. Negishi and A. Suzuki for the palladium-catalyzed cross-coupling reactions, families of organic synthesis that use palladium complexes as catalysts [63]. Recently, Monfared et al. have highlighted the advance in the application of palladium nanoparticles (Pd-NPs) for Hiyama cross-coupling reactions [3]. The investigation showed that Pd-NPs were catalytically highly effective in fluoride-free Hiyama coupling reactions. The importance of the choice of the carrier was also mentioned, with carbon carrier being the most suitable. Pd-NPs have been effective catalysts for the synthesis of various compounds [64–67]. The activity of the Pd-NPs is size and shape dependent. It was revealed that very sharp shaped Pd-NPs show strong catalytic activity for the organic reactions such as Heck, Suzuki and Stille couplings [66]. In a study conducted in our group [68], Pd-NPs supported on SBA-15 typical silica material were revealed to be an efficient catalyst for Suzuki coupling. High performance in terms of turnover frequencies was obtained even under an aqueous system and fairly low temperatures.

Ruthenium nanoparticles as catalysts

Ruthenium was the last of the six platinum group metals to be discovered. Ruthenium-based nanocatalysts featured with an uncommon catalytic behavior are of great implication in many reactions [69–71]. Supported ruthenium nanoparticles (Ru-NPs) are the most widespread heterogeneous catalysts for the hydrogenation of biomass-derived compounds to a variety of attractive fuel components and value-added chemicals [69, 72, 73], with the 5%-Ru/C being the most conventional ones [72–74]. Ruthenium as a Fischer–Tropsch (FT) catalyst is of high scientific interest, as it is working at low temperature and producing high molecular weight hydrocarbons [75, 76]. Ru-NPs act as a FT catalyst as the pure metal, without any promoters. Ru-NPs as catalyst are also used for ammonia and acetic acid production [77]. A study conducted by Ndolomingo and Meijboom shows that low content of ruthenium (1 wt%) on the mesostructured metal oxide supports is highly efficient for the conversion of biomass-derived levulinic acid (LA) to an ideal sustainable liquid fuel, γ-valerolactone (GVL). The best performance (TOF > 493590) with full conversion of LA and > 95% GVL selectivity was obtained from the MnO_2- and TiO_2-based catalysts [78].

Silver nanoparticles as catalysts

Silver metal has been used in numerous technologies and incorporated into a wide range of consumer products that take advantage of their distinct physical, chemical and biological properties [79, 80]. The catalysis of silver nanoparticles (Ag-NPs) has been widely exploited, and it is of great interest in organic synthesis because of their specific reactivity, selectivity and stability in many catalytic systems. Dong and co-workers highlighted some modern advancement of Ag-NP-catalyzed organic reactions [81]. Supported Ag-NPs have been found to be effective catalysts in many reduction processes of functional molecules, including reduction of carbonyl and nitroaromatic compounds [81–83]. Various heterogeneous silver nanocatalysts have been recognized as powerful catalysts for oxidation of alcohols, silanes and olefins, and related oxidative transformations [81, 84]. In a study conducted in our group, Ag-NPs encapsulated within silica nanospheres showed auspicious results in the oxidation of benzyl alcohol [85]. Furthermore, Ag-NPs catalyzed the chemiluminescence from luminol–hydrogen peroxide system with better activity than colloidal Pt and Au [86].

Cobalt nanoparticles as catalysts

Cobalt nanoparticles (Co-NPs) possess magnetic properties that lead to applications in many areas. Stable Co-NPs are a promising class of non-noble metal nanocatalyst for organic synthesis. Several cobalt compounds are oxidation catalysts. However, over the past decade cobalt-based catalysts were widely utilized in reactions involving CO, such as in the hydrogenation of CO into liquid fuels in Fischer–Tropsch process [87–89]. A study conducted by van Deelen et al. indicates that supported cobalt particles of less than 6 nm are less stable in Fischer–Tropsch processes. In addition, it was shown that the stronger interaction between Co and TiO_2 leads to enhanced

catalyst restructuring as compared to SiO_2. Thus, cobalt particles were revealed to be more stable when deposited in SiO_2 than in TiO_2 [88]. Recently, Hertrich et al. have demonstrated the performance of specific heterogeneous Co-NPs synthesized by pyrolysis of preformed cobalt complexes deposited onto various supports in several hydroformylation reactions [90]. It was concluded that the nature of the support and the resulted in situ cobalt complex play a big role on the kinetic behavior and the rate of leaching of the catalysts. In general, the phenanthroline-derived catalysts, Co/phen@TiO_2 and Co/phen@C were shown to be stable, nonvolatile and productive in hydroformylation reactions and thus can conveniently substitute the common but unstable, volatile and toxic cobalt carbonyl complexes in hydroformylation processes. Recently, we have reported on the surface property–activity relations of Co/Sn oxide nanocatalysts evaluated in the oxidation of morin. It was revealed that the catalyst with a small percentage of Co seemed to have the highest number of acidic sites and also had the highest surface area, and thus seemed to be the most performing catalyst [91].

Ni nanoparticles as catalysts

As most of metal nanoparticles, nickel nanoparticles (Ni-NPs) have attracted much attention in many applications due to their potent catalytic activity, high stability and many other valuable properties. Ni-NPs have been recently used to accelerate the rate of CO_2 dissolution, especially under unfavorable water chemistry. The advantages of Ni-NPs as catalyst in the hydration of CO_2 are that its activity is pH independent, compared to the major catalysts such as the enzyme carbonic anhydrase and hypobromous, hypochlorous and boric acids which are effective primarily in the alkaline range [92–94]. Due to their unusual intrinsic properties, Ni-NPs have also been growing interest in organic synthesis compared to the traditional Raney nickel catalyst. Ni-NPs have been used as catalyst for functional group transformations like transfer hydrogenation of carbonyl compounds, reductive amination of aldehydes, alkylation of ketones, oxidative coupling of thiols and synthesis of tetraketones [95]. Recently, Ni-based catalyst has been one of the various catalysts used to convert syngas to methane due to its high activity and moderate cost. To minimize deactivation of the catalyst, common effect due to a build-up of carbon or sintering during this high-temperature methanation reaction, Kamata et al. reported on the development of highly active, suitable and robust Ni-based methanation catalyst, consisting of well-dispersed Ni-NPs encapsulated in mesoporous silica matrix synthesized via a two-step co-precipitation method with high Ni loading up to $\sim$ 40%. The as-synthesized catalyst has shown improved Ni sintering, coking and sulfur resistance compared to a commercial supported Ni methanation catalyst [96]. Another Ni-based methanation catalyst, Ni/La_2O_3/SiO_2, was developed by Li et al. using $LaNiO_3$ with perovskite structure as the precursor loaded on mesoporous silica by the citrate complexing method [97]. It was reported that the resultant catalyst was very stable and exhibited very high activity and high selectivity for CO methanation from syngas. The high stability of the Ni-NPs is due to the fact that Ni-NPs get close to La_2O_3 and confined by the latter which is spread on SiO_2, leading to resistance to carbon deposition, and the interaction between Ni and La_2O_3 improves its resistance to sintering. Mostly for the catalyst prepared by traditional impregnation method, Ni-NPs and La_2O_3 are separately supported on SiO_2.

Synthesis of nanoparticles

Methods of catalytically active nanoparticle (NPs) preparation are very diverse. NPs, either as colloids or supported in some way, may be prepared via different routes. Two generic approaches are usually followed for the production of NPs [98]. These are the top-down [99] and the bottom-up [100]. The former approach essentially refers to the breaking of a solid into smaller particles, while the latter ones involves the preparation of NPs as dispersions by reduction of metal salts or by sonolytic, photolytic or thermal decomposition of metal precursors in various solvents [101]. The bottom-up approach has gained popularity in the preparation of NPs as it gives better control of particle size when compared to the mechanical approach. Due to their high surface area, it is worth mentioning that dispersions of NPs are thermodynamically and intrinsically metastable [102, 103]. Moreover, to hinder sintering and aggregation surface-stabilizing agents have been used in synthesizing many nanomaterials.

Approaches for supported metal nanoparticle preparation

Because of their small size and probable solubility in reaction media, it is not always easy to separate metal nanoparticles, M-NPs, from the solution. To overcome that problem, nanoparticles, NPs, are usually anchored onto a solid support (Fig. 2). The supports are mostly in the form of oxides such as silica aerogels [104], silica spheres [105], silica microemulsions [106], hydrotalcite [107], zeolites [108] and alumina membranes [109] to mention a few. There are a large number of the studies reporting on M-NPs supported on a variety of metal oxides, which some are based on Al [110], Ti [111], Zr [112], Ca [113], Mg [114], Mn [115], Zn [116] and Co [117]. Carbon materials such as activated charcoals (ACs) and graphitic materials or nanomaterials have been also extensively used in heterogeneous catalysis as catalytic supports [118].

In fact, the activity of any metal-supported nanocatalysts depends mostly on the metal loading and its dispersion on the support, with the size of the metal particles being a key factor. Thus, the synthesis of highly dispersed metal nanocatalysts greatly depends on the preparation processes including choice of active chemicals, deposition methods of the active phase, oxidative or reductive treatments, and drying and calcination treatments. Many supported M-NPs are prepared by the succession of methods. Delmon and co-authors [119] have classified three fundamental stages for the preparation of supported M-NPs, that is, preparation of the primary solid, treatment of the primary solid producing the catalyst precursor and activation of the precursor to give the active catalyst.

Fundamental stages for the preparation of supported M-NPs

Preparation of the solid

Four main routes were classified for the preparation of the primary solid [119]: deposition, precipitation or co-precipitation, gel formation and selective removal. Experimental parameters such as aggregate morphology of the support or carrier, quantities, concentrations, stirring conditions, temperature, sequence and duration of each operation are critical for the characteristic of the solid.

(i) Deposition

Various deposition methods can be distinguished including impregnation, ion exchange and gas-phase depositions.

- Deposition by impregnation consists of contacting a solid with a liquid containing the component to be deposited [119]. The nature of both reactants (solid surface and liquid) as well as reaction conditions plays a major role on the type of product. Impregnation can be made via several methods, including impregnation by soaking [120], dry or pore volume impregnation [121], incipient wetness impregnation [121], co-impregnation [122] and successive impregnation [123]. With different rates, diverse processes take place throughout impregnation procedure including selective adsorption of species by Coulomb or van der Waals forces and ion exchange between the charged surface and the electrolyte.
- The processes of deposition by ion exchange are rather similar to those of the impregnation. It is mostly used for solid ion exchange carriers such

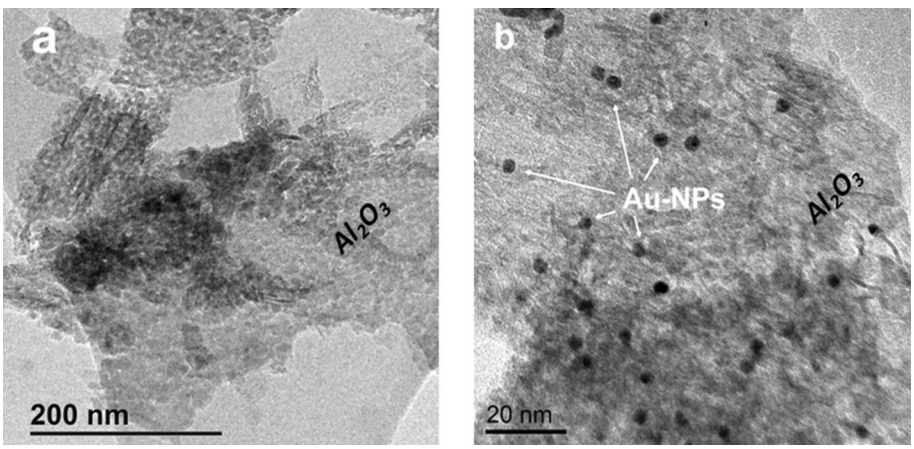

Figure 2 HRTEM images of **a** alumina, Al_2O_3 support and **b** Au-NPs supported on Al_2O_3.

as zeolites. Ion exchange can be non-selective or selective, depending on their chemical structure [124].

- Deposition by gas phase occurs through adsorption from a gas phase. The technique believed to give good dispersion of the active species and ensure very well-controlled distribution [125].

(ii) Precipitation and co-precipitation

Here, precipitation is referred to as precipitation–deposition. In this technique, active species are deposited onto carriers in suspension with an in situ formation or the addition of a precipitating agent. One of the advantages here is that the precipitation requires a lower supersaturation than formation of the novel phase directly from the liquid. Supersaturation can be controlled and maintained at a constant moderate level by a gradual addition of the precipitating agent [119, 126] or by decomposition of an appropriate substance such as urea, ammonium carbonate and sodium hydroxide, which releases the precipitating agent constantly. However, the rate and order of addition of the substances, the mixing procedure, the pH and the maturation process must be carefully controlled.

(iii) Gel formation

The process consists of solutions producing gel- or solid-like substances. The gel can be obtained by freeze drying, polymerization, complexation or addition of a gelling agent [119]. The produced gels retain all the active components from the starting solution. The diffusion is sturdily restricted, and the segregation becomes difficult [120, 127]. The solvent in the starting solution and reaction by-products are removed by evaporation or sublimation, and the gels are thereafter decomposed or further transformed to oxides.

(iv) Selective removal

The method consist of removing one component of the coarse powder alloy by leaching process using, usually NaOH as leaching agent, while leaving the active component in a relatively high dispersion form [119, 128]. The method is not commonly used, but produced important catalysts such as Raney Ni.

Treatment of intermediate solids

The treatments of the precursors or intermediate solid include drying, thermal decomposition, calcination and many other processes. The quality of the product obtained depends on many factors including equal exposition of the particles and adequate quantity of liquid or gas to the reactor [119, 128]. For the equal exposition, it is suggested that all the particles are exposed statistically to precisely very similar series of conditions, which can be ensure by the use of a moving bed (e.g., rotating furnace, fluid bed or spray drying). Very slow process results in better consistency in the distribution of a given element within the catalyst.

Activation of the precursor

The activation of the precursor to give active catalyst differs significantly from case to case. The activation rate depends on the recommendations as discussed above and on the properties of the catalyst [119]. Activation can be done through formation of sulfides (hydrodesulfurization), deammoniation (acidic zeolites) or reduction to metal (hydrogenation catalysts).

Cold plasma method for the preparation of supported M-NPs

Recently, cold plasma, using high electron temperature and low gas temperature combined with impregnation, deposition–precipitation or co-precipitation methods, has been adopted to synthesizing high-performance supported metal catalysts [129]. These catalysts usually have higher activity, selectivity and stability compared to those synthesized by conventional approaches as discussed above. The review by Di et al. revealed that cold plasma is a simple, fast, energy-efficient and eco-friendly method for fabricating heterogeneous nanocatalysts [130]. This process generally consists of calcination and reduction of the metal precursors and thus reduction of the metal ions. The catalysts synthesized by cold plasma mostly possess small and highly distributed metal particles and display enhanced metal–support interaction. Depending on the pressure utilized, this method can be classified into low-pressure (LP) or atmospheric pressure (AP) cold plasma. The former uses inert gases (Ar, etc.) as working gas and energetic electrons as reducing agents [130, 131], while the latter adopted as working gas the hydrogen-containing gases, such as H_2, CH_4 or NH_3, and as reducing agents the generated active hydrogen species [130, 132]. The reduction time can be ten times less for AP cold plasma ($\approx$ 6 min) compared to LP

cold plasma (≈ 60 min). This shows that energetic electrons are less powerful than the active hydrogen species. Lastly, AP cold plasma does not require sophisticated and high-priced vacuum systems.

Laser electrodispersion method for the preparation of supported M-NPs

Laser electrodispersion (LED) method [133] is a propitious method for synthesizing stable supported M-NPs. Here, M-NPs are fashioned and stabilized prior deposition on the support. The method consists of irradiating the metal target by a laser torch. The metal droplets from the surface of the irradiated metal are then splashed, followed by cascade fission and uniform deposition of NPs on the external surface of a support. The metal loadings are exceptionally low (< 0.01 wt%), and the size of the ultimate M-NP is regulated only by the electron work function of the metal. Various metal nanocatalysts formed by this method are immobilized on carbon material or oxide supports [134]. Their investigation revealed that the structure of active sites depends on the properties of both guest metal and host support, and consequently on the nature of the metal–support interaction (MSI) [134, 135].

Some of the features of LED catalysts are (1) the existence of very small oxide layer on the surface of individual M-NP, reducing the possibility of metal particle sintering, (2) particle sizes obtained are very small (∼ 2 nm) and stable; increasing metal loading does not affect the particle size and particle size distribution, (3) the charge state of individual M-NPs (on dielectric supports), creating the possibility of investigating the effect of charging of supported M-NPs on catalytic performance. This phenomenon is ascribed to the thermally activated tunnel charge transfer between neighboring contactless M-NPs [134].

Immobilization of ultrafine M-NPs to high-surface-area materials

The immobilization of ultrafine metal nanoparticles (UM-NPs) to high-surface-area materials is one of the auspicious routes for obtaining high-performance heterogeneous catalysts. The fusion of high-surface-area materials and nanoparticle technology leads to the formation of clean surfaced UM-NPs, which is crucial for catalytic performance [136–138]. Zhu and Xu reviewed recent progress in the preparation of UM-NPs encapsulated in various high-surface-area materials, including metal–organic frameworks (MOFs), ordered mesoporous silica and carbon materials and their applications in catalysis [136]. Due to their confined pore spaces and defined pore diameters of a few nanometers, the encapsulation of UM-NPs in these ordered porous materials inhibit particle growth to a small size regime. This prevents them to aggregate or leach during catalysis. It was reported that the use of nanoporous or two-dimensional nanolayer-structured materials for the immobilization of UM-NPs shows great advantages in catalysis with regard to nucleation control and growth of cleaned surface UM-NPs. In conclusion, high-surface-area materials, particularly with porous feature, can offer large surface and spatial confinement to disperse the UM-NPs. Their channels can interestingly serve as transfer paths for the reactants and products during catalytic reactions [139, 140].

Recently, a non-noble metal sacrificial approach has been developed for the immobilization of highly dispersed noble M-NPs on reduced graphene oxide [141]. Here, a cobalt compound ($Co_3(BO_3)_2$) co-precipitated throughout the reduction of precursors and afterward forfeited by acid etching plays an important role in immobilizing noble M-NPs and prevents them from aggregation. The AgPd-NPs prepared by this approach were revealed to be much smaller than those obtained by the direct deposition method. The resulting ultrafine AgPd nanocatalyst exhibited distinctive high activity for the dehydrogenation of formic acid. Therefore, the sacrificial approach opens up another route for the preparation of high-performance M-NP catalysts. Another approach, weakly capping growth approach, was also reported for the immobilization of UM-NPs [142]. Using this approach, with methanol (water-free) serving as a mild reductant and a weakly capping agent, well-dispersed surfactant-free Pd-NPs have been successfully immobilized on carbon nanospheres. The as-prepared Pd nanocatalysts show an unusual high catalytic activity for 100% selective dehydrogenation of formic acid under mild conditions. The catalytic properties of the prepared catalyst were somehow greatly improved by the tiny size and clean surface of the Pd-NPs. Hence, the use of this remarkably facile approach is expected to open new avenues for designing high-performance ultrafine metal nanocatalysts.

Support effects in heterogeneous catalysis

The effect of supporting nanoparticles, NPs, on various supports has many advantages. One it renders the catalyst in use purely heterogeneous. This helps in catalytic recycling and reusability studies. The effect on catalytic activity of supported NPs is mostly evident when they are supported on different types of supports. In heterogeneous catalysis, the catalysts used are mostly solids and are composed of multiple compounds, with the greatest part being the support. Catalyst supports can be either inert or active in reactions, and in some cases, they might act as a stabilizer to prevent the agglomeration of supported metal nanoparticles, M-NPs. The supports can cooperate with the metal nanoparticles to promote simultaneous and mutually beneficial reactions. Thus, the choice of the appropriate support is a topic of main importance. However, usually the support does not show any catalytic activity on its own. On this support, a catalytically active metal or metal oxide is deposited at low concentrations. The mostly used supports are alumina, silica, titania and carbon materials.

Commonly used supports for the preparation of solid catalysts

Alumina

Alumina, Al_2O_3 is among the most common materials used as a support in heterogeneous catalysis. There are two general classes of aluminas, the low-surface-area aluminas (e.g., alpha alumina, α-Al_2O_3) [143] and the highly porous aluminas (e.g., gamma alumina, γ-Al_2O_3), which are of catalytic interest [143, 144]. Due to its distinctive chemical, thermal and mechanical properties, γ-Al_2O_3 is among the most important support used for metal catalysts [143–145]. Structure and properties of γ-Al_2O_3 had been the subject of various studies [143–148]. γ-Al_2O_3 was conventionally described as a defect spinel (*Fd-3m*) with the formula $Al_{21+1/3}\square_{2+2/3}O_{32}$, where $\square$ denotes a vacancy [144]. Figure 3 shows the illustration of the first two layers in the γ-Al_2O_3 structure.

It has been reported that when γ-Al_2O_3 is derived from amorphous aluminas, it always has a defect cubic spinel structure with vacancies on part of the cation sites [148]. The aluminum ions occupy both tetrahedral and octahedral positions, but there is still dispute regarding the relative partial occupancy in each position [149].

Well-dispersed M-NPs on γ-Al_2O_3 support show a high activity in many reactions. Our studies show that stable γ-Al_2O_3-supported nanocatalysts were very active and also stable in various oxidation reactions [53, 150]. The stability and high performance of the γ-Al_2O_3-based catalysts were also reported in the conversion of ethanol into ethylene oxide [15, 151].

Silica

Silica, SiO_2 is one of the most complex and abundant families of known materials. In addition to a number of distinct crystalline forms which generally consist of tetrahedral SiO_4 units, the amorphous forms of SiO_2 are extensively used as support in catalysis. The high surface area and volume of Santa Barbara Amorphous-type material (SBA-15) and Mobil Composition of Matter (MCM-41) make them the most common types of amorphous ordered mesoporous silica mostly used as support in catalysis. That ordered mesoporous silica is mostly prepared from tetraethyl orthosilicate (TEOS) by reacting it with a template made of micellar rods [152] or by using a simple sol–gel method [153].

A study by Vunain et al. reports on the hydroformylation of 1-octene using SBA-15 and MCM-41 Rh-supported catalysts. All the catalysts showed good active in the studied reaction, with the major products being n-nonanal and 2-methyloctanal. The hexagonal pore structure of the support materials was very influential in directing the activity of the immobilized catalysts. Thus, the SBA-15-supported catalysts (pore diameter 4.0–13.6 nm) were regarded as better catalysts than the MCM-41-based catalysts (pore diameter 2.0–3.2 nm) [154].

Titania

Titanium dioxide, TiO_2 known as titania, is widely used for many applications including catalysis [111]. TiO_2 exists in three crystalline forms: anatase, rutile and brookite, with the first two forms being the most common types [111, 155]. Rutile is the most thermally stable phase of TiO_2, whereas the metastable anatase experiences a phase transition above 600 °C and converts irretrievably into the rutile phase [111, 155]. In its mesoporous structure, TiO_2 is mostly used as a

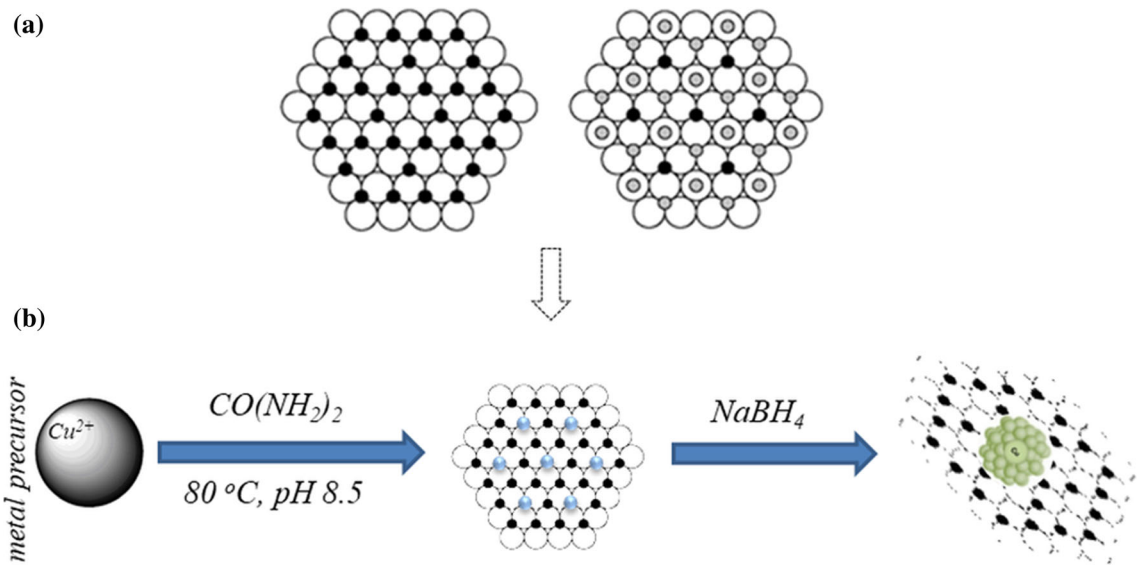

Figure 3 **a** Schematic drawing of the first two layers in the γ-Al_2O_3 structure. Reprinted with permission from [149], **b** scheme for the preparation of γ-Al_2O_3-supported Cu-NPs by deposition precipitation method using urea and sodium borohydride as precipitating and reducing agents, respectively.

support for heterogenous catalyst due to the effect of its strong metal-supported interaction (mostly with noble metals), high surface area stabilizing the catalysts and acid–base property [111]. Compared to rutile, anatase is generally used as a catalytic support because of its high specific surface area and strong interaction with M-NPs.

Ruppert et al. investigated the influence of support on the mixed TiO_2 phases supported Ru and Pt nanoparticles [156]. It was revealed that the activity of Pt increases as the surface area of the anatase phase increases, whereas the activity of Ru is enhanced by using mesoporous support as opposed to microporous support. A synergistic effect between TiO_2, MnO_2 and NiO supports and various metal nanoparticles was investigated [78]. The TiO_2-based nanocatalysts show well-dispersed and smaller particle than the MnO_2- and NiO-based catalysts.

Carbon materials

Carbon, C, the main component of coal and coke, can also be used in heterogeneous catalysis as a catalyst support. Carbon-based materials such as activated carbons (ACs) and graphitic materials are frequently used as catalyst supports due to their properties, such as tunable porosity and surface chemistry, which allow the fixing and dispersion of the active phases [118]. The development of nanostructured carbon materials with different physical forms and shape such as fullerene, carbon nanotubes (CNTs) and nanofibers (CNFs), graphene and mesoporous carbons has undergone spectacular progress. Their remarkable physical properties, such as large surface areas and good electron conductivity incorporated with the good chemical inertness, make them promising support materials for heterogeneous catalysis [157].

Hollow carbon spheres (HCS)- and carbon nanotube (CNT)-supported palladium nanoparticles were very active for the oxidation of benzyl alcohol [158]. It was revealed that both the mean size of palladium particles and supports played a key role in the selective oxidation reaction, and similar results can be obtained from both HCSs and CNTs (both with unfilled cores). Carbon-based materials are still the most practical for the preparation of supported noble metal nanocatalysts, particularly Pt-based catalyst [159].

Addition of metal oxides on supported metal nanocatalysts

Besides oxide support and the catalytically active metal, more complex catalysts contain extra components called additives to improve the efficiency of the catalyst. The role of the additive can be that of a structural promoter, a chemical promoter or a co-

catalyst [160–162]. A structural promoter modifies the structure of the catalyst; it plays a role in stabilization of the catalyst. A chemical promoter by itself has little or no catalytic effect; it improves the effectiveness of the catalyst by interacting with the active component, and a co-catalyst assists in the chemical catalytic process, and it acts along with the main catalyst by for example, providing active oxygen.

The choice of additive or combination of additives is substantial for both activity and selectivity of the catalysts [160–163]. A study on the effect of the addition of CeO_x and/or Li_2O to Cu-, Au- and Ag-supported catalysts was conducted [163]. It was shown that the addition of additive increases the performance of the catalysts. The addition of both oxides showed a greater positive effect compared to that of individual oxides added separately. That synergistic effect has been reported in several studies [164, 165]. Under oxidizing condition, Li_2O probably prevents the oxidation of the metal particles by stabilizing them, while the addition of CeO_x may result in another route of oxygen supply needed. Gluhoi et al. [163, 166, 167] reported that the addition of alkali (earth) metals to γ-Al_2O_3-supported Au catalysts plays a major role on the stabilization of the Au-NPs. Thus, alkali (earth) metals were considered as structural promoters in the investigated reactions. A positive effect of various additives, such as Rb_2O, MgO, BaO, MnO_x, CoO_x and FeO_x to Au/Al_2O_3 for various reactions, has also been reported [160, 165, 168].

Lithium oxide as additive

The promoting effect of adding Li_2O to the supported catalysts has been widely investigated. A fundamental study by Lippits and Nieuwenhuys [15, 151] on the conversion of ethanol into ethylene oxide using γ-Al_2O_3-supported Cu- and Au-NPs shows that Li_2O acts as a structural promoter. The addition of Li_2O also influences the selectivity toward the main product, ethylene oxide. It was shown by de Miguel et al. [169] that Li_2O also has a poisoning effect on the strong acidic sites of the γ-Al_2O_3 and, therefore, can influence the selectivity of the catalyst. Thus, the promoting effect of Li_2O as structural promoter may be twofold. Primo, Li_2O sways the size and shape, and therefore the active sites of the M-NPs, and secondo, it suppress the activity of the support by influencing the acidic sites of the Al_2O_3. Along these lines, it favors the reaction pathway in which the M-NPs are involved.

Ceria as additive

A study by Lippits and co-authors [170] shows that CeO_x acts as a co-catalyst next to the deposited metal particles and results in an increase in the activity of the catalyst. In another study, it was shown that under strongly reducing conditions the addition of CeO_x on the Cu-, Ag- and Au-based catalysts has a positive effect on the oxidation of CO on all three metals. However, in the presence of a small amount of hydrogen a positive effect is observed for Au catalysts and a negative one is observed for Cu and Ag catalysts [163]. Thus, under strongly reducing conditions CeO_x can provide the oxygen for an oxidation, but can also contribute to the oxidation of some M-NPs in a more oxidative environment.

Magnesium, barium, manganese, iron and cobalt oxides as additives

The role of MO_x as additive in various catalytic systems was thoroughly investigated in the past decade. Studies by Nieuwenhuys and co-workers [160, 165, 171] show that MgO and BaO act as structural promoters, as their presence empowers the preparation of small, highly dispersed and stable Au particles on γ-Al_2O_3 and, in this manner, improves both low-temperature CO and H_2 oxidation by O_2 compared to Au/Al_2O_3. While the alkaline earth metal oxides prevents small particles from sintering, the addition of MnO_x, FeO_x or CoO_x to Au/Al_2O_3 implements new routes for supplying active oxygen, e.g., via lattice oxygen. Thus, the transition metal oxides act as co-catalysts in that catalytic system [160, 171].

Perovskite-type oxides as support, catalysts or catalyst precursors

$$t = \frac{r_A + r_X}{\sqrt{2}\,(r_B + r_X)} \tag{1}$$

Perovskite-type oxides (PTOs) are mixed oxides with the general formula of ABO_3, with positions A generally occupied by group I, group II or other large metal ions, and B by transition metal ions of either group 3*d*, 4*d* or 5*d*. The O is nothing other than

oxygen atom [172]. The structural stability of the perovskite is preserved as long as the Goldschmidt tolerance factor (t), as defined in the equation below, lies between 0.8 and 1, where r_A, r_B and r_X are the ionic radii of A, B and oxygen, respectively.

Due to their nature as bimetallic containing transition metals which are abundant, cheap and affective, these PTOs have therefore gained strong interest for application in heterogeneous catalysis. The properties of the PTOs can somehow be adjusted by a partial substitution of A and/or B by other cations, resulting in a general formula of $A_{1-y}A'_yBO_3$, $AB_{1-x}B'_xO_3$ or $A_{1-y}A'_yB_{1-x}B'_xO_3$, which may have a distinctive effect on the catalytic performance [172].

Perovskite-type oxides were mostly used as catalysts or catalyst supports for various systems in heterogeneous catalysis [172–174]. As for most of the oxides, the performance of pure PTOs when utilized as catalysts is lower than when M-NPs are immobilized on them. Recently, PTOs have also been used as catalyst precursors to prepare supported metal catalysts [172, 175]. It was shown that after reducing the metallic ions in the B positions, a number of non-substituted PTOs become active, resulting in PTOs in the form of B/AO_δ. The number δ depends on the valence state of the respective A ion. It was also revealed that the B/AO_δ catalysts could produce small and highly dispersed B-NPs compared to the traditional impregnation method. The choice of PTOs as catalyst precursors is based on their structural arrangement. The B cations are confined in a crystallite and mixed homogeneously at the atomic level. Thus, after reduction the metallic ions/atoms tend to be in interaction, and the reduced active metal would be highly dispersed.

Supporting oxides: nature, surfaces and nanostructuring

Most of the supports used in heterogeneous catalysis are in the oxide form. Over a long period, oxide was mainly regarded as an inert support to disperse and immobilize the M-NPs. Nowadays, various studies have shown that the interaction between the host oxide and the guest metal aggregate may result in significant changes in the properties of the catalyst and hence its activity. Therefore, researcher's perception on the role of oxide support in catalysis has been entirely changed. The complexity of the oxide surface is reflected by the complexity of the interaction of the support with the guest metal. Depending on whether the interaction involves mostly the cations, the surface anions or both, the same metal may behave otherwise. The chemical bonds at the interface of the metal/oxide are in some cases weak and subjugated by dispersion forces and polarization effects. But generally, new chemical bonds are formed when metal and oxide orbitals are mixed [176, 177].

From a chemical perspective, oxides can be categorized into reducible and non-reducible oxides. The binding properties of the two categories of oxides are totally dissimilar, particularly when one permits charge transfer phenomena at the interface of metal/oxide [176]. In the latter category, the oxidation states of the metal ions do not easily change. Simple binary oxides, such as Al_2O_3, SiO_2, ZrO_2, MgO and CaO, belong to this group and are typically wide-band-gap insulators (with a width of 5–9 eV). Their conduction band is consisting basically of empty ns–np cation levels, while their valence band is mostly made of O $2p$ orbitals. A common feature of these oxides is that the top of the valence band, which is deep in energy, lays several eV below the vacuum level. That associated with a conduction band which is sufficiently high in energy, close to the vacuum level. The chemical inertness of this category of oxides is due to a deep position of the valence band which does not permit the extraction of electrons from the $2p$ levels of the O^{2-} ions, and also the high location of the conduction band limits the transfer of the electronic charge. In the former category, metal cation can adopt various oxidation states and show rich redox chemistry. This category includes transition metal and rare earth oxides (e.g., TiO_2, CeO_2, WO_3, etc.). The ionic character in these oxides is usually less pronounced than in the simple oxides. Thus, the O anions have still exiguous oxidizing power, as they are not fully reduced. Reducible oxides can therefore definitely accept electronic charge from a donor species, resulting in the change of the formal oxidation state of the metal cations from M^{n+} to $M^{(n-1)+}$ by trapping excess electrons in localized d or f orbitals. Here, the top of the O $2p$ valence band occupies a higher position, whereas the position of the bottom of the conduction band is lower in energy. This results in a higher reactivity of these oxides [176].

Metal–organic frameworks as support, catalyst precursors or templates

Due to their several distinctive properties, such as high porosity, diverse composition, tunable pore structure and versatile functionality, metal–organic frameworks (MOFs) have arisen as a propitious class of materials in the field of heterogeneous catalysis. MOFs are a subclass of coordination polymers constructed by inorganic nodes (metal clusters and/or ions) with organic ligands, with the special feature that they are porous with strong metal–ligand interactions [178–181]. The microporous structures of MOFs show apparent surface areas of up to 5900 m^2/g, specific pore volumes of up to 2 cm^3/g and a variety of pore sizes and topologies [178]. The synthesis of MOFs is generally carried out by mixing two solutions containing the metal and the organic component, either at room temperature or under aqueous solvothermal conditions. As inorganic nodes, a large variety of metal atoms, including alkaline, alkaline earth, transition and main group metals (in their stable oxidation states), as well as rare earth elements have been effectively used, whereas rigid molecules (i.e., conjugated aromatic systems), including aromatic polycarboxylic molecules, polyazaheterocycles and bipyridines and their derivatives are mostly used as organic components [178]. Rigid molecules are mostly preferred than the floppy ones since they favor the formation of more stable crystalline porous MOFs [182].

MOFs have been demonstrated to serve as a useful platform for the design of supported active nanocatalysts. It is well known that the use of MOFs as catalysts is restricted by their relatively limited chemical and thermal stability [178, 179]. Hence, to satisfy the practical applications of MOFs, three main approaches have been proposed to further enhance their catalytic properties [179, 183–185] through functionalizing the MOF backbone (inorganic nodes or organic linkers) [186], integrating MOFs with functional materials to MOF composites [179] and converting MOFs to functional materials [187]. It was reported by Chen and co-workers that in MOF composites/hybrids, functional materials (e.g., M-NPs, quantum dots, polyoxometalates, molecular species, enzymes, silica and polymers) can cooperatively work with MOFs to show enhanced activity, selectivity and stability in a broad range of catalytic processes [179, 188]. In MOF composites/hybrids, new physical and chemical properties can be elicited by the synergistic effect. Consequently, the remarkable features of MOF composites make them suitable for catalytic applications. Two scenarios are possible when integrating MOFs with functional materials (1) encapsulating guest functional materials in the pores, matrices or layers of MOFs or (2) encapsulating/coating MOFs in/with functional supports/layers. In the former case, MOFs act as porous supports to accommodate functional materials such as M-NPs preventing their leaching and aggregation, whereas in the latter case, functional materials such as carbon and silica can act as shelters to enhance the chemical stability and mechanical strength of MOFs [179, 188, 189].

As a new class of porous materials, MOFs were revealed to be suitable supports for M-NPs [179, 190]. For the synthesis of MOF@M-NP composite, three well-developed methodologies, namely ship-in-bottle, bottle-around-ship and one-pot synthesis [179], enabled the fabrication of monometallic NPs, bimetallic alloy NPs, bimetallic core–shell NPs and polyhedral metal nanocrystals with controlled locations, compositions and shapes within MOFs. However, due to the inherent microstructure of MOFs, it is difficult to fully introduce metal precursors into the pores of host frameworks, causing the deposition of M-NPs on the external surface of MOFs with low stability. To circumvent the challenge, Xu and co-workers developed a double-solvent method to successfully introduce M-NPs inside the pores of the MOFs, without aggregation of M-NPs on their outer surfaces [140, 179, 181]. Hence, ultrafine Pt-NPs were effectively immobilized within the pores of a chromium-based MOF designated as MIL-101. The imaging methods clearly revealed the uniform three-dimensional distributions of the Pt-NPs all over the interior cavities of MOF. The resulting Pt@MOF composites exhibit great performances in gas-phase CO oxidation, liquid-phase ammonia borane hydrolysis and solid-phase ammonia borane thermal dehydrogenation [140]. Double-solvent method combined with a liquid-phase concentration-controlled reduction approach was also used to encapsulate AuNi alloy NPs into MOF [181]. The obtained highly dispersed AuNi-NPs show great performance in the catalysis of hydrolytic dehydrogenation of ammonia borane. For an effective immobilization of ultrafine AuNi-NPs into the MOF nanopores, an overwhelming reduction approach (excess added

reductant) is needed. In contrast, if a modest reduction approach is employed, a severe agglomeration can occur. The double-solvent approach as developed and used here is based on the hydrophilic solvent, water containing the metal precursor (volume water equal to or less than the pore volume of the adsorbent), to be absorbed within the hydrophilic adsorbent pores and the hydrophobic solvent, hexane (in excess) facilitating the impregnation process, by suspending the adsorbent. This method could facilitate the entry of the entire aqueous metal phase into the hydrophilic pores of MOF by capillary force, then minimizing the deposition on the external surface [140, 179, 181]. These results opened up new windows in the development of high-performance supported catalysts by utilizing functionalized cavities of MOFs as hosts especially for the ultrafine non-noble M-NPs. The synthesis of transition M-NPs with a three-layered core–shell structure immobilized by MOF as a cooperative catalyst was also reported [191]. By a double-solvent approach, a Cu, Co and Ni mixed precursor was sensibly introduced into a hydrophilic MOF under moderate conditions. The metal ions were successively in situ reduced with NH_3BH_3 to form tiny Cu@Co@Ni-NPs ($\sim$ 3.3 nm) within MOF pores. The as-synthesized core–shell NPs contain Cu core, Co middle shell and Ni outer shell immobilized by MIL-101. Interestingly, the resultant quadruple-layered Cu@Co@Ni/MOF catalyst exhibited high catalytic performance than most precious metal catalysts for the tandem catalysis of nitroarene reduction by the hydrogen from NH_3BH_3 hydrolysis and CO oxidation.

Though M-NPs stabilized by MOFs have been intensively investigated, determining the specific location of M-NPs relative to MOF particles remains challenging. The assertion for M-NP location into MOF structure are generally based on the sizes of M-NPs and MOF pores, where M-NPs of small sizes than MOF pores are believed to be lodged inside MOFs cavities. Another evidence used is the size-selective catalysis [192, 193], where small substrate shows high conversion, whereas large substrate cannot access the M-NPs inside a MOF and thus not converted. Although facile and usually correct, these methods do not definitely reflect the real situation. Recently, Chen and co-authors have reported on suitable techniques, including high-angle annular dark-field STEM tomography, positron annihilation spectroscopy and hyperpolarized ^{129}Xe NMR spectroscopy, for determining the specific position of M-NPs relative to the MOF particles [194]. Thus, the specific position of M-NPs relative to MOF particles can be definitely localized.

The structural diversity of MOFs has also shown high potential for synthesizing MOF-derived functional materials [187, 195]. MOFs have been utilized as precursors/templates to synthesize M-NPs supported on resulted carbon [196] and metal oxide [197] materials, to mention a few. As template, the permanent nanoscaled cavities and open channels of MOFs offer congenital conditions for small molecules to access. The first attempt on the use of MOFs as templates for preparing nanoporous carbon was reported by Liu et al. [196]. That resulted in the formation of high-specific-surface-area nanoporous carbon, which exhibits important hydrogen uptake as well as excellent performance as an electrode material for a double-layered capacitor. Therefore, the MOF-templated strategy provides a promising way to prepare a variety of nanostructural materials. As a precursor, MOF was used for the first time for the synthesis of platinum-supporting zinc oxide NPs [197]. Taking advantage of the intrinsic metal oxide subunits and pores in MOFs, nanocrystalline ZnO-supported Pt-NPs were prepared by introducing a platinum salt into the pores of MOF ($[Zn_4O(1,4\text{-benzenedicarboxylate})]_3$) followed by heating. By varying the concentration of platinum precursor, the sizes of Pt-NPs can be tuned, and the as-prepared Pt/ZnO nanocatalysts exhibited higher performance for CO oxidation than the conventional Pt/ZnO catalyst.

Metal–support interactions in the design of heterogeneous catalysts

It has been demonstrated that the catalytic properties of the heterogeneous catalysts can be tuned using great variety of metal–support interaction (MSI) types [134, 198]. The variety of such interaction depends on the composition of the specific system and can be classified from very weak (physical adsorption) to very strong (formation of new surface compounds). Depending on the nature of the MSI, the interaction of M-NPs with a support mostly provides completely new properties [134, 198, 199].

Many researchers believe that MSI plays a role in the change in the electronic state of the active metal [134, 200–203]. As an illustration, the high

performance of Pd-based catalysts for hydrodechlorination reactions was associated with the existence of Pd in several oxidation states. In this regard, the mechanism proposed by Gómez-Sainero et al. shows that the R–Cl activation occurs on Pd^{n+} to form [Pd^{n+}–Cl] molecular bond, Pd^0 coordinates R^+ ion by a dative covalent bond, and finally, the activated chemisorbed H_2 reacts with [Pd^{n+}–Cl] and R^+ to form HCl and RH, respectively [134, 202]. Thus, the electron-deficient form of palladium (Pd^{n+}) was obtained from the formation of strong MSI [134, 204].

It was mostly observed that incorporating metal ions into the support structure causes the changes in the electronic state of the guest metal. Usually, MSI leads to the formation of spinel mixed oxides on the catalyst surface, thus resulting in the formation of partially oxidized metal [134, 205, 206]. This phenomenon is clearly explained in the MSI in Ni/Al_2O_3 system in the review by Lokteva and Golubina, where the formation of spinel was generally considered to tune Ni particle size and reduction ability [134]. The incorporation of nickel ions into alumina support leads to the formation of surface nickel aluminate-like species. Firstly, the Ni^{2+} ions in the octahedral positions are replaced by Al^{3+} ions without remarkable distortion of the structure. However, a concurrent creation of cation vacancies generates a structure called substituted nickel oxide. At higher level of substitution, a number of the Al^{3+} ions occupy tetrahedral positions to form an intermediate highly disordered spinel oxide in the locations where NiO contacts with Al_2O_3. The strong binding of nickel with γ-Al_2O_3 is mostly due to the incorporation of Ni^{2+} ions into the tetrahedral vacancies. However, due to a limited number of tetrahedral vacancies in κ-Al_2O_3, nickel only weakly interacts with this support. It was concluded in a liquid-phase catalytic hydrogenation of isoprene that Ni/γ-Al_2O_3 with strong MSI shows excellent performance due to a higher number of hydrogenation sites, resistant to carbon deposition, while the Ni/κ-Al_2O_3 counterpart experiences significant coking due to the presence of hydrogenolytic sites.

In case where preliminary reduced M-NPs are deposited, the effect of MSI on the properties of the catalysts depends on the deposition method used. For laser electrodispersion (LED) technique, the nature of the MSI depends on the nature of the supported metal; as an example, Au or Pd supported on Al_2O_3 by LED technique does not show any indications of their oxidation. However, strong MSI does exist between Al_2O_3 and Ni-NPs deposited by LED method. In catalytic systems obtained by the traditional methods, chemical MSI plays a major role on the properties of the catalysts despite the nature of the supported metal [134, 207].

Computational studies on supported nanoparticles

Over the past decades when the novelty of properties of nanoparticles emerged, there was special emphasis on precise determination of the size of the nanoparticles. In particular, catalytic activity of both unsupported and supported nanoparticles is seen to have a direct relationship with nanoparticle size. In the literature, many researches groups have reported increased activity with the decrease in nanoparticle sizes [208, 209]. This is mainly attributed to increased surface area of the nanoparticles. Although a handful of publications report the contrary [210, 211], it is these few reports that open a window for extensive characterization of the surface of the nanoparticles supported on various supports through the use of computational chemistry.

Among different computational models used, DFT calculations have proved to be the most used and effective in elucidating important aspects of the surfaces atoms. It was recently used as a complementary technique to study surface energy profile of palladium nanoparticles supported on porous hyperlinked polystyrene. Using one-by-one atom addition, Prestianni et al. found that the geometry and energy profiles are strongly influenced by counterbalance between Pd–phenyl and Pd–Pd interactions [210]. They stated that these different interactions are governed by sizes or to be precise atom count. With certain number of atoms, a specific energy profile exists and immediately one atom is added the whole picture changes. Similar work was performed by Zhang et al. using ceria to support gold nanoparticles, identifying different packings, fcc and hcp, with similar energy profiles [212, 213]. Furthermore, the nature of interaction between the gold atoms and the support, through the oxygen species of the support, was revealed to be of a positive nature regardless of the number of gold atoms added.

The review by Tosoni et al. placed more emphasis on gold supported on metal oxides for use in

heterogeneous catalysis [214]. Their review highlights in particular the dependency of the structural geometry of the gold nanoparticles to the number of gold atoms [214, 215]. Planar structures were reported for Au clusters with seven or less atoms based on DFT calculations, while those having eight or more assumed 3-D structures. In cases of catalytic interest, the oxidation state of nanoclusters becomes a priority as activity can be governed by the electronic properties [214]. On the surfaces of oxide supports, the nature of interactions leads to different states of the immobilized metallic atoms. The possibility of electron transfer onto the surface of the metal of the nanocluster or oxidation of the nanocluster all alters the surface and geometric properties of the nanoparticles [212]. To unveil such information, the DFT calculation took center stage in determining the electronic band gaps and charge transfer between nanoparticles and oxide supports.

The information gained through the use of computational chemistry is of great importance for determining the sources of activity and for fine-tuning the development of supported nanoparticle catalysts with high activity for various reactions. However, there is a need to develop advance computational techniques for precise estimations of reactive sites and related energies of nanoparticle-supported interfaces.

Stabilization of metal nanoparticles

Metal nanoparticles, M-NPs, with defined sizes can be tailored through the preparation conditions such as temperature, solvent, pressure and the choice of support or stabilizing agent [216, 217]. The stabilization of M-NPs prevents agglomeration, the thermodynamically favored process that leads to the formation of the bulk metal due to Ostwald ripening [218, 219].

Metal nanoparticles: Ostwald ripening principles

The smaller the nanoparticle, the larger the fraction of exposed surface atoms. Nevertheless, the kinetically stable small NPs can easily aggregate to form larger particles (Fig. 4). The formation of larger particles is governed by the principles of the Ostwald ripening [218, 219]. Thus, thermodynamically more stable larger particles are more energetically favored than smaller ones. With their lower surface-to-volume ratio, the agglomerated particles present a lower energy state with a lower surface energy [220]. The system lowers its overall energy by releasing atoms from the surface of a small particle which diffuse through solution and then attach to the larger particle surface.

Thus, to avoid the agglomeration, small M-NPs require stabilizers to build up a protective layer. The stabilization of NPs during their synthesis can be through ligands, polymers, surfactants or ionic liquids (ILs) [49, 216, 221–224]. Bilayers of surfactant ions lead to an electrostatic stabilization. Ligands or polymers build a protective layer that provides steric coverage to prevent agglomeration [216, 225, 226]. This surface coverage means at least partial deactivation of the M-NPs. On the other hand, the steric (electrosteric) and electrostatic properties of ILs can stabilize M-NPs without additional protective ligands [103, 216, 227, 228].

Ionic liquids as stabilizing agents

Ionic liquids (ILs) are liquid "molten" salts of weakly coordinating cations and anions. They are liquids below 100 °C with high ionic mobility and possess relatively low viscosity [216, 229–231]. Typical cations for ILs are 1-alkyl-3-methylimidazolium and tetraalkylammonium cations, and typical ILs anions are halide anions, hexafluorophosphate (PF_6^-), tetrafluoroborate (BF_4^-), trifluoromethanesulfonate (TfO^-) and bis(trifluoromethylsulfonyl)amide (Tf_2N^-) [216, 224, 232]. The intrinsic "nanostructure" of ILs is caused by electrostatic, hydrogen bonding and van der Waals interactions [216, 229]. Due to their inherent ionic nature, one might expect that ILs can effectively provide a flexible and opportune liquid platform for the synthesis of defined stable metal nanoparticles [103].

The monomeric unit of the structures of 1,3-dialkylimidazolium-based ILs consist of one cation enclosed by at least three anions, and sequentially, each anion is enclosed by at least three cations [103, 216] (Fig. 5a). The inclusion of M-NPs in the ILs network supplies the necessary steric and electrostatic stabilization through the formation of an ion layer around the M-NPs (Fig. 5b). The IL structures provide hydrophilic or hydrophobic regions and a high directional polarizability, which can be

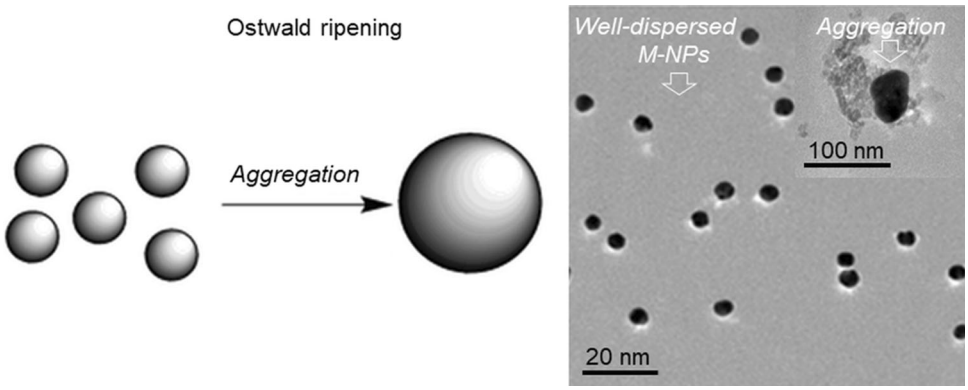

Figure 4 (Left) Schematic presentations of the Ostwald ripening of M-NPs. Adapted with permission from [216], (right) images of well-dispersed M-NPs and their agglomeration.

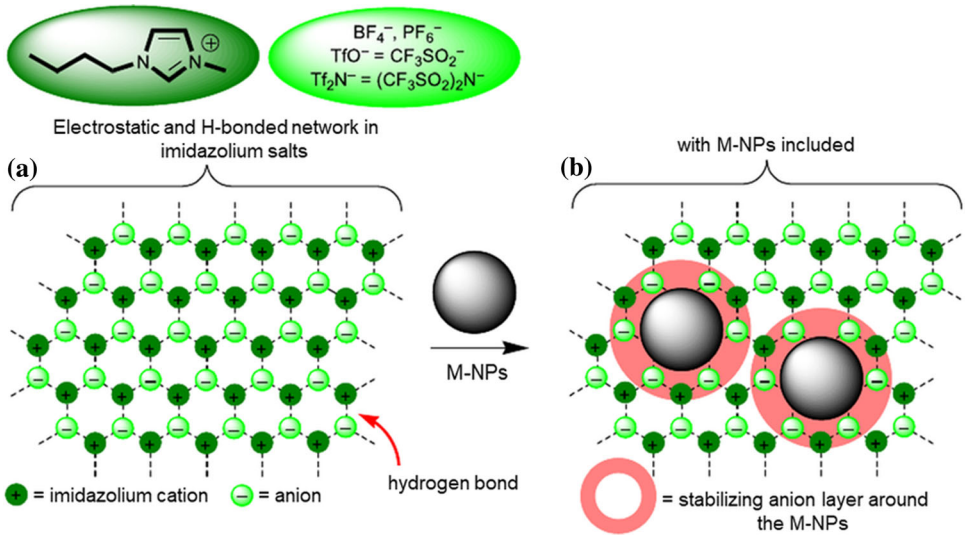

Figure 5 **a** Schematic network structure in 1,3-dialkylimidazolium-based ILs projected in two dimensions and **b** inclusion of M-NPs in the supramolecular IL network. Reprinted with permission from [216].

perpendicularly or parallelly oriented to the included M-NPs; thus, they can adapt to or are adaptable by many species [103].

Studies conducted by ourselves highlighted the role of ILs, especially 1-butyl-3-methylimidazolium hexafluorophosphate and 1-butyl-3-methylimidazolium tetrafluoroborate on the synthesis and stabilization of supported Au- and Cu-NPs. It was shown that the use of ILs resulted in the formation of small ($\leq$ 3.5 nm), stable and reusable nanocatalysts [150, 233]. A series of poly(ionic liquids), PILs materials were also considered as "smart" stabilizer for various M-NPs [234–236]. These PILs can act as M-NP stabilizers, size controllers as well as carriers in reversible phase transfer. The sizes of the M-NPs could be tuned depending on the length of the alkyl chains of PILs, as the size of the alkyl group increases with the increase in the size of M-NPs. The synthesized stable M-NPs using PILs were revealed to be reusable several times and showed good catalytic activity for various reactions.

Dendrimers (polymer) as stabilizing agents

Recently, three-dimensional polymeric material has been used as stabilizing agents for a wide range of transition metals such as Cu, Ru, Pd, Au, Pt and Ag. The 3-D polymeric materials are called dendrimers [237]. Dendrimers consist of the core, the branching groups and the terminal groups. They are capable of hosting a range of transition M-NPs inside their framework [238, 239]. In the process of hosting NPs, as in the concept of dendrimer-encapsulated nanoparticles (DENs), they stabilize NPs by steric effect and minimal ligation effect. The advantage of using dendrimers as stabilizers is the fact that there is minimal passivation of the surface atoms by the interior amide groups. In this concept, mainly the polyamidoamine (PAMAM) dendrimers are widely

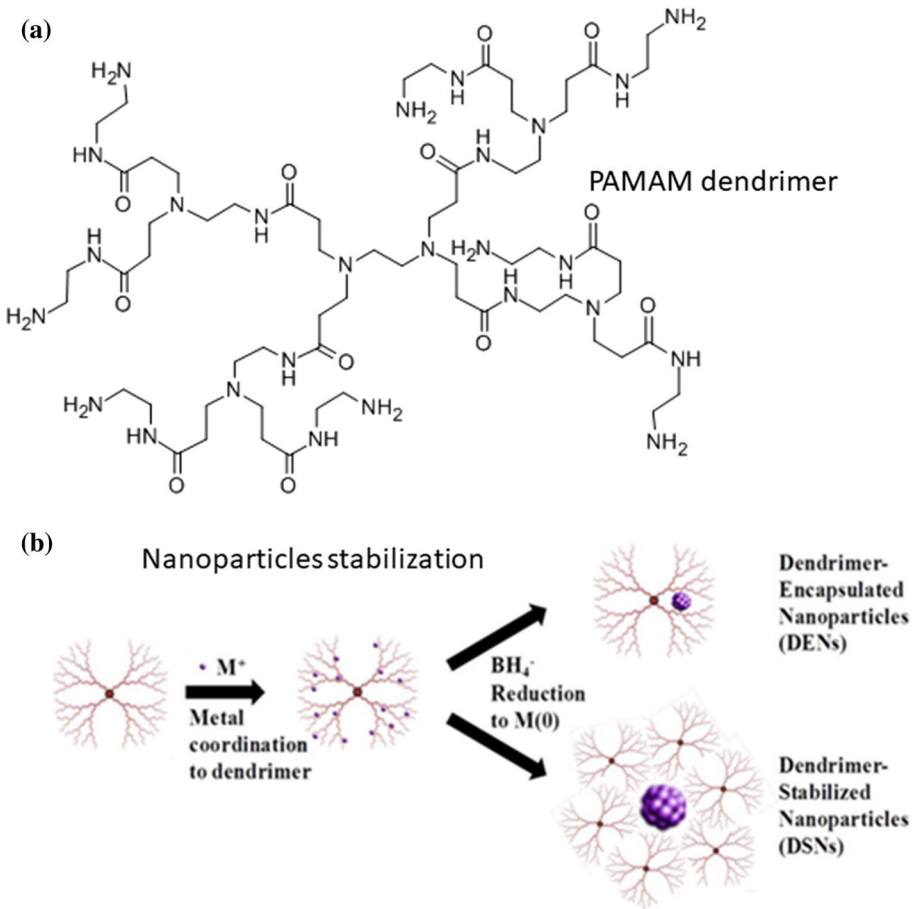

Figure 6 **a** Structure of commercially available PAMAM dendrimer and **b** synthesis and stabilization of transition M-NPs by dendrimers. Reprinted with permission from [241].

used because they are commercially available. In addition to that, the availability of an intermediate donor atom in the form of nitrogen helps during the synthesis of these encapsulated nanoparticles. Nitrogen is capable of binding to both soft and hard Lewis acids. However, since the structure of PAMAM dendrimers has terminal groups, which are sometimes amines, they sometimes form dendrimer-stabilized nanoparticles (DSNs) instead of dendrimer-encapsulated nanoparticles [240]. The principal difference is that in this case the terminal groups are responsible for stabilization of the M-NPs. Figure 6 shows the synthesis and stabilization of M-NPs by dendrimers. Usually, the NPs synthesized using this approach have sizes below 10 nm in diameter [209, 240].

Ligands as stabilizing agents

The use of ligands as M-NP stabilizers is of great interest as it focuses on the precise molecular definition of the catalytic materials [6]. Ligands build a protective layer around the M-NPs that provides steric coverage to prevent aggregation (Fig. 7) [6, 216, 242]. This surface coverage leads to a small change of metal surface properties, which means at least partial deactivation of the M-NPs.

Many ligands have been reported for the synthesis of M-NPs, including thiols, diphosphines, diphosphites, amines and 4-(3-phenylpropyl)pyridine ligands [243]. While the former three ligands exhibited strong interactions with the metal surface, amines showed a different behavior and led to a dynamic ligand exchange. However, the latter simple ligand displayed an unforeseen mode of stabilization with π-coordination of the arene groups at the particle surface. Bronger et al. reported on the use of a novel family of functionalized ligands for the synthesis of Ru-NPs [243]. The multiple donor coordination site-type ligands, *N*-phosphanylamidines $R_2''N–C(R') = N–P(X)R_2$, with X = lone pair (BH_3) were then used for the first time for the stabilization of Ru-NPs. The multiple donor sites of these ligands are directly connected to one another by forming a true electronic

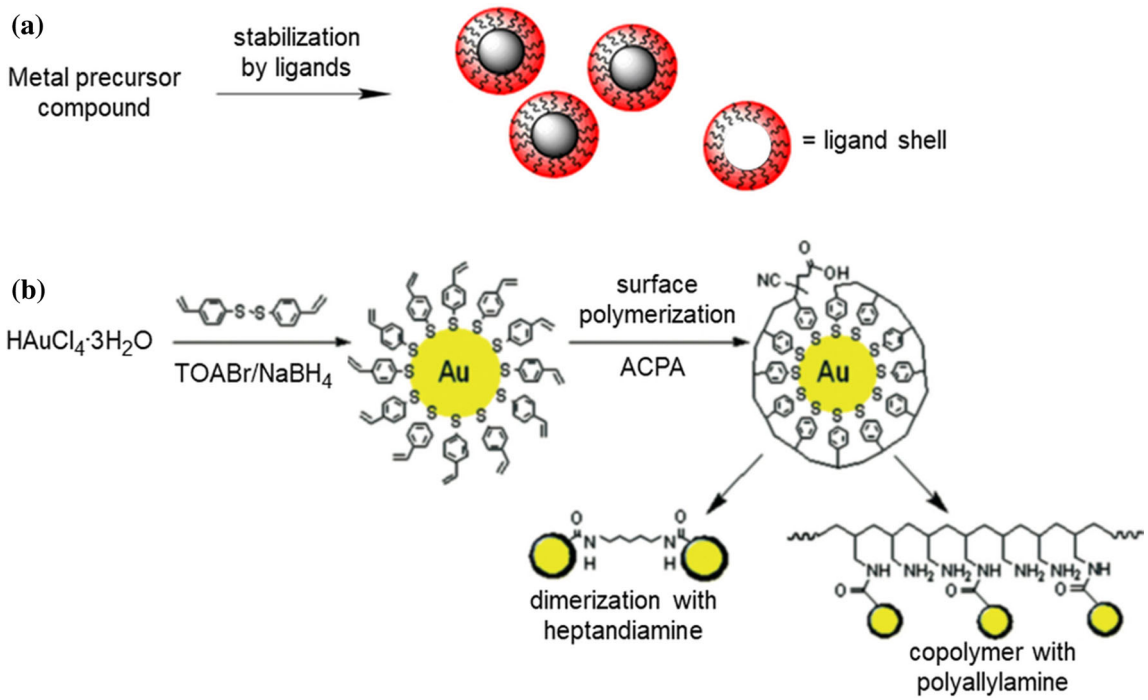

Figure 7 Schematic presentations of **a** the stabilization of M-NPs through protective ligands. Adapted with permission from [216], **b** in situ grafting and polymerization of 2-bis(4-vinylphenyl)disulfide ligand on Au-NPs. With $NaBH_4$ and TOABr being stabilizing and phase transfer agents, respectively, and ACPA the polymerization initiator. Reprinted with permission from [242].

string. These ligands lead to the formation of small Ru-NPs (1.7–3.1 nm) that display narrow size distributions and a hexagonal close packed crystalline structure of ruthenium bulk. Another class of ligands as stabilizer has been investigated by Jadhav et al. [244]. Polymerizable ligands as called are another promising class of stabilizer due to their high surface coverage, possibility to make structural modifications and ability to modify the properties of underlying NPs. It was reported that the use of 2-bis(4-vinylphenyl)disulfide as polymerizable capping ligand for the synthesis of Au-NPs has resulted in the formation of small Au-NPs (2–5 nm in diameter), with well-organized monolayers of 2-bis(4-vinylphenyl)disulfide on the particle surface (Fig. 7) [242, 244].

Determination of the surface area and particle sizes of metal nanoparticles

The interesting unforeseen properties of M-NPs are mainly attributable to their surface. The smaller the nanoparticles, the larger the surface area that provide better dispersion of the active sites and easy diffusion of the reactants [6].

Methods for determining M-NP sizes are very diverse. Current methods for the determination of the sizes of the NPs either as colloids or supported can be divided into many categories including the light scattering methods (e.g., DLS [245] and SAXS [246]), the microscopy method (e.g., TEM [247] and SEM [248]), the localized surface plasmon resonance, LSPR method [249] and the electrospray–differential mobility analysis (ES–DMA) [250]. While microscopy method allows direct NP visualization, the measurement requires sophisticated equipment, tedious sample preparation and often subjective data analysis. The results here are statistically less representative, since only a small population of the NPs is investigated [251]. Unlike imaging-based methods, light scattering and LSPR-based methods which benefit from their ability to probe the M-NPs in solution (eliminating the tedious sample preparation) suffer from poor accuracy [245] and limitations [252], especially for NPs smaller than 35 nm in diameter. Although ES–DMA can accurately measure NPs of

less than 5 nm in diameter, the method requires expensive instrumentation [250].

However, compared to the particle sizes determination, quantification of the M-NP surface area is much more challenging. M-NPs are hardly perfectly spherical or monodispersed, as evident from the imaging methods. They are typically polycrystalline containing diverse crystal facets with junctions, vertices and defects [253, 254]. This can have significant impact on the estimation of the NP surface areas [255]. Surface area of samples of uniform composition can be estimated by BET, a measurement based on the adsorption of a probe gas (usually N_2) onto a solid surface [256, 257]. Although mostly used, this technique does not allow the distinction between the supporting material and the catalytic active species. Generally, specific surface area and the size of supported M-NPs are determined by chemisorption with H_2, O_2 or CO as probe molecules [258–260]. Nevertheless, those methods require expensive instrumentations and are limited by the properties of the support. Thus, chemisorption methods, using organothiols as probe molecules, are theoretically appropriate for the determination of the specific surface area of supported M-NPs [150, 233, 253, 261, 262]. The method, therefore, does not require dedicated and expensive equipment, and tedious sample preparation.

Ligand adsorption methods and approach

Usually long-chained and heterocyclic compounds containing S are used and adsorb on all metal surface atoms [253, 255, 261]. Organothiols strongly and specifically adsorb on the surface of the metals and thus form self-assembling monolayers (SAMs) [263–265]. The basic principle underlying these methods is to suspend under ambient condition a known amount of M-NPs in a known amount of probe ligand [150, 233, 253, 255, 266]. It was reported by Folkers et al. [267] that when thiols are exposed to oxidic supports, no adsorption is observed, except for CuO and AgO. Various studies reported on the supported M-NP surface area determination using organothiol as probe molecules. It was shown that the surface areas of supported M-NPs as determined by organothiol adsorption method are in agreement with those calculated on the basis of the theoretical models and characterization [150, 233, 253, 255, 261, 262]. Table 1 shows some examples.

Supported metal nanoparticles as heterogeneous catalysts

Liquid-/gas-phase oxidation with supported nanocatalysts

The use of supported M-NPs together with green oxidants such as molecular oxygen (O_2), hydrogen peroxide (H_2O_2) and *tert*-butyl hydroperoxide (TBHP) instead of stoichiometric oxidizing reagents represents a desirable approach for the selective

Table 1 Metal surface area and particle size of M-NPs determined by TEM, H_2 and thiol chemisorption methods

Catalyst	TEM		H_2		2-MBI		References
	Particle size (nm)	Surface area ($m^2/g_{met.}$)	Particle size (nm)	Surface area ($m^2/g_{met.}$)	Particle size (nm)	Surface area ($m^2/g_{met.}$)	
Cu/γ-Al_2O_3	3.3 ± 0.5	–	–	–	2.9	230.8	[233]
Au/γAl_2O_3	3.7 ± 0.4	–	–	–	3.6	87.7	[233]
Pt/γ-Al_2O_3	2.4 ± 0.6	–	1.3	216.6	1.7	161.6	[233]
Pd/γ-Al_2O_3	3.7 ± 0.8	–	2.9	173.5	2.7	182.8	[233]
Au/Al_2O_3	5.0 ± 1.7	–	–	–	5.3	59.0	[253]
Au/CeO_2	4.1 ± 2.6	–	–	–	3.1	101.0	[253]
Au/TiO_2	5.9 ± 1.7	–	–	–	5.0	62.0	[253]
Au-NP	10.2 ± 1.3	25.6 ± 7.0	–	–	9.5 ± 0.2	27.4 ± 0.8	[255]

oxidation of organic compounds. It is noteworthy to mention that selective oxidation of hydrocarbons is a broad area of research, and the utilization of hydrocarbons in catalysis is one of the biggest challenges, as forcing conditions are classically required for the activation of C–H bonds [5]. For a clear understanding on how key products are formed, many basic parameters, including nature of the catalysts, reactions time and temperature, solvent type and property, need to be studied and controlled. Several investigations have demonstrated the wide applicability of heterogeneous catalysts emphasizing Au, Ru, Pd and Pt as efficient selective oxidation catalysts [5, 53, 150, 268, 269].

Oxidation of organic dyes as catalytic model reactions

Model reactions are of great catalytic interest as they are used to evaluate the performance of different catalysts and the influence of the carrier system on the catalytic reactions [270]. For a complete kinetic analysis, a model reaction should be easy to monitor, should not take place without the catalyst and should proceed without side reactions. One commonly explored reaction is the oxidation of organic dyes under mild conditions.

Structurally, dyes belong to the chromophoric group, which includes aromatic, heterocyclic and alkenes compounds. Effluents from dyestuffs production may be highly colored, and the removal of that color is of great challenge in the field of environmental chemistry. Advanced oxidation processes (AOPs), which generate highly potent chemical species such as $OH^{\cdot}$ and $O_2^{\cdot-}$, have appeared as a sustainable way to degrade dyes in aqueous media [271–274]. The main concept of these processes is the decomposition of a powerful green oxidant such as H_2O_2 to generate powerful radicals. The oxidant can be used either directly, in concurrence with a catalyst, UV light or both. The advantage of AOPs processes is that they can be carried out at ambient conditions with the possibility of completely mineralizing organic carbon to CO_2.

Oxidation of methylene blue

With regard to its chemical structure, methylene blue (MB), $C_{16}H_{18}N_3SCl$ is a synthetic organic dye that can be classified in the group of azo dyes [275]. It is a potent cationic dye with absorption of light at λ 655 nm. MB is frequently used for dying cotton, wood and silk, and it is particularly resistant to biodegradation [276]. A number of studies on the oxidation of MB have been conducted using the combined effect of H_2O_2 and heterogeneous catalysts [38, 271, 273, 277]. A study by Zhang et al. [271] shows that the oxidation of MB with H_2O_2 using MnO_2 nanorods as catalyst occurs near or on the catalyst surface where the in situ produced free radical species ($HO^{\cdot}$, $HOO^{\cdot}$ or $O_2^{\cdot-}$) serve as oxidizing agents. The complete oxidation of MB produced CO_2, HNO_3, H_2SO_4 and HCl [278–280] and the stoichiometry of the reaction as determined by Salem and El-Maazawi [280] can be written as:

$$C_{16}H_{18}N_3SCl + 52H_2O_2 \longrightarrow \text{M-NPs}16CO_2 + 0.5O_2 + 58H_2O + 3HNO_3 + H_2SO_4 + HCl$$

Even though this reaction is often used as model for the destructive oxidation of organic dyes which are particularly resistant to conventional treatment technologies, a kinetic study and an understanding of the detailed mechanistic aspects of this model reaction are crucial for the evaluation of the performance and the improvement of the nanocatalysts. It is until recently where we have shown both the oxidation and reduction of MB on the NP surface that we unearth some of the mechanistic aspects of this reaction [38, 211, 281]. Just like many organic dyes reduced or oxidized on the surface of nanocatalysts, the oxidation process has been analyzed using the Langmuir–Hinshelwood model, where both reactants are assumed to be adsorbed on the NP surface. The kinetics of the catalytic oxidation of MB with H_2O_2 was studied [38]. Copper-based catalysts were used and were revealed to be very active in the studied reaction, with the activity of 99.4% obtained after 45 min for the most active catalyst. Different intermediate species were detected, and the degradation pathway was then proposed. The catalytic oxidation of MB could be modeled in terms of the Langmuir–Hinshelwood model. Figure 8 illustrate a mechanism of this model, where H_2O_2 reacts on the NP surface leading to adsorbed active species, $HO^{\cdot}$. Alongside, MB adsorbs onto the NP surface and undergoes a surface reaction with the active species, and afterward, the products of the degradation of MB desorb from the surface of the NPs.

This mechanism is also applicable to the reduction by sodium borohydride on Au and Pd surfaces [211]. In the case of reduction, the methylene blue occupies the surface of the nanocatalysts more than the

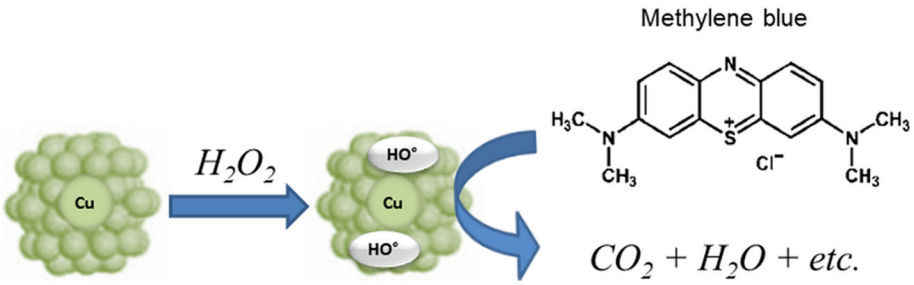

Figure 8 Illustration of Langmuir–Hinshelwood mechanism of the oxidation of MB by H_2O_2 in the presence of Cu-NPs. Reprinted with permission from [38].

Table 2 Catalytic activity of various heterogeneous nanocatalysts for the oxidation of MB

Catalyst	Metal loading (wt%)	Temperature (K)	Time (min)	k_{app} ($min^{-1} \times 10^{-2}$)	MB% decomposition	References
Cu/γ-Al_2O_3	0.70	Room	45	2.94	69.0	[38]
Cu/Li_2O/γ-Al_2O_3	0.51	Room	45	13.6	99.4	[38]
SnO_2	–	Room	70	9.52	100	[282]
α-Fe_2O_3@GO	–	293	80	19.5	≈ 100	[283]
ZnO@GO	–	Room	15	25.4	98.5	[284]
ZnO/graphene	–	Room	90	0.10	≈100	[285]
Mo-K-OMS-2	–	Room	30	7.60	94.0	[286]
ZnO	–	298	120	0.46	≈ 40	[287]
ZnO/graphene	–	298	120	0.92	< 60	[287]
ZnO/graphene/TiO_2	–	298	120	1.97	85.9	[287]

reducing agent. This was shown by the adsorption constants of the two reactants. To the best of our knowledge, there is no many monometallic supported M-NPs reported as catalysts for oxidation of MB. However, the many metal oxides have been used in their nanoscale dimensions. Table 2 shows the comparison of activity of various heterogeneous nanocatalysts for the oxidation of MB.

Oxidation of morin

Morin, $C_{15}H_{10}O_7$, is a polyphenolic dye which belongs to the group of flavonoid plants [288]. It is present in vegetables, tea and fruits, and its chromophore is frequently targeted in the bleaching of laundry [289]. 2,4-Dihydroxybenzoic acid and 2,4,6-trihydroxybenzoic acid are the two oxidation products of morin [290, 291]. But its main oxidation product as proposed by Topalovic [292] is a substituted benzofuranone.

The oxidation of morin by H_2O_2 was previously catalyzed by manganese oxide [293] and colloidal dendrimer-encapsulated Au-NPs [294] with great success. As model reaction, the oxidation of morin with H_2O_2 was also used to investigate the kinetics and the mechanism of the catalysis in the presence of the supported nanocatalysts prepared (in our research group) and to evaluate their activity [150, 233]. The synthesized catalysts were very active, and the oxidation of morin follows the Langmuir–Hinshelwood mechanism on the surface of supported as well as colloidal Au-NPs [150, 294]. In many cases when these NPs are supported on metal oxides, synergistic effects may be observed because of the possibility of participation of the lattice oxygen of the support. However, we have also distinguished between the Mars–van Krevelen and the Langmuir models [295]. In the former mechanism, it is assumed that the lattice oxygen of the metal oxide support, especially reducible metal oxides, participates in the direct oxidation of morin. The Langmuir–Hinshelwood mechanism, which assumes adsorption of both reactants onto the support and reaction of the adsorbed species as the rate-determining step, appeared to be the best mechanism to describe the kinetic of morin oxidation. Thus, the work by Polzer and co-workers on the oxidation of morin by manganese oxide NPs is a confirmation that indeed the oxidation of morin takes place on the surface of NPs rather than being triggered by the lattice oxygen of the metal oxide NPs [293]. A representation of this model as previously explained is shown in Fig. 9.

The presence of polyphenolic groups in the morin structure opens possibility to over-oxidation. Thus, it

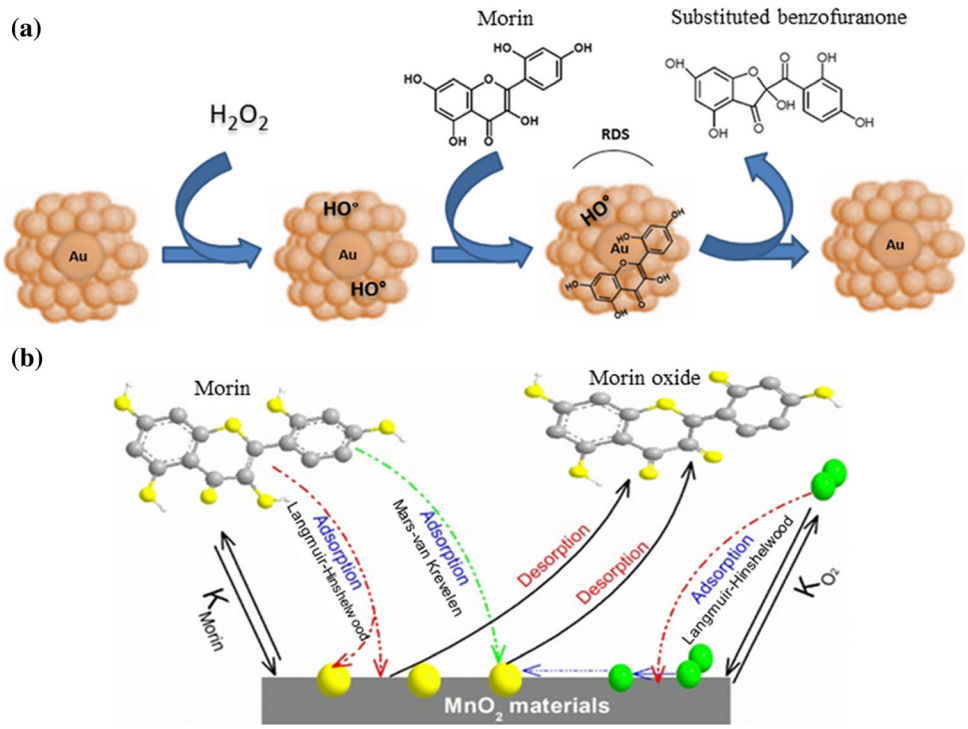

Figure 9 **a** Illustration of Langmuir–Hinshelwood mechanism of the oxidation of morin by H_2O_2 in the presence of Au-NPs. Reprinted with permission from [150], **b** illustration of Langmuir–Hinshelwood and Mars–van Krevelen mechanism for adsorption and desorption of morin on metal oxide surface. Reprinted with permission from [296].

is important to monitor the oxidation process carefully. There are two possible scenarios that might unfold in the over-oxidation process on the NP surface. The first is the oxidation of more than one phenol group. The second possibility is the complete oxidation to many products such as carbon dioxide and water, to mention a few. The reaction is then monitored carefully, more especially if kinetic studies are conducted, through UV–Vis spectroscopy. The appearance and disappearance of isosbestic points are indicative of formation of one and many products, respectively [295]. Thus, kinetic studies on the surface of heterogeneous nanocatalyst are conducted within the first minutes of the reaction, when isosbestic points are still present. Figure 10 shows the appearance and disappearance of isosbestic points in kinetic studies of morin on heterogeneous nanocatalyst.

Besides monometallic supported NPs, many metal oxides have been used in their nanoscale dimensions as catalysts for oxidation of morin. In a study, we conducted using nanometer-sized mesoporous cobalt oxide doped with alkali and alkaline earth metals; we found out that the activity of this material when used as a catalyst is considerably influenced by the nature of the dopant [297]. Thus, the nanometer-sized heterogeneous mesoporous cobalt oxide appeared to be a better catalyst compared to the doped counterparts. The comparison of catalytically active heterogeneous nanocatalysts in morin oxidation is shown in Table 3.

Heterogeneous nanocatalysts for alcohol oxidation

Alcohol oxidation is an important reaction in both academia and industry. The utilization of supported M-NPs and a variety of oxidizing agents (O_2, H_2O_2 or TBHP) on the oxidation of alcohols to the corresponding carbonyl compounds is well explored [5, 10–13, 15, 36, 53, 151, 166, 298].

It was reported by Kaneda and co-authors [298] that Ru-supported NPs were active catalysts for the oxidation of various alcohols. Using toluene as solvent, the oxidation of benzylic and allylic alcohols was performed at 80 °C, with yields in the range of 92–99%. Pd-supported NPs have been also used as catalysts in the oxidation of alcohols [5, 269]. The use of Pt-supported NPs for the liquid-phase aerobic oxidation of alcohols has also been widely explored [5, 299–301]. Crozon et al. [301] reported the efficient liquid-phase oxidation of unsaturated alcohols using Pt-supported NPs at mild conditions, with high conversion of at least 99%. Over the past decade, Au-NPs have emerged as one of the most active nanocatalysts for many reactions. Thus, catalysis by

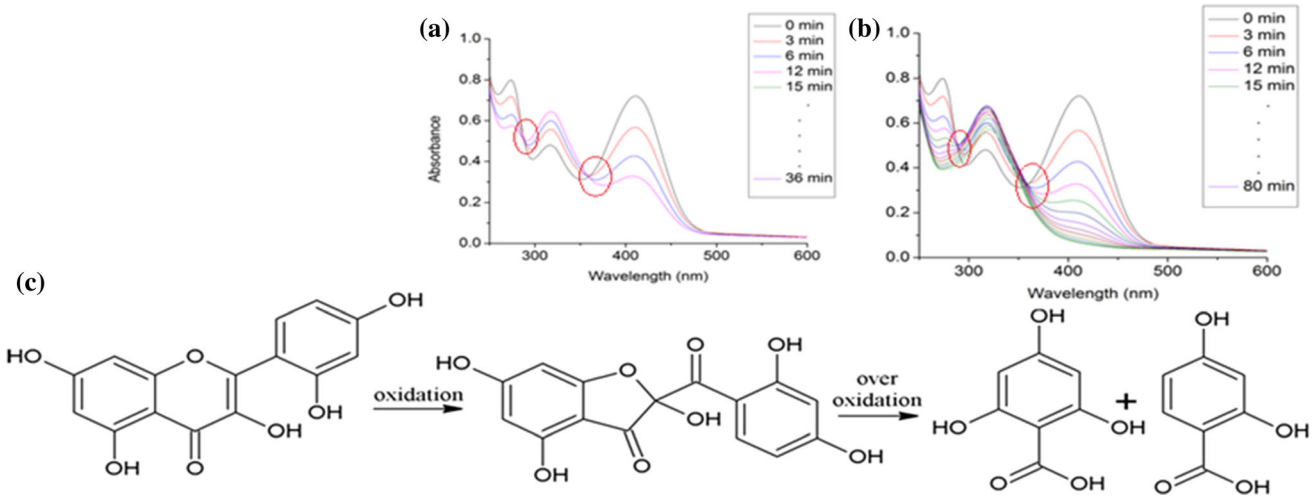

Figure 10 **a** Formation of isosbestic points (circled in red) signifying the oxidation of morin and **b** disappearance of isosbestic points (circled in red) shown in the over-oxidation of morin, **c** reaction scheme for the oxidation of morin and its over-oxidation. Reprinted with permission from [295].

Table 3 Catalytic activity of various heterogeneous nanocatalysts for the oxidation of morin

Catalyst	Metal loading (wt%)	Temperature (K)	Time (min)	k_{app} ($min^{-1} \times 10^{-2}$)	Morin% conversion	References
Au/γ-Al_2O_3	0.69	Room	60	0.50	27.5	[150]
Au/Li_2O/γ-Al_2O_3	0.50	Room	60	0.97	46.4	[150]
Au/Li_2O/γ-Al_2O_3/PF_6	0.52	Room	60	2.01	72.7	[150]
Cu/γ-Al_2O_3	0.70	Room	30	2.96	58.9	[233]
Cu/Li_2O/γ-Al_2O_3	0.51	Room	30	3.51	65.0	[233]
Cu/Li_2O/γ-Al_2O_3/PF_6	0.46	Room	30	3.49	65.1	[233]
MnO_2	–	Room	36	7.8	–	[295]
MnO_2	–	Room	–	0.35	–	[296]
Li/Co_3O_4	–	Room	–	0.10	–	[297]

Au-NPs has been explored extensively in the selective aerobic alcohol oxidation [5, 11, 44, 268, 302] and has been proved highly effective in a variety of reactions. Haider et al. [268] oxidized several alcohols with a full conversion and high selectivity using deposited Au-NPs on Cu-Mg–Al mixed oxides. The activity highly depended on the Cu/Mg molar ratio, with Au/$Cu_5Mg_1Al_2O_x$ showing the highest catalytic activity. Mitsudome et al. [37] reported on hydrotalcite-supported Cu-NPs as catalyst for the oxidant-free dehydrogenation of alcohols. It was revealed that Cu-NPs grafted on hydrotalcite are very active heterogeneous catalysts for the dehydrogenation of various alcohols including less reactive cyclohexanol derivatives.

Selective oxidation of benzyl alcohol to benzaldehyde

Benzyl alcohol is reported to be subjected to different oxidation reactions pathways forming benzaldehyde and benzoic acid, toluene and benzaldehyde or dibenzyl ether depending on the catalyst used (Scheme 1) [10, 53].

Selective oxidation of benzyl alcohol to benzaldehyde is a particularly important commercial process [13, 113, 303–307], as high-quality high-grade benzaldehyde is basically important in perfumery, pharmaceutical and agrochemicals industries. Some studies on liquid-/gas-phase oxidation of benzyl alcohol by supported metal nanocatalysts and O_2, H_2O_2 or TBHP as the oxidant with and without solvent have been reported [10, 11, 53, 158, 308, 309]. Choudary and co-workers [11] reported on Au-NPs supported on TiO_2 and also other metal oxides for the solvent-free

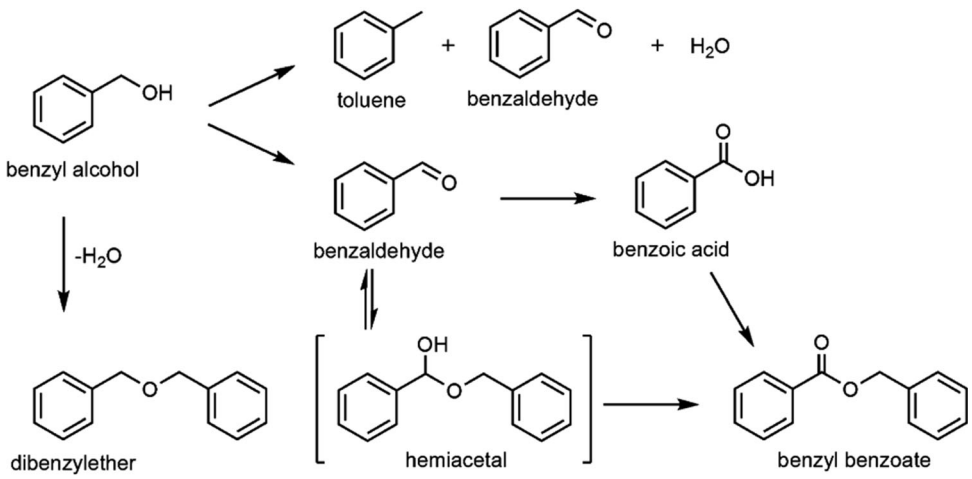

Scheme 1 Reaction scheme for benzyl alcohol oxidation. Adapted with permission from [10].

oxidation of benzyl alcohol to benzaldehyde by TBHP. It was concluded that the catalytic performance is highly influenced by the supports, with Au/TiO_2 and Au/ZrO_2 being the most active and selective catalysts. Another study conducted by the same group [309] revealed that Cu containing layered double hydroxide catalysts showed good activity in the absence of any solvent using TBHP as oxidizing agent. The comparison of the performance of catalytically active supported NPs in the oxidation of benzyl alcohol is shown in Table 4. We have also reported on the performance of the supported Cu and Au nanocatalysts in the solvent-free oxidation of benzyl alcohol to benzaldehyde by TBHP [53]. The Au-based catalysts were revealed to be more active that the Cu-based ones. As the reaction proceeds, the conversion of benzyl alcohol increased, whereas the selectivity to benzaldehyde decreased. The apparent rate constant, k_{app} was revealed to be proportional to the nanocatalyst amount and oxygen present in the system.

Miedziak et al. evaluated the activity of supported bimetallic Au/Pd-NPs synthesized by various methods in the oxidation of benzyl alcohol to benzaldehyde [310]. It was shown that the most performing catalyst, the one prepared by sol immobilization method, produces the narrow-sized particle (~ 4 nm), then followed by deposition–precipitation and impregnation approaches,

Table 4 Performance of the M-NPs supported on various metal oxides in the oxidation of benzyl alcohol to benzaldehyde

Catalyst	Metal loading (wt%)	Conversion of benzyl alcohol (%)	Selectivity (%)		TOF (h^{-1})	References
			Benzaldehyde	Benzyl benzoate		
Au/TiO_2	5.91	63.1	79.2	20.7	108.0	[11]
Au/MnO_2	4.14	54.6	73.2	26.7	140.2	[11]
Au/ZrO_2	3.35	59.5	81.5	18.5	206.1	[11]
$Cu/\gamma\text{-}Al_2O_3$	0.70	70.6	95.6	2.0	668.0	[53]
$Cu/Li_2O/\gamma\text{-}Al_2O_3$	0.51	74.4	96.6	2.1	744.8	[53]
$Au/\gamma\text{-}Al_2O_3$	0.69	73.4	84.4	9.3	2182.7	[53]
$Au/Li_2O/\gamma\text{-}Al_2O_3$	0.50	77.0	90.1	8.7	2437.7	[53]
$Au/Cu/SiO_2$	1.0	89.0	> 99	–	–	[13]
$Au/Pd/TiO_2$	1.0 (1:1)	23.0	74.0	0.4	4830.0	[310]
$Au/Pd/TiO_2$	5.0 (1:1)	74.5	91.6	8.4	607.0	[311]

Turnover frequency (TOF) is defined as the number of moles of benzyl alcohol converted to all products per mole of metal particle in the catalyst per hour

respectively. This is somewhat expected due to the sizes of the particles formed, as the activity of the nanocatalysts is size dependent. The lowest selectivity toward benzaldehyde, with a considerable level of toluene formed, was obtained with the catalysts synthesized by impregnation. One possible reason could be the increase in surface acidity of the catalyst due to the residual chlorine remained on the TiO_2 support during the impregnation method [310, 312]. In the other two preparation methods, the surface acidity could be minimized by an extensive washing of the catalysts. The effects of preparation methods of the supported nanocatalysts and their evaluation in benzyl alcohol oxidation were also investigated by Kumar et al. [313]. Au/SBA-15 nanocatalysts were prepared by using four different approaches, namely homogeneous deposition precipitation, impregnation, microemulsion and polyol. Highly dispersed smaller Au particles (7–8 nm) were obtained from the catalysts synthesized by homogeneous deposition precipitation and had a beneficial effect on the catalytic activity and a longer catalyst life.

Liquid-/gas-phase hydrogenation with supported nanocatalysts

Hydrogenation reactions play a critical role in organic syntheses and are widely used in both laboratory and industrial processes [16, 20, 21]. Several valuable and selective reduction transformations have been discovered, leading to the developments and application of tremendous catalysts. Thus, heterogeneous catalytic hydrogenation is of high importance, especially with increased environmental awareness.

Direct hydrogenation with H_2 gas and transfer hydrogenation using a non-H_2 hydrogen source, such as $LiAlH_4$ (at room temperature) and $NaBH_4$ (at higher temperatures), are the two employed strategies for hydrogenation processes [16]. The former approach is convenient as the hydrogen donors are easy to handle, cheap and readily available. It also does not require intricate experimental setups or hazardous pressurized H_2 gas [16, 314–316]. Although it is convenience, this approach is not environmental-friendly, as the reagents used coproduce a stoichiometric amounts of waste metal salts [20]. The H_2 gas approach is apparently more attractive, in principle providing not only more atom efficient, but it is also more environmental-friendly [20].

Reduction of 4-nitrophenol as catalytic model reactions

The nitrophenols are classified as one of the leading pollutants [317]. They are mostly found in wastewaters from the manufacturing industries. The genotoxicity and carcinogenicity of nitrophenol is not known. However, they have adverse health hazards such as being skin and eyes irritants and they also cause inflammation. Thus, it becomes priority to convert nitrophenols to value-added chemicals. The reduction of 4-nitrophenol (4NIP) to 4-aminophenol (4AMP) has been utilized more frequently. This reaction is mostly carried out because it is a clean reaction, it only produces one product and it is easy to execute. Also it can be followed by simple spectroscopic techniques such the UV–Vis spectroscopy. The use of NPs as catalysts for this reaction has seen the number of publication increase significantly. They have been applied as both colloidal NPs [209, 318] and supported NPs [199, 319].

The nature of this reaction has been the subject of debate for a long time. However, it has since been established that the reaction takes place on the surface of the nanoparticulate catalysts [266]. This triggered surface kinetic studies using NPs as catalysts. The use of M-NPs enabled the determination of the kinetic mechanism governing this reaction [199, 320]. The Langmuir–Hinshelwood mechanism has been the most successful kinetic model describing this reaction compared to other model such as Elay–Rideal model. The reduction of 4NIP by $NaBH_4$ in the presence of the M-NPs as catalysts requires adsorption of both reactants onto the catalyst surface prior to the reaction according to the Langmuir–Hinshelwood mechanism. The Langmuir–Hinshelwood mechanism also assumes that the adsorption onto the surface of the two reactants is reversible and fast, and desorption of the product is irreversible and fast. It then means that the reaction of the adsorbed species is the rate-determining step. We have shown that this mechanism best describes the reduction of 4NIP catalyzed by both colloidal and supported NPs [199, 321, 322]. When metallic NPs are supported on native supports such as silica and titania, the activity is attributed to only the metallic nanoparticles. However, when supported on metal oxide supports, which are sometimes catalytically active for this

reaction, the catalytic activity is enhanced [199, 323]. There are many explanations for this phenomenon, which one of them being the hydrogen spillover [324]. However, the most widely accepted explanation is the electron relay mechanism [325, 326]. Most first row transition metal oxides are electron conductive that eases the way electrons are transferred on their surface. More importantly, the M-NP surfaces are electron-rich and these electrons assist in the reduction reaction. Thus, the movement of electrons from the NPs' surface to the support and vice versa enhances the reduction of 4NIP. Figure 11 shows the adsorption of reactants onto the surface and the electron relay mechanism involving supported NPs.

This phenomenon is not limited to 4NIP but also provides a foundation for analysis of other nitrophenol reduction reactions catalyzed by heterogeneous NPs. Table 5 provides literature rate constants for 4NIP reduction by $NaBH_4$ catalyzed by supported transition M-NPs at 25 °C.

Heterogeneous nanocatalysts for the hydrogenation of biomass-derived compounds

The consumption and significant depletion of fossil fuel resources including its impact on the environment have been raising concerns on a possible use of renewable and environmental-friendly energy resources [73, 332–335]. Abundantly available biomass is therefore viewed as a potential energy resource for the production of biofuels and many value-added chemicals [334–341]. With an estimated production of 170 billion tons per year through photosynthesis, biomass can potentially become the world's largest sustainable energy source [342, 343]. It is one of the cost-effective ways to derive energy, and it also strives on feature of being a greener (carbon neutral) process. In addition, most of the

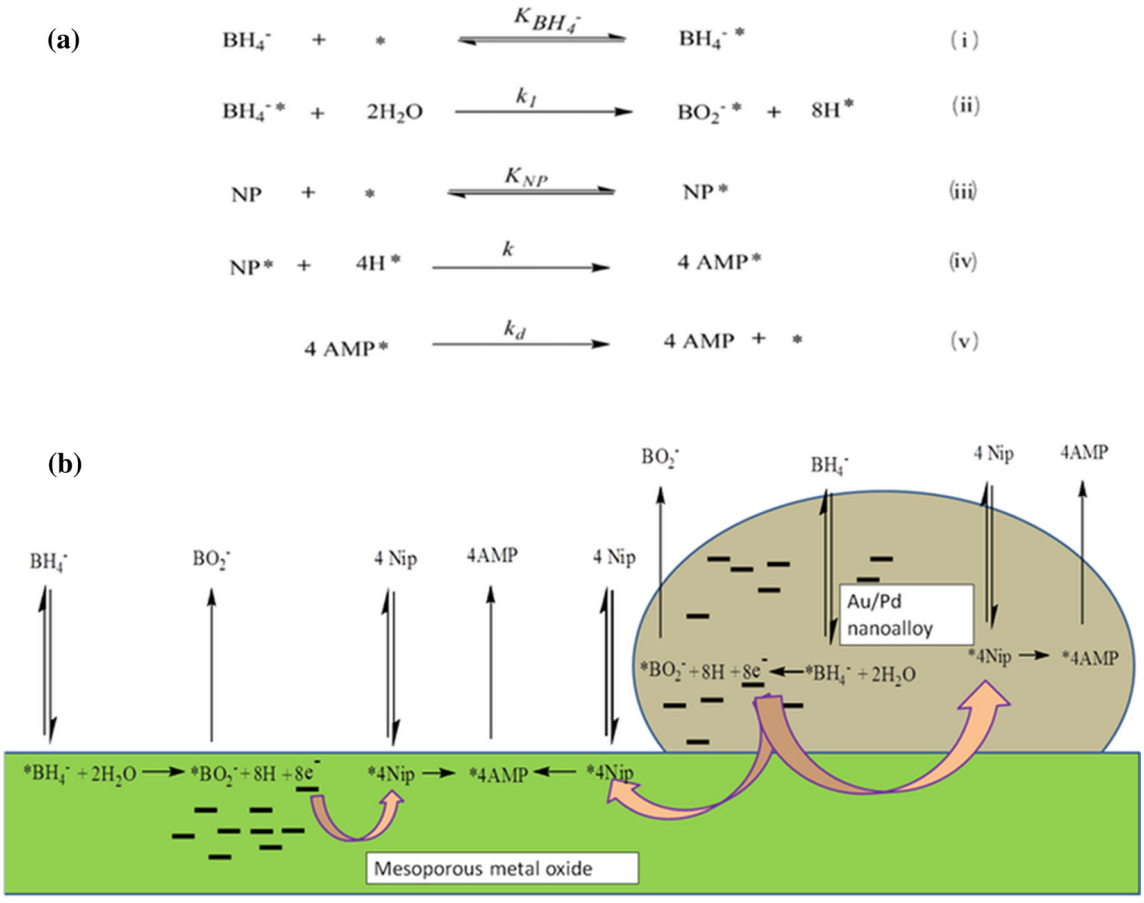

Figure 11 Illustration of the reaction mechanism of 4NIP reduction on the surface of supported M-NPs; **a** evolution of hydrogen from borohydride and adsorption and reduction of 4 NPs on the surface. Reprinted with permission from [209]; **b** adsorption onto the surface of the support and NPs, and the electron relay mechanism. Reprinted with permission from [199].

Table 5 Comparison of catalytic activity of heterogeneous transition M-NPs in the reduction of 4-nitrophenol

Catalyst	M-NP content (μmol)	Rate constant ($s^{-1} \times 10^{-2}$)	References
Au–Fe_2O_3	1.9	1.10	[327]
Au@ZrO_2	248	0.80	[327]
Au/CeO_2	91	1.30	[328]
Cu_2O@CMK-8	–	2.21	[329]
Pd/SBA-15	–	1.20	[330]
Pd/SiO_2–NH_2	–	0.11	[331]

functional groups necessary for synthesis of platform chemicals can be found in biomass.

During the past decade, heterogeneous catalysts have been widely investigated for the hydrogenation of biomass-derived compounds with good yield obtained [338, 344–351]. Therefore, the selective transformations of a set of biomass feedstocks such as cellulose or carbohydrates to the platform intermediates including levulinic acid and furfural and their conversion to prospective biofuels and value-added chemicals have received strong attention [335, 347, 352]. Due to their unique fuel properties, γ-valerolactone (GVL) and 2-methylfuran (2-MF) are among the mostly attractive potential fuel components [346, 347, 353–355]. While the transformation of levulinic acid to GVL involves the hydrogenation and ring formation [346, 347], the conversion of furfural to 2-MF firstly requires selective hydrogenation of the aldehyde group (–C=O) with no breaking of the conjugated ring system (–C=C–C=C–) and then hydrogenolysis of the C–O bond, where supplementary energy is needed [347, 356, 357]. However, a flexible route for the conversion of furfural to 2-MF was suggested by Stevens and co-workers [346], in which a twin catalyst system in combination with supercritical CO_2 in a continuous-flow reactor yield 90% 2-MF.

Hydrogenation of levulinic acid to γ-valerolactone

Levulinic acid, LA, a typical biosourced material, usually produced from cellulose and lignocellulose through a conventional hydrolysis process has gained strong interest as an intermediate for a variety of fuel components and value-added chemicals, such as γ-valerolactone, GVL [73, 358–361]. GVL a low-toxic hydrocarbon molecule is mostly attractive for its excellent characteristics of an ideal liquid fuel [351, 353–355]. In comparison with other liquid fuels such as ethanol, GVL displays better lubricity and higher energy density [362]. In addition to its unique fuel properties, GVL is also receiving attention due to its application in pharmaceutical, perfume and food industries [362–364]. As the selectivity is mostly challenging, GVL can further be hydrogenated to 2-methyltetrahydrofuran via the formation of 1,4-pentanediol (Scheme 2) [341].

Several studies have been focusing on the synthesis of GVL from LA in various catalytic systems. Many reaction conditions were evaluated, with the temperature between 100 and 265 °C, and H_2 pressures ranging from 5 to 60 bar [156, 359, 365, 366]. High-pressure H_2 is generally reported as the hydrogen source for the synthesis of GVL from LA [349, 367, 368], and homogeneous [341, 353, 369, 370] or heterogeneous [349, 350, 371, 372] catalysts are generally used for an efficient conversion and selectivity. Most of these catalysts consist of noble metals, such as Ru [72, 338], Pt [72, 156], Ir [72, 339] and Pd [72, 371]. A variety of supported metal-based catalyzed hydrogenations of LA to GVL with excellent results has been reported [156, 339, 346, 350, 351, 355, 363, 366, 373], of which Ru led to the best results. The most common catalysts for this reaction are 5%-Ru/C and 10%-Pd/C [72, 342, 374], with the 5%-Ru/C being the most typical ones [72, 74, 375]. Table 6 shows the performance of various supported nanocatalysts in the hydrogenation of LA to GVL.

Manzer [72] reported on the performance of (5 w %) Ni, Ru, Rh, Pd, Re, Ir and Pt, supported on activated carbon and presented Ru as the best performing nanocatalyst. Recently, Piskun and co-workers [351] have reported in the hydrogenation of LA in an aqueous system over TiO_2-, C- and Al_2O_3-supported Ru nanocatalysts [361]. The Ru/C was revealed to be the most active catalyst, while Ru/Al_2O_3 catalyst was the less active. Bimetallic catalyzed conversion of LA to GVL has also been investigated [366, 377, 378]. Yang et al. emphasized the good performance of the Ru/Ni/C catalyst in the formation of GVL from LA [366]. We have recently

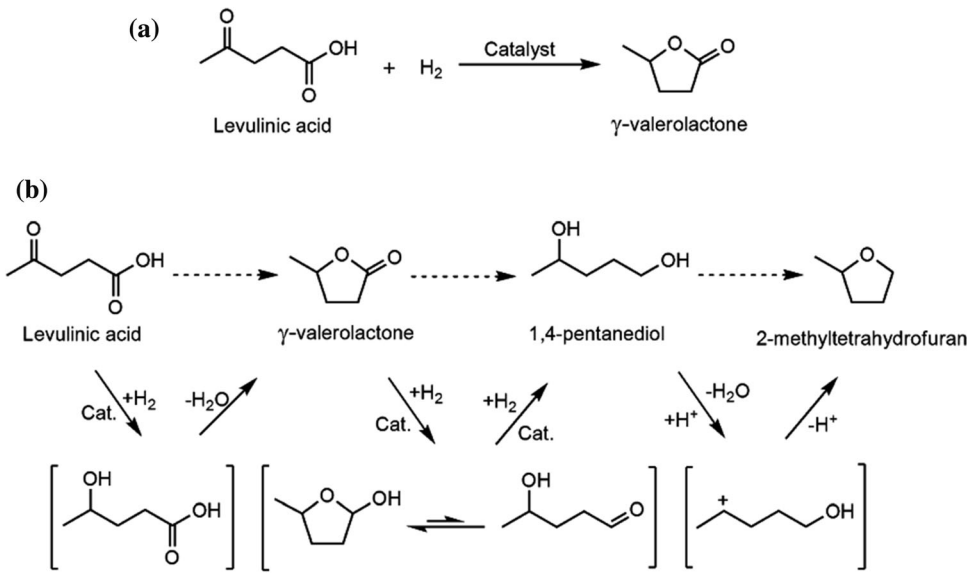

Scheme 2 **a** Catalytic hydrogenation of levulinic acid to γ-valerolactone, **b** proposed mechanism for the catalytic hydrogenation of levulinic acid. Adapted with permission from [341].

Table 6 Comparison of the activity and selectivity of supported M-NP-catalyzed hydrogenation of LA to GVL

Catalyst	Metal loading (wt%)	Solvent	Temperature (K)	Pressure (bar)	Time (h)	LA conversion (%)	GVL selectivity (%)	TOF (h^{-1})	References
Ru@Meso-SiO_2	0.39	Dioxane	423	10	5	100	100	6555	[350]
Pt@Mezo-SiO_2	0.40	Water	423	10	5	88	98	5112	[350]
Ru/TiO_2	1.0	Water	347	40	4	100	99.9	7676	[376]
Ru/C	0.5	Water	363	45	6	92	78	–	[351]
Au–Pd/TiO_2	1.0	Dioxane	473	40	5	90	97.5	360	[338]
Ru–Pd/TiO_2	1.0	Dioxane	473	40	0.5	99	99.6	2160	[338]
Cu–ZrO_2	–	Water	473	35	5	100	100	–	[365]
Cu–ZrO_2	–	Methanol	473	35	5	100	90	–	[365]

demonstrated that Pt- and Ru-NPs supported on mesoporous SiO_2 and TiO_2 are highly efficient in the hydrogenation of LA, with a selectivity to GVL of > 97% [350]. The utilization of noble metal-free catalysts in the hydrogenation of LA was also reported. The Cu catalyst prepared from the hydrotalcite precursor was revealed to be selective at 91% yield of GVL [347].

Hydrogenation of glycerol to 1,2-propanediol and low-chain hydrocarbons

The biodiesel industry is considered one of the fast-growing sectors in energy production. One of the aspects that make it the most attractive field is the virtue of using cost-effective ways to derive energy. It also strives on virtue of being a much greener process. However, on the dark side is the prospect of producing excessively by-products including glycerol. This will lead to undesirable environmental problems, as it will be a tedious task to store these compounds. Their conversion into value-added chemicals is now the center of attention. Although glycerol can be converted using various ways such as biotechnological routes, catalysis by heterogeneous nanomaterials is one of the widely studied areas. More emphasis has been placed on the hydrogenation of glycerol for the production of light alcohols such 1.3-propanol. These light alcohols find use as fuels. The hydrogenation of glycerol yields various

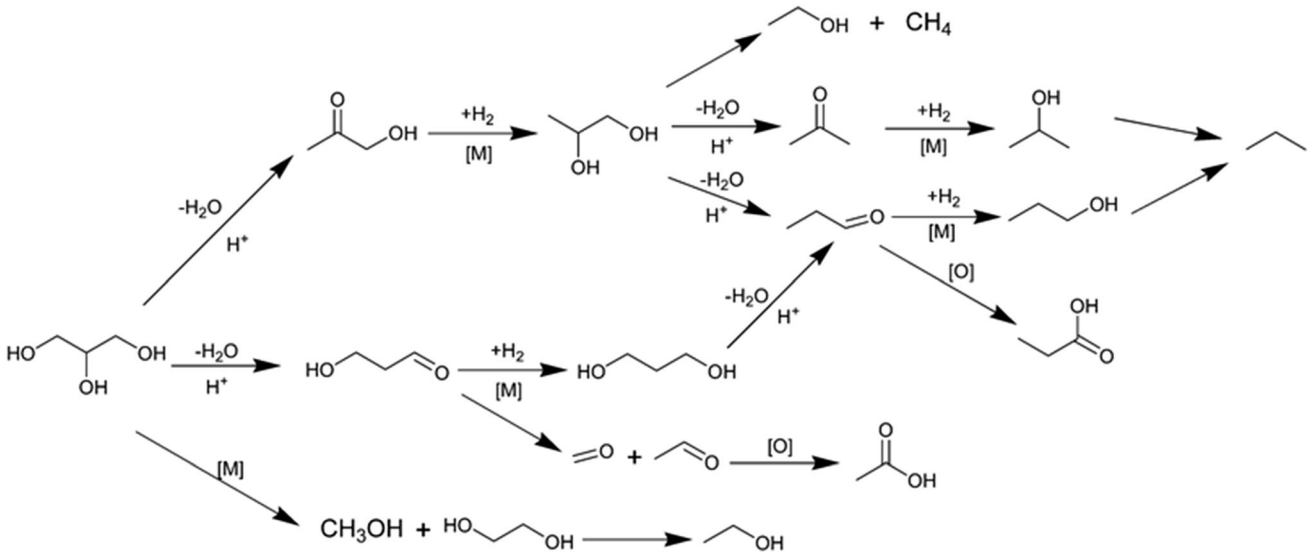

Scheme 3 Illustration of glycerol hydrogenation to various intermediates and products. Reprinted with permission from [379].

Scheme 4 Hydrogenation of glycerol over supported transition M-NPs to low-chain hydrocarbons. Reprinted with permission from [380].

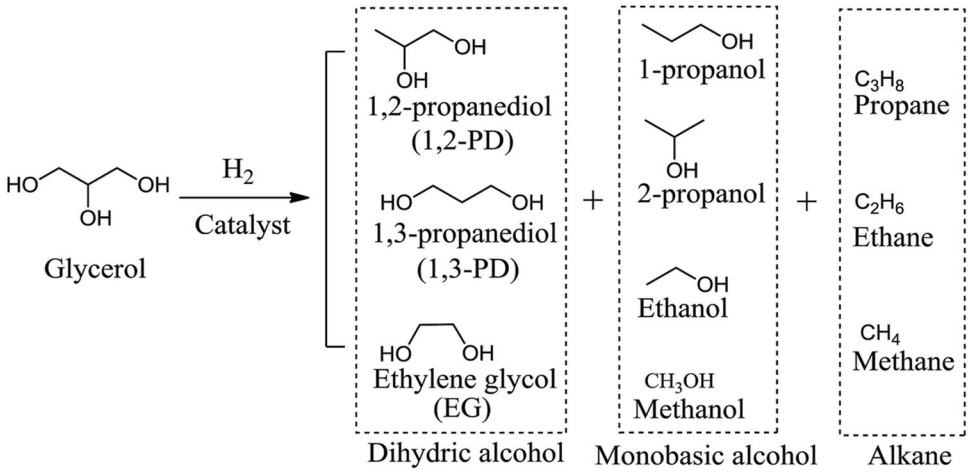

intermediates and products such propane and methane. All these find use in important industrial processes. Zhu et al. reported the conversion of biomass-derived glycerol to propanol on supported M-NPs [379]. Their chosen silica-, tungsten- and zirconia-derived supports together with Pt-NPs showed selectivities toward propanols of above 90% at high glycerol conversions. The schematic representation of glycerol hydrogenation to various products is given in Scheme 3.

From that scheme, it is important to note that the formation of propanediols is not shown. The formation of propanediols as intermediates is the mostly observed route in the hydrogenolysis of glycerol. These propanediols are further hydrogenated to yield propanols, which will eventually form low alkane chains. The low alkanes are used as fuel sources in various transportation modes. The work of Wang et al. proved that the use of cheap transition M-NPs of Cu, Ni and Co can effectively yield high selectivities toward 1,2-propanediol (1,2-PD) at mild reaction conditions [380]. Scheme 4 shows the hydrogenation of glycerol to propane, ethane and methane.

Among the cheap transition metals, Cu appeared to be the widely used. Different synthetic protocols have been used to synthesize these Cu-based NPs, and high glycerol conversion (> 40%) and high selectivities (> 91%) toward 1,2-PD were observed. Similar results were obtained for supported Ni-NPs, more especially concerning the selectivity. The more precious M-NPs supported on various supports did not show significant deviations from these results in

terms of percentage conversion; however, the selectivity trend toward 1,2-PD appeared to be lagging behind compared with those observed when Cu- and Ni-NPs are used. Among the more precious M-NPs, Ir, Pt and Ru showed poor selectivity toward 1,2-PD [380]. Table 7 gives a comparison between cheap transition M-NPs and precious M-NPs for the hydrogenation of glycerol to 1,2-PD.

Kinetic of the liquid-/gas-phase reaction over a solid catalyst

To study the feasibility of the catalytic systems, detailed kinetic studies of the reaction are essential. The quantification of the kinetics of the catalytic systems implies both characterizing the order of the reaction and providing a kinetic model for future reactor development [388]. The order of a reaction is crucial in that it enables an understanding of the mechanism of the reaction and efficient classification of specific chemical reactions. Kinetic data could be modeled according to a new developed model or an existing method. Because most of the catalytic reactions take place on the particle surface, the kinetics of the model reactions can be treated in terms of the classical Langmuir–Hinshelwood model [389].

The analysis of the kinetic data using Langmuir–Hinshelwood model yields the kinetic constant, k, of the surface reaction together with the thermodynamic adsorption constants K for each reactants [389–391]. In the Langmuir–Hinshelwood model, both reactants compete for the surface sites on catalyst surface; that is, to react, both reactants must be adsorbed onto the surface. The rate at which the reactants adsorb on the catalyst surface is proportional to the frequency of the collision of the adsorbate with the surface and the probability of the adsorption. Thus, mathematically, the adsorption rate can be written as [392]:

$$r_{\mathrm{ad}} = \frac{p \cdot \sigma \cdot f(\theta)}{(2 \cdot \pi \cdot m \cdot k_{\mathrm{B}} \cdot T)^{1/2}} \cdot \mathrm{e}^{-E_{\mathrm{ad}}/RT} \tag{2}$$

where r_{ad} is the adsorption rate, p the pressure, σ the probability on the exact adsorption energy E_{ad} of the molecule for the adsorption, $f(\theta)$ the free adsorption site; θ surface coverage, m the mass of the molecule, K_{B} the Boltzmann's constant and T the absolute temperature.

Unlike adsorption, desorption is always an activated process, and the rate of desorption on a uniform surface can be written as [392]:

$$r_{\mathrm{des}} = k_{\mathrm{des}}(\theta) \cdot f'(\theta) \cdot \mathrm{e}^{-E_{\mathrm{des}}(\theta)/RT} \tag{3}$$

where k_{des} is the rate of desorption, $f'(\theta)$ the occupied site and E_{des} the activation energy of desorption. On a uniform surface, both k_{des} and E_{des} depend on θ.

Furthermore, in the Langmuir isotherm it is assumed that adsorption does not depend on the degree of surface coverage and adsorption and desorption are in equilibrium (only applicable to ideal systems). To keep the analysis as general as possible, the Langmuir isotherm is usually combined to the Freundlich isotherm to provide a model that better describes "non-ideal" systems [293, 322, 389, 390]. The Freundlich isotherm takes into consideration the fact that at higher surface coverage, the adsorption

Table 7 Comparison between supported base M-NPs and precious M-NPs for the hydrogenation of glycerol to 1,2-propanediol (1,2-PD)

Catalyst	Metal loading (wt%)	Temperature (K)	Pressure (MPa)	Time (h)	Glycerol% conversion	1,2-PD% selectivity	References
Cu/SiO_2	–	513	8	5	51.9	96.6	[381]
$CuO/CuFe_2O_4$	–	463	4.1	10	47	92	[382]
Ni/SiO_2	–	523	6	–	25.6	70.2	[383]
Ni/Al_2O_3-$CuCr_2O_4$	–	473	1.5	8	32.1	94.1	[384]
Ni/SiO_2-Al_2O_3	–	473	2.5	8	30	98	[385]
Ir-ReO_x/SiO_2	–	393	8	4	21.7	6.7	[386]
Ru/SiO_2	–	513	8	5	18	90.2	[387]

rate decreases and a full surface coverage is never reached.

$$\theta_i = \frac{(K_i \cdot c_i)^{n_i}}{1 + \sum_{j=1}^{N} (K_j \cdot c_j)^{n_j}} \quad (4)$$

where θ_i and K_i are the surface coverage of the compound i and its corresponding adsorption constant, respectively, and c_i the concentration of the compound i in solution.

Synopsis and outlook

This review presents a general overview of supported M-NPs with emphasis on Cu, Au, Pt, Pd, Ru, Ag, Co and Ni nanoparticles, NPs (active phase), their synthesis methodologies, their features and their advantages and application as catalysts for various oxidation and hydrogenation reactions. A brief view of the ligand adsorption-based technique for M-NP surface area determination and kinetic models of the liquid-/gas-phase reaction over M-NPs is also provided.

The performance of supported M-NP catalysts depends on their nature, surface area, sizes, shapes and synergistic effect. Their relationship is a critical factor on the performances of the catalysts. The following recommendations are necessary for a good performance of the catalyst: (1) the use of an appropriate synthesis method; size and electronic state of metal on the surface of catalyst can be tuned using appropriate preparation method, (2) the choice of an appropriate carrier (synergistic effect); sizes and distribution of M-NPs on the support surface depend on the nature of both metal and support, and can be tailored through the preparation conditions such as temperature, pressure, stirring speed and duration, (3) investigation of the metal–support interaction; the interaction between the support and M-NPs is very significant for the catalytic stability and activity, (4) stabilization of the M-NPs; the catalytic properties of M-NPs are directly related to the size of the nanoparticles (exposed surface area), and nanometer-sized catalyst particles can undergo easy sintering, (5) determination of the exposed (true) surface area of the NPs; the activity and selectivity of heterogeneous catalysts benefit strongly from a high active surface area, and (6) kinetic assessment of the catalytic activities of supported M-NPs on the studied reactions by investigating different aspects including NP concentration, reactant concentration, solvent effect, pressure, temperature, steering speed and duration, and attempt to understand the mechanistic aspects that are indispensable for catalyst and parameters improvement.

Acknowledgements

This work is financially supported by the University of Johannesburg and in the part by the National Research Foundation of South Africa (Grant specific unique reference numbers (UID) 85386, 117997).

Compliance with ethical standards

Conflict of interest The authors declare no competing financial interest.

References

[1] Cuenya BR, Behafarid F (2015) Nanocatalysis: size-and shape-dependent chemisorption and catalytic reactivity. Surf Sci Rep 70:135–187

[2] Schlögl R, Abd Hamid SB (2004) Nanocatalysis: mature science revisited or something really new? Angew Chem Int Ed 43:1628–1637

[3] Monfared A, Mohammadi R, Ahmadi S, Nikpassand M, Hosseinian A (2019) Recent advances in the application of nano-catalysts for Hiyama cross-coupling reactions. RSC Adv 9:3185–3202

[4] Navalón S, García H (2016) Nanoparticles for catalysis. Nanomaterials 6:123

[5] Dimitratos N, Lopez-Sanchez JA, Hutchings GJ (2012) Selective liquid phase oxidation with supported metal nanoparticles. Chem Sci 3:20–44

[6] Astruc D (2008) Nanoparticles and catalysis. Wiley, New York

[7] Shang L, Bian T, Zhang B, Zhang D, Wu L, Tung C, Yin Y, Zhang T (2014) Graphene-supported ultrafine metal nanoparticles encapsulated by mesoporous silica: robust catalysts for oxidation and reduction reactions. Angew Chem 126:254–258

[8] Xia Y, Yang H, Campbell CT (2013) Nanoparticles for catalysis. Acc Chem Res 46:1671–1672

[9] Philippot K, Serp P (2013) Nanomaterials in catalysis. Wiley-VCH, Weinheim

[10] Albonetti S, Mazzoni R, Cavani F (2014) Homogeneous, heterogeneous and nanocatalysis. In: Cardona F, Parmeggiani C (eds) Transition metal catalysis in aerobic alcohol

oxidation. Royal Society of Chemistry, Cambridge, pp 1–39

[11] Choudhary VR, Dumbre DK, Bhargava SK (2009) Oxidation of benzyl alcohol to benzaldehyde by tert-butyl hydroperoxide over nanogold supported on TiO_2 and other transition and rare-earth metal oxides. Ind Eng Chem Res 48:9471–9478

[12] Albonetti S, Pasini T, Lolli A, Blosi M, Piccinini M, Dimitratos N, Lopez-Sanchez JA, Morgan DJ, Carley AF, Hutchings GJ (2012) Selective oxidation of 5-hydroxymethyl-2-furfural over TiO_2-supported gold–copper catalysts prepared from preformed nanoparticles: effect of Au/Cu ratio. Catal Today 195:120–126

[13] Della Pina C, Falletta E, Rossi M (2008) Highly selective oxidation of benzyl alcohol to benzaldehyde catalyzed by bimetallic gold–copper catalyst. J Catal 260:384–386

[14] Pritchard J, Kesavan L, Piccinini M, He Q, Tiruvalam R, Dimitratos N, Lopez-Sanchez JA, Carley AF, Edwards JK, Kiely CJ (2010) Direct synthesis of hydrogen peroxide and benzyl alcohol oxidation using Au–Pd catalysts prepared by sol immobilization. Langmuir 26:16568–16577

[15] Lippits MJ, Nieuwenhuys BE (2010) Direct conversion of ethanol into ethylene oxide on copper and silver nanoparticles: effect of addition of CeO_x and Li_2O. Catal Today 154:127–132

[16] Wang D, Astruc D (2015) The golden age of transfer hydrogenation. Chem Rev 115:6621–6686

[17] Simakova OA, Davis RJ, Murzin DY (2013) Selective hydrogenation reactions. In: Biomass process over gold catalysts. Springer Briefs in Molecular Science. Springer, Heidelberg, pp 39–40

[18] Liao F, Huang Y, Ge J, Zheng W, Tedsree K, Collier P, Hong X, Tsang SC (2011) Morphology-dependent interactions of ZnO with Cu nanoparticles at the materials' interface in selective hydrogenation of CO_2 to CH_3OH. Angew Chem Int Ed 50:2162–2165

[19] Hou R (2017) Selective hydrogenation of 1,3-butadiene on Pd–Ni bimetallic catalyst: from model surfaces to supported catalysts. In: Catalytic and process study of the selective hydrogenation of acetylene and 1,3-butadiene. Springer theses. Springer, Singapore, pp 45–72

[20] Smith AM, Whyman R (2014) Review of methods for the catalytic hydrogenation of carboxamides. Chem Rev 114:5477–5510

[21] Pritchard J, Filonenko GA, van Putten R, Hensen EJM, Pidko EA (2015) Heterogeneous and homogeneous catalysis for the hydrogenation of carboxylic acid derivatives: history, advances and future directions. Chem Soc Rev 44:3808–3833

[22] Ouyang G, Wang CX, Yang GW (2009) Surface energy of nanostructural materials with negative curvature and related size effects. Chem Rev 109:4221–4247

[23] Schmid G (2004) Nanoparticles: from theory to application. Wiley-VCH, Weinheim

[24] Astruc D, Lu F, Aranzaes JR (2005) Nanoparticles as recyclable catalysts: the frontier between homogeneous and heterogeneous catalysis. Angew Chem Int Ed 44:7852–7872

[25] Thielbeer F, Donaldson K, Bradley M (2011) Zeta potential mediated reaction monitoring on nano and microparticles. Bioconjug Chem 22:144–150

[26] Polshettiwar V, Varma RS (2010) Green chemistry by nanocatalysis. Green Chem 12:743–754

[27] Aiken JD III, Lin Y, Finke RG (1996) A perspective on nanocluster catalysis: polyoxoanion and $(n\text{-}C_4H_9)_4N$ + stabilized Ir(0) ~ 300 nanocluster 'soluble heterogeneous catalysts'. J Mol Catal A Chem 114:29–51

[28] Antonels NC (2014) The evaluation of dendrimer encapsulated ruthenium nanoparticles, immobilised on silica, as catalysts in various catalytic reactions and the effect of ionic liquids on the catalytic activity. University of Johannesburg, Johannesburg

[29] Belyakova OA, Slovokhotov YL (2003) Structures of large transition metal clusters. Russ Chem Bull 52:2299–2327

[30] Kidwai M (2010) Nanoparticles in green catalysis. In: Handbook of green chemistry. Online, Wiley Online Library, pp 81–92

[31] Toshima N (2003) In: Liz-Marzan LM, Kamat PV (eds) Nanoscale materials, vol 444. Kluwer Acad. Pub., London, pp 79–96

[32] Thathagar MB, Beckers J, Rothenberg G (2002) Copper-catalyzed Suzuki cross-coupling using mixed nanocluster catalysts. J Am Chem Soc 124:11858–11859

[33] Calo V, Nacci A, Monopoli A, Ieva E, Cioffi N (2005) Copper bronze catalyzed heck reaction in ionic liquids. Org Lett 7:617–620

[34] Lipshutz BH, Taft BR (2006) Heterogeneous copper-in-charcoal-catalyzed click chemistry. Angew Chem Int Ed 45:8235–8238

[35] Jammi S, Sakthivel S, Rout L, Mukherjee T, Mandal S, Mitra R, Saha P, Punniyamurthy T (2009) CuO nanoparticles catalyzed C–N, C–O, and C–S cross-coupling reactions: scope and mechanism. J Org Chem 74:1971–1976

[36] Ranu BC, Dey R, Chatterjee T, Ahammed S (2012) Copper nanoparticle-catalyzed carbon–carbon and carbon–heteroatom bond formation with a greener perspective. Chemsuschem 5:22–44

[37] Mitsudome T, Mikami Y, Ebata K, Mizugaki T, Jitsukawa K, Kaneda K (2008) Copper nanoparticles on hydrotalcite

as a heterogeneous catalyst for oxidant-free dehydrogenation of alcohols. Chem Commun 39:4804–4806
[38] Ndolomingo MJ, Meijboom R (2015) Kinetic analysis of catalytic oxidation of methylene blue over γ-Al_2O_3 supported copper nanoparticles. Appl Catal A Gen 506:33–43
[39] Hutchings GJ, Haruta M (2005) A golden age of catalysis: a perspective. Appl Catal A Gen 291:2–5
[40] Haruta M (2005) Catalysis: gold rush. Nature 437:1098–1099
[41] Sermon PA, Bond GC, Wells PB (1979) Hydrogenation of alkenes over supported gold. J Chem Soc Faraday 1 Trans Phys Chem Condens Phases 75:385–394
[42] Bond GC (1972) The catalytic properties of gold. Gold Bull 5:11–13
[43] Schwank J (1985) Gold in bimetallic catalysts. Gold Bull 18:2–10
[44] Hashmi ASK, Hutchings GJ (2006) Gold catalysis. Angew Chem Int Ed 45:7896–7936
[45] Hutchings GJ, Brust M, Schmidbaur H (2008) Gold—an introductory perspective. Chem Soc Rev 37:1759–1765
[46] Corma A, Serna P (2006) Chemoselective hydrogenation of nitro compounds with supported gold catalysts. Science 313:332–334
[47] Hutchings GJ (1996) Catalysis: a golden future. Gold Bull 29:123–130
[48] Haruta M, Kobayashi T, Sano H, Yamada N (1987) Novel gold catalysts for the oxidation of carbon monoxide at a temperature far below 0 C. Chem Lett 16:405–408
[49] Abad A, Concepción P, Corma A, García H (2005) A collaborative effect between gold and a support induces the selective oxidation of alcohols. Angew Chem Int Ed 44:4066–4069
[50] Malta G, Kondrat SA, Freakley SJ, Davies CJ, Lu L, Dawson S, Thetford A, Gibson EK, Morgan DJ, Jones W (2017) Identification of single-site gold catalysis in acetylene hydrochlorination. Science 355:1399–1403
[51] Hashmi ASK, Rudolph M (2008) Gold catalysis in total synthesis. Chem Soc Rev 37:1766–1775
[52] Marion N, Nolan SP (2008) N-Heterocyclic carbenes in gold catalysis. Chem Soc Rev 37:1776–1782
[53] Ndolomingo MJ, Meijboom R (2017) Selective liquid phase oxidation of benzyl alcohol to benzaldehyde by tert-butyl hydroperoxide over γ-Al_2O_3 supported copper and gold nanoparticles. Appl Surf Sci 398:19–32
[54] Wang C, Daimon H, Onodera T, Koda T, Sun S (2008) A general approach to the size-and shape-controlled synthesis of platinum nanoparticles and their catalytic reduction of oxygen. Angew Chem Int. Ed 47:3588–3591
[55] Tan TL, Wang L-L, Zhang J, Johnson DD, Bai K (2015) Platinum nanoparticle during electrochemical hydrogen evolution: adsorbate distribution, active reaction species, and size effect. ACS Catal 5:2376–2383
[56] Ovejero G, Rodríguez A, Vallet A, García J (2011) Studies in catalytic wet air oxidation as a process to destroy CI Basic Yellow 11 in aqueous stream over platinum catalyst. Color Technol 127:10–17
[57] Gomes HT, Samant PV, Serp P, Kalck P, Figueiredo JL, Faria JL (2004) Carbon nanotubes and xerogels as supports of well-dispersed Pt catalysts for environmental applications. Appl Catal B Environ 54:175–182
[58] Daas BM, Ghosh S (2016) Fuel cell applications of chemically synthesized zeolite modified electrode (ZME) as catalyst for alcohol electro-oxidation—a review. J Electroanal Chem 783:308–315
[59] Lange J, Price R, Ayoub PM, Louis J, Petrus L, Clarke L, Gosselink H (2010) Valeric biofuels: a platform of cellulosic transportation fuels. Angew Chem Int Ed 49:4479–4483
[60] Liu X, Guo Y, Xu W, Wang Y, Gong X, Guo Y, Guo Y, Lu G (2011) Catalytic properties of Pt/Al_2O_3 catalysts in the aqueous-phase reforming of ethylene glycol: effect of the alumina support. Kinet Catal 52:817–822
[61] Stanislaus A, Marafi A, Rana MS (2010) Recent advances in the science and technology of ultra low sulfur diesel (ULSD) production. Catal Today 153:1–68
[62] Bingwa N, Ndolomingo MJ, Noh J-H, Antonels N, Haumann M, Meijboom R (n.d) Synergistic effect of mesoporous transition metal oxides and Pt nanoparticles in aerobic oxidation of ethanol and ionic liquid induced selectivity. Manuscript under review
[63] Smidt J, Hafner W, Jira R, Sedlmeier J, Sieber R, Rüttinger R, Kojer H (1959) Katalytische Umsetzungen von Olefinen an Platinmetall-Verbindungen Das Consortium-Verfahren zur Herstellung von Acetaldehyd. Angew Chem 71:176–182
[64] Reddy CB, Bharti R, Kumar S, Das P (2016) Supported palladium nanoparticles-catalyzed decarboxylative coupling approaches to aryl alkynes, indoles and pyrrolines synthesis. RSC Adv. 6:71117–71121
[65] Kumar S, Chaudhary A, Bhattacherjee D, Thakur V, Das P (2017) Supported palladium nanoparticles as switchable catalyst for aldehyde conjugate/s and acetate ester syntheses from alcohols. New J Chem 41:3242–3245
[66] Shiju NR, Guliants VV (2009) Recent developments in catalysis using nanostructured materials. Appl Catal A Gen 356:1–17
[67] Shah D, Kaur H (2016) Supported palladium nanoparticles: a general sustainable catalyst for microwave enhanced carbon-carbon coupling reactions. J Mol Catal A Chem 424:171–180

[68] Ncube P, Hlabathe T, Meijboom R (2015) Palladium nanoparticles supported on mesoporous silica as efficient and recyclable heterogenous nanocatalysts for the Suzuki C–C coupling reaction. J Clust Sci 26:1873–1888

[69] Iqbal S, Kondrat SA, Jones DR, Schoenmakers DC, Edwards JK, Lu L, Yeo BR, Wells PP, Gibson EK, Morgan DJ (2015) Ruthenium nanoparticles supported on carbon: an active catalyst for the hydrogenation of lactic acid to 1, 2-propanediol. ACS Catal 5:5047–5059

[70] Tan J, Cui J, Cui X, Deng T, Li X, Zhu Y, Li Y (2015) Graphene-modified Ru nanocatalyst for low-temperature hydrogenation of carbonyl groups. ACS Catal 5:7379–7384

[71] Sun J, Li X, Taguchi A, Abe T, Niu W, Lu P, Yoneyama Y, Tsubaki N (2013) Highly-dispersed metallic Ru nanoparticles sputtered on H-beta zeolite for directly converting syngas to middle isoparaffins. ACS Catal 4:1–8

[72] Manzer LE (2004) Catalytic synthesis of α-methylene-γ-valerolactone: a biomass-derived acrylic monomer. Appl Catal A Gen 272:249–256

[73] Bozell JJ, Petersen GR (2010) Technology development for the production of biobased products from biorefinery carbohydrates—the US Department of Energy's "Top 10" revisited. Green Chem 12:539–554

[74] Protsenko II, Nikoshvili LZ, Matveeva VG, Sulman EM, Rebrov E (2016) Selective hydrogenation of levulinic acid to gamma-valerolactone using polymer-based ru-containing catalysts. Chem Eng Trans 52:679–684

[75] Frohning CD, Kölbel H, Ralek M, Rottig W, Schnur F, Schulz H (1977) Fischer–Tropsch synthese. In: Falbe J (ed) Chemierohstoffe Aus Kohle, pp 218–219

[76] Vannice MA (1975) The catalytic synthesis of hydrocarbons from H_2CO mixtures over the group VIII metals: III. Metal–support effects with Pt and Pd catalysts. J Catal 40:129–134

[77] Kitano M, Kanbara S, Inoue Y, Kuganathan N, Sushko PV, Yokoyama T, Hara M, Hosono H (2015) Electride support boosts nitrogen dissociation over ruthenium catalyst and shifts the bottleneck in ammonia synthesis. Nat Commun 6:6731

[78] Ndolomingo MJ, Meijboom R (2019) Noble and base-metal nanoparticles supported on mesoporous metal oxides: efficient catalysts for the selective hydrogenation of levulinic acid to γ-valerolactone. Catal Lett 149:2807–2822

[79] Sun Y (2013) Controlled synthesis of colloidal silver nanoparticles in organic solutions: empirical rules for nucleation engineering. Chem Soc Rev 42:2497–2511

[80] Rizzello L, Pompa PP (2014) Nanosilver-based antibacterial drugs and devices: mechanisms, methodological drawbacks, and guidelines. Chem Soc Rev 43:1501–1518

[81] Dong XY, Gao ZW, Yang KF, Zhang WQ, Xu LW (2015) Nanosilver as a new generation of silver catalysts in organic transformations for efficient synthesis of fine chemicals. Catal Sci Technol 5:2554–2574

[82] Gawande MB, Guo H, Rathi AK, Branco PS, Chen Y, Varma RS, Peng D-L (2013) First application of core-shell Ag@ Ni magnetic nanocatalyst for transfer hydrogenation reactions of aromatic nitro and carbonyl compounds. RSC Adv 3:1050–1054

[83] Bingwa N, Meijboom R (2015) Evaluation of catalytic activity of Ag and Au dendrimer-encapsulated nanoparticles in the reduction of 4-nitrophenol. J Mol Catal A Chem 396:1–7

[84] Chaki NK, Tsunoyama H, Negishi Y, Sakurai H, Tsukuda T (2007) Effect of Ag-doping on the catalytic activity of polymer-stabilized Au clusters in aerobic oxidation of alcohol. J Phys Chem C 111:4885–4888

[85] Nemanashi-Maumela M, Nongwe I, Motene RC, Davids BL, Meijboom R (2017) Au and Ag nanoparticles encapsulated within silica nanospheres using dendrimers as dual templating agent and their catalytic activity. Mol Catal 438:184–196

[86] Guo JZ, Cui H, Zhou W, Wang W (2008) Ag nanoparticle-catalyzed chemiluminescent reaction between luminol and hydrogen peroxide. J Photochem Photobiol A Chem 193:89–96

[87] Khodakov AY, Chu W, Fongarland P (2007) Advances in the development of novel cobalt Fischer–Tropsch catalysts for synthesis of long-chain hydrocarbons and clean fuels. Chem Rev 107:1692–1744

[88] van Deelen TW, Nijhuis JJ, Krans NA, Zečević J, de Jong KP (2018) Preparation of Cobalt nanocrystals supported on metal oxides to study particle growth in Fischer–Tropsch catalysts. ACS Catal 8:10581–10589

[89] Sadek R, Chalupka KA, Mierczynski P, Rynkowski J, Gurgul J, Dzwigaj S (2019) Cobalt based catalysts supported on two kinds of beta zeolite for application in Fischer–Tropsch synthesis. Catalysts 9:497

[90] Hertrich MF, Scharnagl FK, Pews-Davtyan A, Kreyenschulte CR, Lund H, Bartling S, Jackstell R, Beller M (2019) Supported cobalt nanoparticles for hydroformylation reactions. Chem Eur J 25:5534–5538

[91] Bingwa N, Ndolomingo MJ, Mabate T, Dube S, Meijboom R (2019) Surface property–activity relations of Co/Sn oxide nanocatalysts evaluated using a model reaction: surface characterization study. Catal Lett 149:2940–2949

[92] Seo S, Perez GA, Tewari K, Comas X, Kim M (2018) Catalytic activity of nickel nanoparticles stabilized by adsorbing polymers for enhanced carbon sequestration. Sci Rep 8(11786):1–11

[93] Seo S, Nguyen M, Mastiani M, Navarrete G, Kim M (2017) Microbubbles loaded with nickel nanoparticles: a perspective for carbon sequestration. Anal Chem 89:10827–10833
[94] Bhaduri GA, Šiller L (2013) Nickel nanoparticles catalyse reversible hydration of carbon dioxide for mineralization carbon capture and storage. Catal Sci Technol 3:1234–1239
[95] Khurana JM, Vij K (2012) Nickel nanoparticles: a highly efficient catalyst for one pot synthesis of tetraketones and biscoumarins. J Chem Sci 124:907–912
[96] Kamata H, Tian ZQ, Izumi Y, Choong CKS, Chang J, Schreyer M, Chen L, Borgna A (2018) Dispersed and high loading Ni catalyst stabilized in porous SiO_2 matrix for substituted natural gas production. Catal Today 299:193–200
[97] Li S, Tang H, Gong D, Ma Z, Liu Y (2017) Loading Ni/La_2O_3 on SiO_2 for CO methanation from syngas. Catal Today 297:298–307
[98] Naito M, Yokoyama T, Hosokawa K, Nogi K (2018) Nanoparticle technology handbook. Elsevier, Amsterdam
[99] Merkel TJ, Herlihy KP, Nunes J, Orgel RM, Rolland JP, DeSimone JM (2009) Scalable, shape-specific, top-down fabrication methods for the synthesis of engineered colloidal particles. Langmuir 26:13086–13096
[100] Wang X, Zhuang J, Peng Q, Li Y (2005) A general strategy for nanocrystal synthesis. Nature 437:121–124
[101] Peng Z, Yang H (2009) Designer platinum nanoparticles: control of shape, composition in alloy, nanostructure and electrocatalytic property. Nano Today 4:143–164
[102] Ferrando R, Jellinek J, Johnston RL (2008) Nanoalloys: from theory to applications of alloy clusters and nanoparticles. Chem Rev 108:845–910
[103] Dupont J, Scholten JD (2010) On the structural and surface properties of transition-metal nanoparticles in ionic liquids. Chem Soc Rev 39:1780–1804
[104] Gurav JL, Jung I-K, Park H-H, Kang ES, Nadargi DY (2010) Silica aerogel: synthesis and applications. J Nanomater 2010:1–11
[105] Jiang Z-J, Liu C-Y, Sun L-W (2005) Catalytic properties of silver nanoparticles supported on silica spheres. J Phys Chem B 109:1730–1735
[106] Hori K, Matsune H, Takenaka S, Kishida M (2006) Preparation of silica-coated Pt metal nanoparticles using microemulsion and their catalytic performance. Sci Technol Adv Mater 7:678–684
[107] He L, Lin Q, Liu Y, Huang Y (2014) Unique catalysis of Ni–Al hydrotalcite derived catalyst in CO_2 methanation: cooperative effect between Ni nanoparticles and a basic support. J Energy Chem 23:587–592
[108] Peng X, Cheng K, Kang J, Gu B, Yu X, Zhang Q, Wang Y (2015) Impact of hydrogenolysis on the selectivity of the Fischer–Tropsch synthesis: diesel fuel production over mesoporous Zeolite-Y-supported cobalt nanoparticles. Angew Chem Int Ed 54:4553–4556
[109] Cheng D, Jin W, Zhan X, Chen F (2016) Alumina membrane coated activated carbon: a novel strategy to enhance the mechanical properties of a solid catalyst. RSC Adv. 6:10229–10232
[110] Raybaud P, Chizallet C, Mager-Maury C, Digne M, Toulhoat H, Sautet P (2013) From γ-alumina to supported platinum nanoclusters in reforming conditions: 10 years of DFT modeling and beyond. J Catal 308:328–340
[111] Bagheri S, Muhd Julkapli N, Bee Abd Hamid S (2014) Titanium dioxide as a catalyst support in heterogeneous catalysis. Sci World J 2014:1–21. https://doi.org/10.1155/2014/727496
[112] Ntais S, Isaifan RJ, Baranova EA (2014) An X-ray photoelectron spectroscopy study of platinum nanoparticles on yttria-stabilized zirconia ionic support: insight into metal support interaction. Mater Chem Phys 148:673–679
[113] Mori K, Hara T, Mizugaki T, Ebitani K, Kaneda K (2004) Hydroxyapatite-supported palladium nanoclusters: a highly active heterogeneous catalyst for selective oxidation of alcohols by use of molecular oxygen. J Am Chem Soc 126:10657–10666
[114] Kantam ML, Chakravarti R, Pal U, Sreedhar B, Bhargava S (2008) nanocrystalline magnesium oxide-stabilized palladium (0): an efficient and reusable catalyst for selective reduction of nitro compounds. Adv Synth Catal 350:822–827
[115] Wang LC, Liu Y-M, Chen M, Cao Y, He H-Y, Fan K-N (2008) MnO_2 nanorod supported gold nanoparticles with enhanced activity for solvent-free aerobic alcohol oxidation. J Phys Chem C 112:6981–6987
[116] Wu H, Wang L, Zhang J, Shen Z, Zhao J (2011) Catalytic oxidation of benzene, toluene and p-xylene over colloidal gold supported on zinc oxide catalyst. Catal Commun 12:859–865
[117] Yamada Y, Yano K, Xu Q, Fukuzumi S (2010) Cu/Co_3O_4 nanoparticles as catalysts for hydrogen evolution from ammonia borane by hydrolysis. J Phys Chem C 114:16456–16462
[118] Pérez-Mayoral E, Calvino-Casilda V, Soriano E (2016) Metal-supported carbon-based materials: opportunities and challenges in the synthesis of valuable products. Catal Sci Technol 6:1265–1291
[119] Haber J, Block JH, Delmon B (1995) Manual of methods and procedures for catalyst characterization (Technical Report). Pure Appl Chem 67(1995):1257–1306
[120] Poncelet G, Martens J, Delmon B, Grange P, Jacobs PA (1995) Preparation of catalysts VI: scientific bases for the

preparation of heterogeneous catalysts. Elsevier, Amsterdam

[121] Ertl G, KnÃ H, Weitkamp J (2008) Preparation of solid catalysts. Wiley, New York

[122] Qiu S, Zhang X, Liu Q, Wang T, Zhang Q, Ma L (2013) A simple method to prepare highly active and dispersed Ni/MCM-41 catalysts by co-impregnation. Catal Commun 42:73–78

[123] Del Angel G, Bonilla A, Pena Y, Navarrete J, Fierro JLG, Acosta DR (2003) Effect of lanthanum on the catalytic properties of PtSn/γ-Al_2O_3 bimetallic catalysts prepared by successive impregnation and controlled surface reaction. J Catal 219:63–73

[124] Agnihotry SA, Sharma N, Deepa M (2002) Ion exchange derived precursor materials for deposition of WO_3 electrochromic films: spectroscopic investigations. J Sol-Gel Sci Technol 24:265–270

[125] Jones AC, Hitchman ML (2009) Chemical vapour deposition: precursors, processes and applications. Royal Society of Chemistry, Cambridge

[126] Schüth F, Hesse M, Unger KK (2008) In: Rostrup-Nielsen JR, Ertl G, Knözinger H, Schüth F, Weitkamp J (eds) Handbook of heterogeneous catalysis, pp 100–109

[127] Rochas C, Rinaudo M (1984) Mechanism of gel formation in κ-carrageenan. Biopolym Orig Res Biomol 23:735–745

[128] Murzin D (2013) Engineering catalysis. Walter de Gruyter, Berlin

[129] Taghvaei H, Heravi M, Rahimpour MR (2017) Synthesis of supported nanocatalysts via novel non-thermal plasma methods and its application in catalytic processes. Plasma Process Polym 14(1600204):1–20

[130] Di L, Zhang J, Zhang X (2018) A review on the recent progress, challenges, and perspectives of atmospheric-pressure cold plasma for preparation of supported metal catalysts. Plasma Process Polym 15(1700234):1–19

[131] Wang W, Wang Z, Wang J, Zhong C, Liu C (2017) Highly active and stable Pt–Pd alloy catalysts synthesized by room-temperature electron reduction for oxygen reduction reaction. Adv Sci 4:1600486-1–1600486-9

[132] Wang X, Xu W, Liu N, Yu Z, Li Y, Qiu J (2015) Synthesis of metallic Ni–Co/graphene catalysts with enhanced hydrodesulfurization activity via a low-temperature plasma approach. Catal Today 256:203–208

[133] Kozhevin VM, Yavsin DA, Kouznetsov VM, Busov VM, Mikushkin VM, Nikonov SY, Gurevich SA, Kolobov A (2000) Granulated metal nanostructure deposited by laser ablation accompanied by cascade drop fission. J Vac Sci Technol B Microelectron Nanom Struct Process Meas Phenom 18:1402–1405

[134] Lokteva ES, Golubina EV (2019) Metal–support interactions in the design of heterogeneous catalysts for redox processes. Pure Appl Chem 91:609–631

[135] Rostovshchikova TN, Lokteva ES, Kavalerskaya NE, Gurevich SA, Kozhevin VM, Yavsin DA (2013) Surface density of particles in the design of nanostructured catalysts. Theor Exp Chem 49:40–45

[136] Zhu Q-L, Xu Q (2016) Immobilization of ultrafine metal nanoparticles to high-surface-area materials and their catalytic applications. Chemistry 1:220–245

[137] Zhu Q-L, Xu Q (2014) Metal–organic framework composites. Chem Soc Rev 43:5468–5512

[138] Campelo JM, Luna D, Luque R, Marinas JM, Romero AA (2009) Sustainable preparation of supported metal nanoparticles and their applications in catalysis. ChemSusChem Chem Sustain Energy Mater 2:18–45

[139] Zhong H, Liu C, Wang Y, Wang R, Hong M (2016) Tailor-made porosities of fluorene-based porous organic frameworks for the pre-designable fabrication of palladium nanoparticles with size, location and distribution control. Chem Sci 7:2188–2194

[140] Aijaz A, Karkamkar A, Choi YJ, Tsumori N, Rönnebro E, Autrey T, Shioyama H, Xu Q (2012) Immobilizing highly catalytically active Pt nanoparticles inside the pores of metal–organic framework: a double solvents approach. J Am Chem Soc 134:13926–13929

[141] Chen Y, Zhu Q-L, Tsumori N, Xu Q (2015) Immobilizing highly catalytically active noble metal nanoparticles on reduced graphene oxide: a non-noble metal sacrificial approach. J Am Chem Soc 137:106–109

[142] Zhu Q-L, Tsumori N, Xu Q (2015) Immobilizing extremely catalytically active palladium nanoparticles to carbon nanospheres: a weakly-capping growth approach. J Am Chem Soc 137:11743–11748

[143] Maciver DS, Tobin HH, Barth RT (1963) Catalytic aluminas I. Surface chemistry of eta and gamma alumina. J Catal 2:485–497

[144] Rozita Y, Brydson R, Scott AJ (2010) An investigation of commercial gamma-Al_2O_3 nanoparticles. J Phys Conf Ser 241:12096-1–12096-4

[145] Krokidis X, Raybaud P, Gobichon AE, Rebours B, Euzen P, Toulhoat H (2001) Theoretical study of the dehydration process of boehmite to γ-alumina. J Phys Chem B 105:5121–5130

[146] Lippens BC, De Boer JH (1964) Study of phase transformations during calcination of aluminum hydroxides by selected area electron diffraction. Acta Crystallogr 17:1312–1321

[147] Vaezifar S, Faghihian H, Kamali M (2008) The influence of alumina used as a support on the catalytic properties of Pt/

Sn/Al_2O_3 systems in the dehydrogenation of isobutane. J Iran Chem Res 1:19–24

[148] Levin I, Bendersky LA, Brandon DG, Rühle M (1997) Cubic to monoclinic phase transformations in alumina. Acta Mater 45:3659–3669

[149] Halvarsson M (2016) CVD alumina. http://fy.chalmers.se/~f10mh/Halvarsson/CVD_alumina.html. Accessed 22 June 2016

[150] Ndolomingo MJ, Meijboom R (2016) Kinetics of the catalytic oxidation of morin on γ-Al_2O_3 supported gold nanoparticles and determination of gold nanoparticles surface area and sizes by quantitative ligand adsorption. Appl Catal B Environ 199:142–154

[151] Lippits MJ, Nieuwenhuys BE (2010) Direct conversion of ethanol into ethylene oxide on gold-based catalysts: effect of CeO_x and Li_2O addition on the selectivity. J Catal 274:142–149

[152] Trewyn BG, Nieweg JA, Zhao Y, Lin VS-Y (2008) Biocompatible mesoporous silica nanoparticles with different morphologies for animal cell membrane penetration. Chem Eng J 137:23–29

[153] Nandiyanto ABD, Kim S-G, Iskandar F, Okuyama K (2009) Synthesis of spherical mesoporous silica nanoparticles with nanometer-size controllable pores and outer diameters. Microporous Mesoporous Mater 120:447–453

[154] Vunain E, Ncube P, Jalama K, Meijboom R (2018) Confinement effect of rhodium(I) complex species on mesoporous MCM-41 and SBA-15: effect of pore size on the hydroformylation of 1-octene. J Porous Mater 25:303–320

[155] Xu J, Li K, Shi W, Li R, Peng T (2014) Rice-like brookite titania as an efficient scattering layer for nanosized anatase titania film-based dye-sensitized solar cells. J Power Sources 260:233–242

[156] Ruppert AM, Grams J, Jędrzejczyk M, Matras-Michalska J, Keller N, Ostojska K, Sautet P (2015) Titania-supported catalysts for levulinic acid hydrogenation: influence of support and its impact on γ-valerolactone yield. Chemsuschem 8:1538–1547

[157] Dai H (2001) Carbon nanotubes: synthesis, structure, properties, and applications. In: Dresselhaus MS, Dresselhaus G, Avouris P (eds) Topics in applied physics, vol 80. Springer, pp 29–54

[158] Ravat V, Nongwe I, Meijboom R, Bepete G, Coville NJ (2013) Pd on boron-doped hollow carbon spheres–PdO particle size and support effects. J Catal 305:36–45

[159] Lam E, Luong JHT (2014) Carbon materials as catalyst supports and catalysts in the transformation of biomass to fuels and chemicals. ACS Catal 4:3393–3410

[160] Gluhoi AC, Bogdanchikova N, Nieuwenhuys BE (2005) The effect of different types of additives on the catalytic activity of Au/Al_2O_3 in propene total oxidation: transition metal oxides and ceria. J Catal 229:154–162

[161] Lippits MJ (201) Catalytic behavior of Cu, Ag and Au nanoparticles. A comparison

[162] Lee J-K, Kung MC, Kung HH (2008) Cooperative catalysis: a new development in heterogeneous catalysis. Top Catal 49:136–144

[163] Lippits MJ, Gluhoi AC, Nieuwenhuys BE (2007) A comparative study of the effect of addition of CeO_x and Li_2O on γ-Al_2O_3 supported copper, silver and gold catalysts in the preferential oxidation of CO. Top Catal 44:159–165

[164] Gluhoi AC, Lin SD, Nieuwenhuys BE (2004) The beneficial effect of the addition of base metal oxides to gold catalysts on reactions relevant to air pollution abatement. Catal Today 90:175–181

[165] Gluhoi AC, Bogdanchikova N, Nieuwenhuys BE (2005) Alkali (earth)-doped Au/Al_2O_3 catalysts for the total oxidation of propene. J Catal 232:96–101

[166] Gluhoi AC, Nieuwenhuys BE (2007) Structural and chemical promoter effects of alkali (earth) and cerium oxides in CO oxidation on supported gold. Catal Today 122:226–232

[167] Gluhoi AC (2005) Fundamental studies focused on understanding of gold catalysis. Faculty of Mathematics & Natural Sciences, Institute of Chemistry, Leiden University, Leiden

[168] Gluhoi AC, Tang X, Marginean P, Nieuwenhuys BE (2006) Characterization and catalytic activity of unpromoted and alkali (earth)-promoted Au/Al_2O_3 catalysts for low-temperature CO oxidation. Top Catal 39:101–110

[169] de Miguel SR, Caballero Martinez A, Castro AA, Scelza OA (1996) Effect of lithium addition upon γ-Al2O3 for isopropanol dehydration. J Chem Technol Biotechnol Int Res Process Environ Clean Technol 65:131–136

[170] Lippits MJ, Iwema RRHB, Nieuwenhuys BE (2009) A comparative study of oxidation of methanol on γ-Al_2O_3 supported group IB metal catalysts. Catal Today 145:27–33

[171] Grisel RJH, Weststrate CJ, Goossens A, Crajé MWJ, Van der Kraan AM, Nieuwenhuys BE (2002) Oxidation of CO over $Au/MO_x/Al_2O_3$ multi-component catalysts in a hydrogen-rich environment. Catal Today 72:123–132

[172] Yang Q, Liu G, Liu Y (2017) Perovskite-type oxides as the catalyst precursors for preparing supported metallic nanocatalysts: a review. Ind Eng Chem Res 57:1–17

[173] Grabowska E (2016) Selected perovskite oxides: characterization, preparation and photocatalytic properties—a review. Appl. Catal. B Environ. 186:97–126

[174] Lam SM, Sin JC, Mohamed AR (2017) A newly emerging visible light-responsive $BiFeO_3$ perovskite for photocatalytic applications: a mini review. Mater Res Bull 90:15–30

[175] Chen J, He Z, Li G, An T, Shi H, Li Y (2017) Visible-light-enhanced photothermocatalytic activity of ABO_3-type perovskites for the decontamination of gaseous styrene. Appl Catal B Environ 209:146–154

[176] Pacchioni G, Freund HJ (2018) Controlling the charge state of supported nanoparticles in catalysis: lessons from model systems. Chem Soc Rev 47:8474–8502

[177] Tosoni S, Pacchioni G (2017) Trends in adhesion energies of gold on MgO (100), Rutile TiO_2 (110), and CeO_2 (111) surfaces: a comparative DFT study. J Phys Chem C 121:28328–28338

[178] Corma A, García H, Llabrés i Xamena FX (2010) Engineering metal organic frameworks for heterogeneous catalysis. Chem Rev 110:4606–4655

[179] Chen L, Xu Q (2019) Metal-organic framework composites for catalysis. Matter 1:57–89

[180] Cui Y, Li B, He H, Zhou W, Chen B, Qian G (2016) Metal–organic frameworks as platforms for functional materials. Acc Chem Res 49:483–493

[181] Zhu QL, Li J, Xu Q (2013) Immobilizing metal nanoparticles to metal–organic frameworks with size and location control for optimizing catalytic performance. J Am Chem Soc 135:10210–10213

[182] Hawxwell SM, Espallargas GM, Bradshaw D, Rosseinsky MJ, Prior TJ, Florence AJ, van de Streek J, Brammer L (2007) Ligand flexibility and framework rearrangement in a new family of porous metal–organic frameworks. Chem Commun 15:1532–1534

[183] Jiao L, Wang Y, Jiang H, Xu Q (2018) Metal–organic frameworks as platforms for catalytic applications. Adv Mater 30(1703663):1–23

[184] Xu C, Fang R, Luque R, Chen L, Li Y (2019) Functional metal–organic frameworks for catalytic applications. Coord Chem Rev 388:268–292

[185] Tu W, Xu Y, Yin S, Xu R (2018) Rational design of catalytic centers in crystalline frameworks. Adv Mater 30(1707582):1–29

[186] Kang Y-S, Lu Y, Chen K, Zhao Y, Wang P, Sun W-Y (2019) Metal–organic frameworks with catalytic centers: from synthesis to catalytic application. Coord Chem Rev 378:262–280

[187] Dang S, Zhu Q-L, Xu Q (2018) Nanomaterials derived from metal–organic frameworks. Nat Rev Mater 3(17075):1–14

[188] Chen L, Luque R, Li Y (2017) Controllable design of tunable nanostructures inside metal–organic frameworks. Chem Soc Rev 46:4614–4630

[189] O'Neill LD, Zhang H, Bradshaw D (2010) Macro-/microporous MOF composite beads. J Mater Chem 20:5720–5726

[190] Li G, Zhao S, Zhang Y, Tang Z (2018) Metal-organic frameworks encapsulating active nanoparticles as emerging composites for catalysis: recent progress and perspectives. Adv Mater 30(1800702):1–43

[191] Sun J-L, Chen Y-Z, Ge B-D, Li J-H, Wang G-M (2018) Three-shell Cu@Co@Ni nanoparticles stabilized with a metal–organic framework for enhanced tandem catalysis. ACS Appl Mater Interfaces 11:940–947

[192] Lu G, Li S, Guo Z, Farha OK, Hauser BG, Qi X, Wang Y, Wang X, Han S, Liu X (2012) Imparting functionality to a metal–organic framework material by controlled nanoparticle encapsulation. Nat Chem 4:310–316

[193] Yang Q, Xu Q, Yu S, Jiang H (2016) Pd nanocubes@ ZIF-8: integration of plasmon-driven photothermal conversion with a metal-organic framework for efficient and selective catalysis. Angew Chem Int Ed 55:3685–3689

[194] Chen Y-Z, Gu B, Uchida T, Liu J, Liu X, Ye B-J, Xu Q, Jiang H-L (2019) Location determination of metal nanoparticles relative to a metal–organic framework. Nat Commun 10(3462):1–10

[195] Gadipelli S, Travis W, Zhou W, Guo Z (2014) A thermally derived and optimized structure from ZIF-8 with giant enhancement in CO_2 uptake. Energy Environ Sci 7:2232–2238

[196] Liu B, Shioyama H, Akita T, Xu Q (2008) Metal-organic framework as a template for porous carbon synthesis. J Am Chem Soc 130:5390–5391

[197] Liu B, Han S, Tanaka K, Shioyama H, Xu Q (2009) Metal–organic framework (MOF) as a precursor for synthesis of platinum supporting zinc oxide nanoparticles. Bull Chem Soc Jpn 82:1052–1054

[198] Ruppert AM, Weckhuysen BM (2008) Metal–support interactions. In: Handbook of heterogeneous catalysis, pp 1178–1188

[199] Bingwa N, Patala R, Noh J-H, Ndolomingo MJ, Tetyana S, Bewana S, Meijboom R (2017) Synergistic effects of gold–palladium nanoalloys and reducible supports on the catalytic reduction of 4-nitrophenol. Langmuir 33:7086–7095

[200] Munoz M, de Pedro ZM, Casas JA, Rodriguez JJ (2014) Improved γ-alumina-supported Pd and Rh catalysts for hydrodechlorination of chlorophenols. Appl Catal A Gen 488:78–85

[201] Baeza JA, Calvo L, Gilarranz MA, Rodriguez JJ (2014) Effect of size and oxidation state of size-controlled rhodium nanoparticles on the aqueous-phase hydrodechlorination of 4-chlorophenol. Chem Eng J 240:271–280

[202] Gómez-Sainero LM, Seoane XL, Fierro JLG, Arcoya A (2002) Liquid-phase hydrodechlorination of CCl_4 to $CHCl_3$ on Pd/carbon catalysts: nature and role of Pd active species. J Catal 209:279–288

[203] Ordóñez S, Díaz E, Bueres RF, Asedegbega-Nieto E, Sastre H (2010) Carbon nanofibre-supported palladium catalysts as model hydrodechlorination catalysts. J Catal 272:158–168

[204] Baeza JA, Calvo L, Gilarranz MA, Mohedano AF, Casas JA, Rodriguez JJ (2012) Catalytic behavior of size-controlled palladium nanoparticles in the hydrodechlorination of 4-chlorophenol in aqueous phase. J Catal 293:85–93

[205] Ewbank JL, Kovarik L, Diallo FZ, Sievers C (2015) Effect of metal–support interactions in Ni/Al_2O_3 catalysts with low metal loading for methane dry reforming. Appl Catal A Gen 494:57–67

[206] Molina CB, Calvo L, Gilarranz MA, Casas JA, Rodriguez JJ (2009) Pd–Al pillared clays as catalysts for the hydrodechlorination of 4-chlorophenol in aqueous phase. J Hazard Mater 172:214–223

[207] Lokteva ES, Peristyy AA, Kavalerskaya NE, Golubina EV, Yashina LV, Rostovshchikova TN, Gurevich SA, Kozhevin VM, Yavsin DA, Lunin VV (2012) Laser electrodispersion as a new chlorine-free method for the production of highly effective metal-containing supported catalysts. Pure Appl Chem 84:495–508

[208] Cao S, Tao FF, Tang Y, Li Y, Yu J (2016) Size-and shape-dependent catalytic performances of oxidation and reduction reactions on nanocatalysts. Chem Soc Rev 45:4747–4765

[209] Bingwa N, Meijboom R (2014) Kinetic evaluation of dendrimer-encapsulated palladium nanoparticles in the 4-nitrophenol reduction reaction. J Phys Chem C 118:19849–19858

[210] Prestianni A, Ferrante F, Sulman EM, Duca D (2014) Density functional theory investigation on the nucleation and growth of small palladium clusters on a hyper-cross-linked polystyrene matrix. J Phys Chem C 118:21006–21013

[211] Ncube P, Bingwa N, Baloyi H, Meijboom R (2015) Catalytic activity of palladium and gold dendrimer-encapsulated nanoparticles for methylene blue reduction: a kinetic analysis. Appl Catal A Gen 495:63–71

[212] Cortese R, Schimmenti R, Prestianni A, Duca D (2018) DFT calculations on subnanometric metal catalysts: a short review on new supported materials. Theor Chem Acc 137(59):2–8

[213] Zhang C, Michaelides A, King DA, Jenkins SJ (2010) Positive charge states and possible polymorphism of gold nanoclusters on reduced ceria. J Am Chem Soc 132:2175–2182

[214] Tosoni S, Pacchioni G (2019) Oxide-supported gold clusters and nanoparticles in catalysis: a computational chemistry perspective. ChemCatChem 11:73–89

[215] Häkkinen H, Landman U (2000) Gold clusters (Au_N, $2 < \sim N < \sim 10$) and their anions. Phys Rev B 62:R2287–R2290

[216] Janiak C (2013) Ionic liquids for the synthesis and stabilization of metal nanoparticles. Zeitschrift Für Naturforsch B 68:1059–1089

[217] An K, Alayoglu S, Ewers T, Somorjai GA (2012) Colloid chemistry of nanocatalysts: a molecular view. J Colloid Interface Sci 373:1–13

[218] Lou XW, Yuan C, Rhoades E, Zhang Q, Archer LA (2006) Encapsulation and Ostwald ripening of Au and Au–Cl complex nanostructures in silica shells. Adv Funct Mater 16:1679–1684

[219] Ostwald WZ (1901) Blocking of Ostwald ripening allowing long-term stabilization. Phys Chem 37:385

[220] Kim M, Phan VN, Lee K (2012) Exploiting nanoparticles as precursors for novel nanostructure designs and properties. CrystEngComm 14:7535–7548

[221] Ma Z, Yu J, Dai S (2010) Preparation of inorganic materials using ionic liquids. Adv Mater 22:261–285

[222] Roucoux A, Schulz J, Patin H (2002) Reduced transition metal colloids: a novel family of reusable catalysts? Chem Rev 102:3757–3778

[223] Scholten JD, Leal BC, Dupont J (2011) Transition metal nanoparticle catalysis in ionic liquids. ACS Catal 2:184–200

[224] Hardacre C, Parvulescu V (2014) Catalysis in ionic liquirds: from catalyst synthesis to application. Royal Society of Chemistry, Cambridge

[225] Bönnemann H, Richards RM (2001) Nanoscopic metal particles–synthetic methods and potential applications. Eur J Inorg Chem 2001:2455–2480

[226] Pan C, Pelzer K, Philippot K, Chaudret B, Dassenoy F, Lecante P, Casanove M-J (2001) Ligand-stabilized ruthenium nanoparticles: synthesis, organization, and dynamics. J Am Chem Soc 123:7584–7593

[227] Neouze M-A (2010) About the interactions between nanoparticles and imidazolium moieties: emergence of original hybrid materials. J Mater Chem 20:9593–9607

[228] Vollmer C, Janiak C (2011) Naked metal nanoparticles from metal carbonyls in ionic liquids: easy synthesis and stabilization. Coord Chem Rev 255:2039–2057

[229] Weingärtner H (2008) Understanding ionic liquids at the molecular level: facts, problems, and controversies. Angew Chem Int Ed 47:654–670

[230] Xiao D, Rajian JR, Cady A, Li S, Bartsch RA, Quitevis EL (2007) Nanostructural organization and anion effects on the temperature dependence of the optical Kerr effect spectra of ionic liquids. J Phys Chem B 111:4669–4677

[231] Kuwabata S, Tsuda T, Torimoto T (2010) Room-temperature ionic liquid. A new medium for material production and analyses under vacuum conditions. J Phys Chem Lett 1:3177–3188

[232] Plechkova NV, Seddon KR (2008) Applications of ionic liquids in the chemical industry. Chem Soc Rev 37:123–150

[233] Ndolomingo MJ, Meijboom R (2016) Determination of the surface area and sizes of supported copper nanoparticles through organothiol adsorption–chemisorption. Appl Surf Sci 390:224–235

[234] Qian W, Texter J, Yan F (2017) Frontiers in poly (ionic liquid) s: syntheses and applications. Chem Soc Rev 46:1124–1159

[235] Vijayakrishna K, Charan KTP, Manojkumar K, Venkatesh S, Pothanagandhi N, Sivaramakrishna A, Mayuri P, Kumar AS, Sreedhar B (2016) Ni nanoparticles stabilized by poly (ionic liquids) as chemoselective and magnetically recoverable catalysts for transfer hydrogenation reactions of carbonyl compounds. ChemCatChem 8:1139–1145

[236] Charan KTP, Pothanagandhi N, Vijayakrishna K, Sivaramakrishna A, Mecerreyes D, Sreedhar B (2014) Poly (ionic liquids) as "smart" stabilizers for metal nanoparticles. Eur Polym J 60:114–122

[237] Zimmerman SC (1999) Dendritic macromolecules: concepts, syntheses, perspectives. J Chem Educ 76:31

[238] Scott RWJ, Wilson OM, Crooks RM (2005) Synthesis, characterization, and applications of dendrimer-encapsulated nanoparticles. J Phys Chem B 109:692–704

[239] Kim Y-G, Oh S-K, Crooks RM (2004) Preparation and characterization of 1–2 nm dendrimer-encapsulated gold nanoparticles having very narrow size distributions. Chem Mater 16:167–172

[240] Deraedt C, Ye R, Ralston WT, Toste FD, Somorjai GA (2017) Dendrimer-stabilized metal nanoparticles as efficient catalysts for reversible dehydrogenation/hydrogenation of N-heterocycles. J Am Chem Soc 139:18084–18092

[241] Noh J-H, Meijboom R (2014) Catalytic evaluation of dendrimer-templated Pd nanoparticles in the reduction of 4-nitrophenol using Langmuir-Hinshelwood kinetics. Appl Surf Sci 320:400–413

[242] Krüger C, Agarwal S, Greiner A (2008) Stoichiometric functionalization of gold nanoparticles in solution through a free radical polymerization approach. J Am Chem Soc 130:2710–2711

[243] Bronger R, Le TD, Bastin S, García-Antón J, Citadelle C, Chaudret B, Lecante P, Igau A, Philippot K (2011) Multisite coordination N-phosphanylamidine ligands as stabilizers for the synthesis of ruthenium nanoparticles. New J Chem 35:2653–2660

[244] Jadhav SA, Brunella V, Scalarone D (2015) Polymerizable ligands as stabilizers for nanoparticles. Part Part Syst Charact 32:417–428

[245] Khlebtsov BN, Khlebtsov NG (2011) On the measurement of gold nanoparticle sizes by the dynamic light scattering method. Colloid J 73:118–127

[246] Bienert R, Emmerling F, Thünemann AF (2009) The size distribution of'gold standard'nanoparticles. Anal Bioanal Chem 395:1651–1660

[247] Pyrz WD, Buttrey DJ (2008) Particle size determination using TEM: a discussion of image acquisition and analysis for the novice microscopist. Langmuir 24:11350–11360

[248] Goldstein JI, Newbury DE, Michael JR, Ritchie NWM, Scott JHJ, Joy DC (2017) Scanning electron microscopy and X-ray microanalysis. Springer, Berlin

[249] Willets KA, Van Duyne RP (2007) Localized surface plasmon resonance spectroscopy and sensing. Annu Rev Phys Chem 58:267–297

[250] Guha S, Li M, Tarlov MJ, Zachariah MR (2012) Electrospray–differential mobility analysis of bionanoparticles. Trends Biotechnol 30:291–300

[251] Couteau O, Roebben G (2011) Measurement of the size of spherical nanoparticles by means of atomic force microscopy. Meas Sci Technol 22(065101):1–8

[252] Haiss W, Thanh NTK, Aveyard J, Fernig DG (2007) Determination of size and concentration of gold nanoparticles from UV–Vis spectra. Anal Chem 79:4215–4221

[253] Janz A, Köckritz A, Yao L, Martin A (2010) Fundamental calculations on the surface area determination of supported gold nanoparticles by alkanethiol adsorption. Langmuir 26:6783–6789

[254] Perumal S, Hofmann A, Scholz N, Rühl E, Graf C (2011) Kinetics study of the binding of multivalent ligands on size-selected gold nanoparticles. Langmuir 27:4456–4464

[255] Gadogbe M, Ansar SM, He G, Collier WE, Rodriguez J, Liu D, Chu I-W, Zhang D (2013) Determination of colloidal gold nanoparticle surface areas, concentrations, and sizes through quantitative ligand adsorption. Anal Bioanal Chem 405:413–422

[256] Sing KSW (1998) Adsorption methods for the characterization of porous materials. Adv Colloid Interface Sci 76:3–11

[257] Brunauer S, Emmett PH, Teller E (1938) Adsorption of gases in multimolecular layers. J Am Chem Soc 60:309–319

[258] Anderson JA (2012) Supported metals in catalysis. World Scientific, Singapore

[259] Berndt H, Pitsch I, Evert S, Struve K, Pohl M-M, Radnik J, Martin A (2003) Oxygen adsorption on Au/Al_2O_3 catalysts

and relation to the catalytic oxidation of ethylene glycol to glycolic acid. Appl Catal A Gen 244:169–179

[260] Chiorino A, Manzoli M, Menegazzo F, Signoretto M, Vindigni F, Pinna F, Boccuzzi F (2009) New insight on the nature of catalytically active gold sites: quantitative CO chemisorption data and analysis of FTIR spectra of adsorbed CO and of isotopic mixtures. J Catal 262:169–176

[261] Clément M, Ménard H, Rowntree PA (2008) Determination of the surface area of Pd and nanometric Au aggregates supported on a micrometric solid support by thiol adsorption and GC–MS. Langmuir 24:8045–8049

[262] Van Vegten N, Haider P, Maciejewski M, Krumeich F, Baiker A (2009) Chemisorption of methyl mercaptane on titania-supported Au nanoparticles: viability of Au surface area determination. J Colloid Interface Sci 339:310–316

[263] Ulman A (1996) Formation and structure of self-assembled monolayers. Chem Rev 96:1533–1554

[264] Dubois LH, Nuzzo RG (1992) Synthesis, structure, and properties of model organic surfaces. Annu Rev Phys Chem 43:437–463

[265] Hinterwirth H, Kappel S, Waitz T, Prohaska T, Lindner W, Lämmerhofer M (2013) Quantifying thiol ligand density of self-assembled monolayers on gold nanoparticles by inductively coupled plasma–mass spectrometry. ACS Nano 7:1129–1136

[266] Mahmoud MA, Garlyyev B, El-Sayed MA (2013) Determining the mechanism of solution metallic nanocatalysis with solid and hollow nanoparticles: homogeneous or heterogeneous. J Phys Chem C 117:21886–21893

[267] Folkers JP, Gorman CB, Laibinis PE, Buchholz S, Whitesides GM, Nuzzo RG (1995) Self-assembled monolayers of long-chain hydroxamic acids on the native oxide of metals. Langmuir 11:813–824

[268] Haider P, Baiker A (2007) Gold supported on Cu–Mg–Al-mixed oxides: strong enhancement of activity in aerobic alcohol oxidation by concerted effect of copper and magnesium. J Catal 248:175–187

[269] Punniyamurthy T, Velusamy S, Iqbal J (2005) Recent advances in transition metal catalyzed oxidation of organic substrates with molecular oxygen. Chem Rev 105:2329–2364

[270] Herves P, Perez-Lorenzo M, Liz-Marzan LM, Dzubiella J, Lu Y, Ballauff M (2012) Catalysis by metallic nanoparticles in aqueous solution: model reactions. Chem Soc Rev 41:5577–5587

[271] Zhang W, Yang Z, Wang X, Zhang Y, Wen X, Yang S (2006) Large-scale synthesis of β-MnO_2 nanorods and their rapid and efficient catalytic oxidation of methylene blue dye. Catal Commun 7:408–412

[272] Grabowski LR, Van Veldhuizen EM, Pemen AJM, Rutgers WR (2007) Breakdown of methylene blue and methyl orange by pulsed corona discharge. Plasma Sources Sci Technol 16:226–232

[273] Zhang L, Nie Y, Hu C, Hu X (2011) Decolorization of methylene blue in layered manganese oxide suspension with H_2O_2. J Hazard Mater 190:780–785

[274] Salem IA (2000) Kinetics of the oxidative color removal and degradation of bromophenol blue with hydrogen peroxide catalyzed by copper(II)-supported alumina and zirconia. Appl Catal B Environ 28:153–162

[275] El-Dein AM, Libra JA, Wiesmann U (2003) Mechanism and kinetic model for the decolorization of the azo dye Reactive Black 5 by hydrogen peroxide and UV radiation. Chemosphere 52:1069–1077

[276] Asahi R, Morikawa T, Ohwaki T, Aoki K, Taga Y (2001) Visible-light photocatalysis in nitrogen-doped titanium oxides. Science 293:269–271

[277] Zhou L, Song W, Chen Z, Yin G (2013) Degradation of organic pollutants in wastewater by bicarbonate-activated hydrogen peroxide with a supported cobalt catalyst. Environ Sci Technol 47:3833–3839

[278] Sopajaree K (1997) Photocatalytic oxidation of methylene blue by titanium dioxide in an integrated photoreactor-membrane filtration unit. Doctoral dissertation, University of Texas at Arlington

[279] Mills A, Davies RH, Worsley D (1993) Water purification by semiconductor photocatalysis. Chem Soc Rev 22:417–425

[280] Salem IA, El-Maazawi MS (2000) Kinetics and mechanism of color removal of methylene blue with hydrogen peroxide catalyzed by some supported alumina surfaces. Chemosphere 41:1173–1180

[281] Ilunga AK, Meijboom R (2016) Catalytic oxidation of methylene blue by dendrimer encapsulated silver and gold nanoparticles. J Mol Catal A Chem 411:48–60

[282] Elango G, Roopan SM (2016) Efficacy of SnO_2 nanoparticles toward photocatalytic degradation of methylene blue dye. J Photochem Photobiol B Biol 155:34–38

[283] Liu Y, Jin W, Zhao Y, Zhang G, Zhang W (2017) Enhanced catalytic degradation of methylene blue by α-Fe_2O_3/-graphene oxide via heterogeneous photo-Fenton reactions. Appl Catal B Environ 206:642–652

[284] Atchudan R, Edison TNJI, Perumal S, Karthikeyan D, Lee YR (2016) Facile synthesis of zinc oxide nanoparticles decorated graphene oxide composite via simple solvothermal route and their photocatalytic activity on methylene blue degradation. J Photochem Photobiol B Biol 162:500–510

[285] Edison TNJI, Atchudan R, Lee YR (2016) Optical sensor for dissolved ammonia through the green synthesis of silver nanoparticles by fruit extract of Terminalia chebula. J Clust Sci 27:683–690

[286] Sriskandakumar T, Opembe N, Chen C-H, Morey A, King'ondu C, Suib SL (2009) Green decomposition of organic dyes using octahedral molecular sieve manganese oxide catalysts. J Phys Chem A 113:1523–1530

[287] Nuengmatcha P, Chanthai S, Mahachai R, Oh WC (2016) Sonocatalytic performance of ZnO/graphene/TiO_2 nanocomposite for degradation of dye pollutants (methylene blue, texbrite BAC-L, texbrite BBU-L and texbrite NFW-L) under ultrasonic irradiation. Dye Pigment 134:487–497

[288] Wieprecht T, Heinz U, Xia J, Schlingloff G, Dannacher J (2004) Terpyridine-manganese complexes: a new class of bleach catalysts for detergent applications. J Surfactants Deterg 7:59–66

[289] Dannacher JJ (2006) Catalytic bleach: most valuable applications for smart oxidation chemistry. J Mol Catal A Chem 251:159–176

[290] Colombini MP, Andreotti A, Baraldi C, Degano I, Łucejko JJ (2007) Colour fading in textiles: a model study on the decomposition of natural dyes. Microchem J 85:174–182

[291] Osman A, Makris DP (2011) Oxidation of morin (2′,3,4′,5,7-pentahydroxylavone) with a peroxidase homogenate from onion. Int Food Res J 18:1085–1089

[292] Topalovic T (2007) Catalytic bleaching of cotton: molecular and macroscopic aspects. University of Twente, Twente

[293] Polzer F, Wunder S, Lu Y, Ballauff M (2012) Oxidation of an organic dye catalyzed by MnO_x nanoparticles. J Catal 289:80–87

[294] Nemanashi M, Meijboom R (2015) Catalytic behavior of different sizes of dendrimer-encapsulated Au_n nanoparticles in the oxidative degradation of morin with H_2O_2. Langmuir 31:9041–9053

[295] Bingwa N, Bewana S, Haumann M, Meijboom R (2017) Revisiting kinetics of morin oxidation: surface kinetics analysis. Appl Surf Sci 426:497–503

[296] Ilunga AK, Legodi IR, Gumbi S, Meijboom R (2018) Isothermic adsorption of morin onto the reducible mesoporous manganese oxide materials surface. Appl Catal B Environ 224:928–939

[297] Bingwa N, Bewana S, Ndolomingo MJ, Mawila N, Mogudi B, Ncube P, Carleschi E, Doyle BP, Haumann M, Meijboom R (2018) Effect of alkali and alkaline earth metal dopants on catalytic activity of mesoporous cobalt oxide evaluated using a model reaction. Appl Catal A Gen 555:189–195

[298] Yamaguchi K, Mori K, Mizugaki T, Ebitani K, Kaneda K (2000) Creation of a monomeric Ru species on the surface of hydroxyapatite as an efficient heterogeneous catalyst for aerobic alcohol oxidation. J Am Chem Soc 122:7144–7145

[299] Mallat T, Baiker A (1994) Oxidation of alcohols with molecular oxygen on platinum metal catalysts in aqueous solutions. Catal Today 19:247–283

[300] Besson M, Gallezot P (2000) Selective oxidation of alcohols and aldehydes on metal catalysts. Catal Today 57:127–141

[301] Crozon A-B, Besson M, Gallezot P (1998) Oxidation of 9-decen-1-ol (rosalva) by air in aqueous media on platinum catalysts. New J Chem 22:269–273

[302] Della Pina C, Falletta E, Prati L, Rossi M (2008) Selective oxidation using gold. Chem Soc Rev 37:2077–2095

[303] Pagliaro M, Campestrini S, Ciriminna R (2005) Ru-based oxidation catalysis. Chem Soc Rev 34:837–845

[304] Schultz MJ, Adler RS, Zierkiewicz W, Privalov T, Sigman MS (2005) Using mechanistic and computational studies to explain ligand effects in the palladium-catalyzed aerobic oxidation of alcohols. J Am Chem Soc 127:8499–8507

[305] ten Brink G-J, Arends IWCE, Sheldon RA (2000) Green, catalytic oxidation of alcohols in water. Science 287:1636–1639

[306] Vazylyev M, Sloboda-Rozner D, Haimov A, Maayan G, Neumann R (2005) Strategies for oxidation catalyzed by polyoxometalates at the interface of homogeneous and heterogeneous catalysis. Top Catal 34:93–99

[307] Bolm C, Beller M (2004) Transition metals for organic synthesis. Wiley-VCH, Weinheim

[308] Xiao S, Zhang C, Chen R, Chen F (2015) Selective oxidation of benzyl alcohol to benzaldehyde with H_2O_2 in water on epichlorohydrin-modified Fe_3O_4 microspheres. New J Chem 39:4924–4932

[309] Choudhary VR, Dumbre DK, Uphade BS, Narkhede VS (2004) Solvent-free oxidation of benzyl alcohol to benzaldehyde by tert-butyl hydroperoxide using transition metal containing layered double hydroxides and/or mixed hydroxides. J Mol Catal A Chem 215:129–135

[310] Miedziak PJ, He Q, Edwards JK, Taylor SH, Knight DW, Tarbit B, Kiely CJ, Hutchings GJ (2011) Oxidation of benzyl alcohol using supported gold–palladium nanoparticles. Catal Today 163:47–54

[311] Enache DI, Edwards JK, Landon P, Solsona-Espriu B, Carley AF, Herzing AA, Watanabe M, Kiely CJ, Knight DW, Hutchings GJ (2006) Solvent-free oxidation of primary alcohols to aldehydes using Au-Pd/TiO_2 catalysts. Science 311:362–365

[312] Meenakshisundaram S, Nowicka E, Miedziak PJ, Brett GL, Jenkins RL, Dimitratos N, Taylor SH, Knight DW, Bethell

D, Hutchings GJ (2010) Oxidation of alcohols using supported gold and gold–palladium nanoparticles. Faraday Discuss 145:341–356

[313] Kumar A, Kumar VP, Srikanth A, Vishwanathan V, Chary KVR (2016) Vapor phase oxidation of benzyl alcohol over nano Au/SBA-15 catalysts: effect of preparation methods. Catal Lett 146:35–46

[314] Wang C, Wu X, Xiao J (2008) Broader, greener, and more efficient: recent advances in asymmetric transfer hydrogenation. Chem Asian J 3:1750–1770

[315] Wu X, Xiao J (2007) Aqueous-phase asymmetric transfer hydrogenation of ketones—a greener approach to chiral alcohols. Chem Commun 24:2449–2466

[316] Clapham SE, Hadzovic A, Morris RH (2004) Mechanisms of the H_2-hydrogenation and transfer hydrogenation of polar bonds catalyzed by ruthenium hydride complexes. Coord Chem Rev 248:2201–2237

[317] Vincent T, Guibal E (2003) Chitosan-supported palladium catalyst. 3. Influence of experimental parameters on nitrophenol degradation. Langmuir 19:8475–8483

[318] Feng ZV, Lyon JL, Croley JS, Crooks RM, Vanden Bout DA, Stevenson KJ (2009) Synthesis and catalytic evaluation of dendrimer-encapsulated Cu nanoparticles. An undergraduate experiment exploring catalytic nanomaterials. J Chem Educ 86:368–372

[319] Lee J, Park JC, Song H (2008) A nanoreactor framework of a Au@SiO_2 yolk/shell structure for catalytic reduction of p-nitrophenol. Adv Mater 20:1523–1528

[320] Evangelista V, Acosta B, Miridonov S, Smolentseva E, Fuentes S, Simakov A (2015) Highly active Au-CeO_2@ZrO_2 yolk–shell nanoreactors for the reduction of 4-nitrophenol to 4-aminophenol. Appl Catal B Environ 166:518–528

[321] Nemanashi M, Meijboom R (2013) Synthesis and characterization of Cu, Ag and Au dendrimer-encapsulated nanoparticles and their application in the reduction of 4-nitrophenol to 4-aminophenol. J Colloid Interface Sci 389:260–267

[322] Antonels NC, Meijboom R (2013) Preparation of well-defined dendrimer Encapsulated ruthenium nanoparticles and their evaluation in the reduction of 4-nitrophenol according to the Langmuir-Hinshelwood approach. Langmuir 29:13433–13442

[323] An K, Alayoglu S, Musselwhite N, Plamthottam S, Melaet G, Lindeman AE, Somorjai GA (2013) Enhanced CO oxidation rates at the interface of mesoporous oxides and Pt nanoparticles. J Am Chem Soc 135:16689–16696

[324] Karim W, Spreafico C, Kleibert A, Gobrecht J, VandeVondele J, Ekinci Y, van Bokhoven JA (2017) Catalyst support effects on hydrogen spillover. Nature 541:68–71

[325] Wang Q, Zhang Y, Zhou Y, Zhang Z, Xu Y, Zhang C, Sheng X (2015) Synthesis of dendrimer-templated Pt nanoparticles immobilized on mesoporous alumina for p-nitrophenol reduction. New J Chem 39:9942–9950

[326] El-Bahy ZM (2013) Preparation and characterization of Pt-promoted NiY and CoY catalysts employed for 4-nitrophenol reduction. Appl Catal A Gen 468:175–183

[327] Lin F, Doong R (2011) Bifunctional Au–Fe_3O_4 heterostructures for magnetically recyclable catalysis of nitrophenol reduction. J Phys Chem C 115:6591–6598

[328] Zhou Z, Kooi S, Flytzani-Stephanopoulos M, Saltsburg H (2008) The role of the interface in CO oxidation on Au/CeO_2 multilayer nanotowers. Adv Funct Mater 18:2801–2807

[329] Rath PC, Saikia D, Mishra M, Kao H-M (2018) Exceptional catalytic performance of ultrafine Cu_2O nanoparticles confined in cubic mesoporous carbon for 4-nitrophenol reduction. Appl Surf Sci 427:1217–1226

[330] Morère J, Tenorio MJ, Torralvo MJ, Pando C, Renuncio JAR, Cabanas A (2011) Deposition of Pd into mesoporous silica SBA-15 using supercritical carbon dioxide. J Supercrit Fluids 56:213–222

[331] Liu X, Zhao X, Zhu L, Liu N, Tian T (2018) Palladium nanoparticles covered on amine-functionalized mesoporous hollow SiO_2 spheres for the reduction of 4-nitrophenol. Catal Lett 148:173–180

[332] Chow LCH (2011) China's energy future: a framing comment. Eurasian Geogr Econ 52:523–528

[333] Hassan H, Lim JK, Hameed BH (2016) Recent progress on biomass co-pyrolysis conversion into high-quality bio-oil. Bioresour Technol 221:645–655

[334] Gallezot P (2012) Conversion of biomass to selected chemical products. Chem Soc Rev 41:1538–1558

[335] Bond JQ, Alonso DM, Wang D, West RM, Dumesic JA (2010) Integrated catalytic conversion of γ-valerolactone to liquid alkenes for transportation fuels. Science 327:1110–1114

[336] Serrano-Ruiz JC, West RM, Dumesic JA (2010) Catalytic conversion of renewable biomass resources to fuels and chemicals. Annu Rev Chem Biomol Eng 1:79–100

[337] Biddy MJ, Davis R, Humbird D, Tao L, Dowe N, Guarnieri MT, Linger JG, Karp EM, Salvachúa D, Vardon DR (2016) The techno-economic basis for coproduct manufacturing to enable hydrocarbon fuel production from lignocellulosic biomass. ACS Sustain Chem Eng 4:3196–3211

[338] Luo W, Sankar M, Beale AM, He Q, Kiely CJ, Bruijnincx PCA, Weckhuysen BM (2015) High performing and stable supported nano-alloys for the catalytic hydrogenation of levulinic acid to γ-valerolactone. Nat Commun 6(6540):1–10

[339] Li W, Xie J-H, Lin H, Zhou Q-L (2012) Highly efficient hydrogenation of biomass-derived levulinic acid to γ-valerolactone catalyzed by iridium pincer complexes. Green Chem 14:2388–2390

[340] Climent MJ, Corma A, Iborra S (2014) Conversion of biomass platform molecules into fuel additives and liquid hydrocarbon fuels. Green Chem 16:516–547

[341] Geilen F, Engendahl B, Harwardt A, Marquardt W, Klankermayer J, Leitner W (2010) Selective and flexible transformation of biomass-derived platform chemicals by a multifunctional catalytic system. Angew Chem 122:5642–5646

[342] Yan Z, Lin L, Liu S (2009) Synthesis of γ-valerolactone by hydrogenation of biomass-derived levulinic acid over Ru/C catalyst. Energy Fuels 23:3853–3858

[343] Amenuvor G, Makhubela BCE, Darkwa J (2016) Efficient solvent-free hydrogenation of levulinic acid to γ-valerolactone by pyrazolylphosphite and pyrazolylphosphinite ruthenium(II) complexes. ACS Sustain Chem Eng 4:6010–6018

[344] Hu Q, Yang L, Fan G, Li F (2016) Hydrogenation of biomass-derived compounds containing a carbonyl group over a copper-based nanocatalyst: insight into the origin and influence of surface oxygen vacancies. J Catal 340:184–195

[345] Kong X, Wu S, Jin Y, Liu L, Liu J (2017) Continuous hydrogenation of ethyl levulinate to γ-valerolactone over Cu-Zn/ZrO_2 catalyst with alumina binder. Energy Fuels 31:12232–12237

[346] Stevens JG, Bourne RA, Twigg MV, Poliakoff M (2010) Real-time product switching using a twin catalyst system for the hydrogenation of furfural in supercritical CO_2. Angew Chem 122:9040–9043

[347] Yan K, Liao J, Wu X, Xie X (2013) A noble-metal free Cu-catalyst derived from hydrotalcite for highly efficient hydrogenation of biomass-derived furfural and levulinic acid. RSC Adv 3:3853–3856

[348] Li Z, Zuo M, Jiang Y, Tang X, Zeng X, Sun Y, Lei T, Lin L (2016) Stable and efficient CuCr catalyst for the solvent-free hydrogenation of biomass derived ethyl levulinate to γ-valerolactone as potential biofuel candidate. Fuel 175:232–239

[349] Shimizu K, Kanno S, Kon K (2014) Hydrogenation of levulinic acid to γ-valerolactone by Ni and MoO_x co-loaded carbon catalysts. Green Chem 16:3899–3903

[350] Nemanashi M, Noh J-H, Meijboom R (2018) Hydrogenation of biomass-derived levulinic acid to γ-valerolactone catalyzed by mesoporous supported dendrimer-derived Ru and Pt catalysts: an alternative method for the production of renewable biofuels. Appl Catal A Gen 550:77–89

[351] Piskun AS, de Haan JE, Wilbers E, van de Bovenkamp HH, Tang Z, Heeres HJ (2016) Hydrogenation of levulinic acid to γ-valerolactone in water using millimeter sized supported Ru catalysts in a packed bed reactor. Acs Sustain Chem Eng 4:2939–2950

[352] Dutta S (2012) Catalytic materials that improve selectivity of biomass conversions. RSC Adv 2:12575–12593

[353] Omoruyi U, Page S, Hallett J, Miller PW (2016) Homogeneous catalyzed reactions of levulinic acid: to γ-valerolactone and beyond. Chemsuschem 9:2037–2047

[354] Xie C, Song J, Zhou B, Hu J, Zhang Z, Zhang P, Jiang Z, Han B (2016) Porous hafnium phosphonate: novel heterogeneous catalyst for conversion of levulinic acid and esters into γ-valerolactone. ACS Sustain Chem Eng 4:6231–6236

[355] Wright WRH, Palkovits R (2012) Development of heterogeneous catalysts for the conversion of levulinic acid to γ-valerolactone. Chemsuschem 5:1657–1667

[356] Baijun L, Lianhai L, Bingchun W, Tianxi C, Iwatani K (1998) Liquid phase selective hydrogenation of furfural on Raney nickel modified by impregnation of salts of heteropolyacids. Appl Catal A Gen 171:117–122

[357] Sitthisa S, Resasco DE (2011) Hydrodeoxygenation of furfural over supported metal catalysts: a comparative study of Cu, Pd and Ni. Catal Lett 141:784–791

[358] Zhong H, Li Q, Liu J, Yao G, Wang J, Zeng X, Huo Z, Jin F (2017) New method for highly efficient conversion of biomass-derived levulinic acid to γ-valerolactone in water without precious metal catalysts. ACS Sustain Chem Eng 5:6517–6523

[359] Wang S, Huang H, Dorcet V, Roisnel T, Bruneau C, Fischmeister C (2017) Efficient Iridium catalysts for base-free hydrogenation of levulinic acid. Organometallics 36:3152–3162

[360] Pileidis FD, Titirici M (2016) Levulinic acid biorefineries: new challenges for efficient utilization of biomass. Chemsuschem 9:562–582

[361] Zhang J, Chen J, Guo Y, Chen L (2015) Effective upgrade of levulinic acid into γ-valerolactone over an inexpensive and magnetic catalyst derived from hydrotalcite precursor. ACS Sustain Chem Eng 3:1708–1714

[362] Horváth IT, Mehdi H, Fábos V, Boda L, Mika LT (2008) γ-Valerolactone—a sustainable liquid for energy and carbon-based chemicals. Green Chem 10:238–242

[363] Alonso DM, Wettstein SG, Dumesic JA (2013) Gamma-valerolactone, a sustainable platform molecule derived from lignocellulosic biomass. Green Chem 15:584–595

[364] Tang X, Zeng X, Li Z, Hu L, Sun Y, Liu S, Lei T, Lin L (2014) Production of γ-valerolactone from lignocellulosic biomass for sustainable fuels and chemicals supply. Renew Sustain Energy Rev 40:608–620

[365] Hengne AM, Rode CV (2012) Cu–ZrO_2 nanocomposite catalyst for selective hydrogenation of levulinic acid and its ester to γ-valerolactone. Green Chem 14:1064–1072

[366] Yang Y, Gao G, Zhang X, Li F (2014) Facile fabrication of composition-tuned Ru–Ni bimetallics in ordered mesoporous carbon for levulinic acid hydrogenation. ACS Catal 4:1419–1425

[367] Delhomme C, Schaper LA, Zhang-Preße M, Raudaschl-Sieber G, Weuster-Botz D, Kühn FE (2013) Catalytic hydrogenation of levulinic acid in aqueous phase. J Organomet Chem 724:297–299

[368] Tukacs JM, Király D, Strádi A, Novodarszki G, Eke Z, Dibó G, Kégl T, Mika LT (2012) Efficient catalytic hydrogenation of levulinic acid: a key step in biomass conversion. Green Chem 14:2057–2065

[369] Fábos V, Mika LT, Horváth IT (2014) Selective conversion of levulinic and formic acids to γ-valerolactone with the shvo catalyst. Organometallics 33:181–187

[370] Joo F, Tóth Z, Beck MT (1977) Homogeneous hydrogenations in aqueous solutions catalyzed by transition metal phosphine complexes. Inorg Chim Acta 25:L61–L62

[371] Deng L, Zhao Y, Li J, Fu Y, Liao B, Guo Q (2010) Conversion of levulinic acid and formic acid into γ-valerolactone over heterogeneous catalysts. Chemsuschem 3:1172–1175

[372] Wang J, Jaenicke S, Chuah G-K (2014) Zirconium-Beta zeolite as a robust catalyst for the transformation of levulinic acid to γ-valerolactone via Meerwein–Ponndorf–Verley reduction. RSC Adv 4:13481–13489

[373] Al-Shaal MG, Wright WRH, Palkovits R (2012) Exploring the ruthenium catalysed synthesis of γ-valerolactone in alcohols and utilisation of mild solvent-free reaction conditions. Green Chem 14:1260–1263

[374] Galletti AMR, Antonetti C, De Luise V, Martinelli M (2012) A sustainable process for the production of γ-valerolactone by hydrogenation of biomass-derived levulinic acid. Green Chem 14:688–694

[375] Selva M, Gottardo M, Perosa A (2012) Upgrade of biomass-derived levulinic acid via Ru/C-catalyzed hydrogenation to γ-valerolactone in aqueous–organic–ionic liquids multiphase systems. ACS Sustain Chem Eng 1:180–189

[376] Tan J, Cui J, Deng T, Cui X, Ding G, Zhu Y, Li Y (2015) Water-promoted hydrogenation of levulinic acid to γ-valerolactone on supported ruthenium catalyst. ChemCatChem 7:508–512

[377] Braden DJ, Henao CA, Heltzel J, Maravelias CC, Dumesic JA (2011) Production of liquid hydrocarbon fuels by catalytic conversion of biomass-derived levulinic acid. Green Chem 13:1755–1765

[378] Wettstein SG, Bond JQ, Alonso DM, Pham HN, Datye AK, Dumesic JA (2012) RuSn bimetallic catalysts for selective hydrogenation of levulinic acid to γ-valerolactone. Appl Catal B Environ 117:321–329

[379] Zhu S, Zhu Y, Hao S, Zheng H, Mo T, Li Y (2012) One-step hydrogenolysis of glycerol to biopropanols over Pt–$H_4SiW_{12}O_{40}/ZrO_2$ catalysts. Green Chem 14:2607–2616

[380] Wang Y, Zhou J, Guo X (2015) Catalytic hydrogenolysis of glycerol to propanediols: a review. RSC Adv 5:74611–74628

[381] Vasiliadou ES, Eggenhuisen TM, Munnik P, De Jongh PE, De Jong KP, Lemonidou AA (2014) Synthesis and performance of highly dispersed Cu/SiO_2 catalysts for the hydrogenolysis of glycerol. Appl Catal B Environ 145:108–119

[382] Xiao Z, Jin S, Wang X, Li W, Wang J, Liang C (2012) Preparation, structure and catalytic properties of magnetically separable Cu–Fe catalysts for glycerol hydrogenolysis. J Mater Chem 22:16598–16605

[383] van Ryneveld E, Mahomed AS, van Heerden PS, Green MJ, Friedrich HB (2011) A catalytic route to lower alcohols from glycerol using Ni-supported catalysts. Green Chem 13:1819–1827

[384] Marinoiu A, Ionita G, Gáspár CL, Cobzaru C, Marinescu D, Teodorescu C, Oprea S (2009) Selective hydrogenolysis of glycerol to propylene glycol using heterogeneous catalysts. React Kinet Mech Catal 99:111–118

[385] Marinoiu A, Ionita G, Gáspár C-L, Cobzaru C, Oprea S (2009) Glycerol hydrogenolysis to propylene glycol. React Kinet Catal Lett 97:315–320

[386] Amada Y, Shinmi Y, Koso S, Kubota T, Nakagawa Y, Tomishige K (2011) Reaction mechanism of the glycerol hydrogenolysis to 1,3-propanediol over Ir–ReO_x/SiO_2 catalyst. Appl Catal B Environ 105:117–127

[387] Vasiliadou ES, Lemonidou AA (2011) Parameters affecting the formation of 1,2-propanediol from glycerol over Ru/SiO_2 catalyst. Org Process Res Dev 15:925–931

[388] Zhang JS, Delgass WN, Fisher TS, Gore JP (2007) Kinetics of Ru-catalyzed sodium borohydride hydrolysis. J Power Sources 164:772–781

[389] Wunder S, Polzer F, Lu Y, Mei Y, Ballauff M (2010) Kinetic analysis of catalytic reduction of 4-nitrophenol by metallic nanoparticles immobilized in spherical polyelectrolyte brushes. J Phys Chem C 114:8814–8820

[390] Rill C, Kolar ZI, Kickelbick G, Wolterbeek HT, Peters JA (2009) Kinetics and thermodynamics of adsorption on hydroxyapatite of the [^{160}Tb] terbium complexes of the bone-targeting ligands DOTP and BPPED. Langmuir 25:2294–2301

[391] Wunder S, Lu Y, Albrecht M, Ballauff M (2011) Catalytic activity of faceted gold nanoparticles studied by a model reaction: evidence for substrate-induced surface restructuring. ACS Catal 1:908–916

[392] Vannice MA, Joyce WH (2005) Kinetics of catalytic reactions. Springer, Berlin